Synthesis and Characterization of Toughened Thermally Rearranged Polymers, Poly(2,6-Dimethylphenylene-oxide) Based Copolymers and Polymer Blends for Gas Separation Membranes

Wenrui Zhang

Dissertation submitted to the Faculty of Virginia Polytechnic Institute and State University in partial fulfillment of the requirements for the degree of

DOCTOR OF PHILOSOPHY

In

Macromolecular Science and Engineering

Committee Members:

Dr. Judy S. Riffle, Chairman

Dr. S. Richard Turner

Dr. Richey M. Davis

Dr. Charles E. Frazier

Dr. Sue J. Mecham

02/27/2017
Blacksburg, VA

Keywords: gas separation membrane, polyhydroxyimides, thermally rearranged polymers, poly(phenylene oxide), UV-crosslinking.

Abstract

Synthesis and Characterization of Toughened Thermally Rearranged Polymers, Poly(2,6-Dimethylphenylene-oxide) Based Copolymers and Polymer Blends for Gas Separation Membranes

Wenrui Zhang

Thermally rearranged (TR) polymers have outstanding gas separation properties, but are limited in their industrial application due to being mechanically brittle. A series of low volume fraction of a poly(arylene ether sulfone) (PAES) block was introduced into the TR precursor polyhydroxyimide (PI) chain to improve mechanical properties without compromising gas transport properties. The multiblock copolyhydroxyimide incorporated the PAES in systematically varied amounts and copolymerized it with 4,4'-(hexafluoroisopropylidene)diphthalic anhydride and 3,3'-dihydroxy-4,4'-diaminobiphenyl. Before thermal rearrangement, the PI-co-PAES precursors exhibited much more improved mechanical properties (tensile stress and strain at break) than those of homo polyimide precursor. After thermal rearrangement, tensile stress and strain at break of all TR copolymers decreased comparing to their corresponding precursors, but improved comparing to the homo TR polymer.

Poly(phenylene oxide) (PPO) based copolymers (Chapter 4) and polymer blends (Chapter 5) were also studied for use as gas separation membranes. The polymer materials were cast into films, then crosslinked in the solid state with UV light. The

ketone and benzylic methyl groups crosslinked upon exposure to UV light. For the study of PPO copolymers, copolymers were prepared by polycondensation of a difunctional PPO oligomer with 4,4'-difluorobenzophenone or 1,3-bis(4-fluorobenzoyl)benzene respectively. This study offers a means for fabrication of membrane films, fibers or composites, as well as tuning of gas transport properties through crosslinking in the solid state. While for the study of PPO polymer blends, PPO polymers with M_n's from 2000-22,000 g/mole were synthesized and blended with a poly(arylene ether ketone) derived from bisphenol A and difluorobenzophenone (BPA-PAEK). The crosslinked blends had improved gas selectivities over their linear counterparts. The 90/10 wt/wt 22k PPO/BPA PAEK crosslinked blends gained the most O_2/N_2 selectivity and maintained a high permeability.

General Audience Abstract

Synthesis and Characterization of Toughened Thermally Rearranged Polymers, Poly(2,6-Dimethylphenylene-oxide) Based Copolymers and Polymer Blends for Gas Separation Membranes

Wenrui Zhang

Membrane gas separation has become a fast-growing industrial technology because of its many advantages over traditional separation technologies including low capital cost and energy consumption relative to thermal distillation methods, and higher operational flexibility. Currently, membrane gas separation is widely used in processing raw natural gas to meet certain specifications before delivery to pipelines. Researches in this dissertation mainly focus on synthesis and characterization of membrane gas separation materials. In chapter 3, one type of thermally rearranged copolymer membrane was obtained, which could be potentially used in industrial field due to its improved mechanical property. In chapter 4 and 5, a series of poly(phenylene oxide) based copolymers and blends were studied. After UV-crosslinking reaction, poly(phenylene oxide) membranes showed improved gas selectivities over their linear counterparts.

Acknowledgements

I would like to express my greatest gratitude to Dr. James E. McGrath as my research advisor when I first started my graduate student career. It was a huge honor to work for such a great scientist in polymer science, and I'll always remember his kindness and generosity for his students. The research performed in this dissertation can all be traced back towards his brilliant mind, and I hope he would be proud to see it brought to fruition. I also would like to extend my warmest appreciation to my advisor Dr. Judy S. Riffle for her encouragement and guidance during my research transition after the unfortunate passing of Dr. McGrath. Dr. Riffle also contributed tremendously towards much of my scientific writing, and selflessly led our research group moving forward. Furthermore, I would like to thank my committee members, Dr. S. Richard Turner, Dr. Richey M. Davis, Dr. Charles E. Frazier and Dr. Sue J. Mecham who have been invaluable and continually giving in their advice and support. I also appreciate Dr. John J. Lesko for graciously substituting in the absence of a committee member during my final defense.

A warm appreciation is extended to the McGrath-Riffle research group for discussions and helping me maintain my sanity in the laboratory, especially Hailun Borjigin, Jarrett Rowlett, and Andrew Shaver. Thanks are extended to the life-long friends I acquired during my years in Blacksburg. I wish all of them success in their careers. Especially, I would like to thank my loving family including my parents Zuguang Zhang and Xingqun Fu, my wife Yixi Liu, and my daughter Cassie Zhang

for their love and inspiration. Thanks for believing in me when I did not believe in myself.

Attribution

Chapter 3: TOUGHENED THERMALLY REARRANGED POLYMERS FOR GAS SEPARATION MEMBRANES

To be submitted

Britannia Vondrasek, M.S. (Department of Macromolecular Science and Engineering) is a Ph.D. candidate at Virginia Tech. Ms. Vondrasek was a co-author on this paper and performed the mechanical property test on polymer films.

Gregory C. Miller, B.S. (Department of Macromolecular Science and Engineering) is a Ph.D. candidate at Virginia Tech. Mr. Miller was a co-author on this paper and performed TGA test on polymer films.

Shreya Roy Choudhury, B.S. (Department of Macromolecular Science and Engineering) is a Ph.D. candidate at Virginia Tech. Ms. Choudhury was a co-author on this paper and performed SEC test on polymer films.

Ran Liu, B.S. (Department of Macromolecular Science and Engineering) is a Ph.D. candidate at Virginia Tech. Mr. Liu was a co-author on this paper and performed monomer synthesis.

Sue J. Mecham, Ph.D. (Department of Chemistry) is currently a research scientist at the University of North Carolina at Chapel Hill. Dr. Mecham was a coauthor on this paper and contributed to the SEC analysis of the polymers.

J. J. Lesko, Ph.D. (Department of Engineering) is a professor at Virginia Tech. Dr. Lesko was a co-author on this paper and assisted in revisions of the final document.

James E. McGrath, Ph.D. (Department of Macromolecular Science and Engineering) was a professor at Virginia Tech. Dr. McGrath was a co-author on this paper and co-principal investigator for the grants supporting this research.

Benny D. Freeman, Ph.D. (Department of Chemical Engineering) is currently a professor at the University of Texas at Austin. Dr. Freeman was a co-author on this paper, co-principal investigator for the grants supporting this research and assisted in

revisions of the final document.

Judy S. Riffle, Ph.D. (Department of Macromolecular Science and Engineering) is a professor at Virginia Tech. Dr. Riffle was a co-author on this paper, co-principal investigator for the grants supporting this research and contributed revisions to the final document.

Chapter 4: POLY(PHENYLENE-OXIDE) BASED COPOLYMERS FOR GAS SEPARATION MEMBRANES

Chapter 4 was published in Journal of Materials Chemistry A

Jarrett R. Rowlett, Ph.D. is currently a membrane research scientist at NL Chemical Technology Inc. Dr. Rowlett was a co-author on this paper and contributed revisions to the final document.

Qiang Liu, Ph.D. is currently a Senior Engineer at The Dow Chemical Company.

Dr. Liu was a co-author on this paper and contributed to the gas transport testing of the polymer films.

Joshua D. Moon, B.S. (Department of Chemical Engineering) is currently a Ph.D candidate at the University of Texas at Austin. Mr. Moon was a co-author on this paper and contributed to the gas transport testing of the polymer films.

Michelle E. Dose, B.S. (Department of Chemical Engineering) is currently a Ph.D candidate at the University of Texas at Austin. Ms. Dose was a co-author on this paper and contributed to the gas transport testing of the polymer films.

James E. McGrath, Ph.D. (Department of Macromolecular Science and Engineering) was a professor at Virginia Tech. Dr. McGrath was a co-author on this paper and co-principal investigator for the grants supporting this research.

Benny D. Freeman, Ph.D. (Department of Chemical Engineering) is currently a professor at the University of Texas at Austin. Dr. Freeman was a co-author on this paper, co-principal investigator for the grants supporting this research and assisted in revisions of the final document.

Judy S. Riffle, Ph.D. (Department of Macromolecular Science and Engineering) is a

professor at Virginia Tech. Dr. Riffle was a co-author on this paper, co-principal investigator for the grants supporting this research and contributed revisions to the final document.

Chapter 5: POLY(PHENYLENE-OXIDE) BASED POLYMER BLENDS FOR GAS SEPARATION MEMBRANES

Chapter 5 was published in Polymer.

Andy Shaver, Ph.D. is currently a scientist at Westland Technologies Inc. Dr. Shaver was a co-author on this paper and contributed revisions to the final document.

Joshua D. Moon, B.S. (Department of Chemical Engineering) is currently a Ph.D candidate at the University of Texas at Austin. Mr. Moon was a co-author on this paper and contributed to the gas transport testing of the polymer films.

Donald Savacool, B.S. is currently a chemical engineer at Universal Fibers, Inc. Mr. Savacool was a co-author on this paper and contributed to film casting.

Gurtej Narang, B.S. (Department of Macromolecular Science and Engineering) is a Ph.D. candidate at Virginia Tech. Mr. Narang was a co-author on this paper and performed UV test.

Gregory C. Miller, B.S. (Department of Macromolecular Science and Engineering) is a Ph.D. candidate at Virginia Tech. Mr. Miller was a co-author on this paper and performed TGA and DSC test on polymer films.

Britannia Vondrasek, M.S. (Department of Macromolecular Science and Engineering) is a Ph.D. candidate at Virginia Tech. Ms. Vondrasek was a co-author on this paper and performed the mechanical property test on polymer films.

J. J. Lesko, Ph.D. (Department of Engineering) is a professor at Virginia Tech. Dr. Lesko was a co-author on this paper and assisted in revisions of the final document.

James E. McGrath, Ph.D. (Department of Macromolecular Science and Engineering) was a professor at Virginia Tech. Dr. McGrath was a co-author on this paper and co-principal investigator for the grants supporting this research.

Benny D. Freeman, Ph.D. (Department of Chemical Engineering) is currently a

professor at the University of Texas at Austin. Dr. Freeman was a co-author on this paper, co-principal investigator for the grants supporting this research and assisted in revisions of the final document.

Judy S. Riffle, Ph.D. (Department of Macromolecular Science and Engineering) is a professor at Virginia Tech. Dr. Riffle was a co-author on this paper, co-principal investigator for the grants supporting this research and contributed revisions to the final document.

Table of Contents

List of Figures

List of Tables

CHAPTER 1: LITERATURE REVIEW

1.1 Introduction

1.1.1 History of Membrane Gas Separation

Many early studies were focused on natural materials. In the middle of the 18th century, Jean Antoine Nollet reported the first semi-permeable membrane which was a pig bladder. Nollet realized that ethanol passed through the pig bladder faster than water.[1] About 100 years later, John Kearsley Mitchell recognized that hydrogen passes through the wall of balloons made of natural rubber.[2] Further experiments were carried out by Thomas Graham in 1866 in order to show that gases permeate rubber materials at different rates. He also stated that the rate of diffusion of a gas is inversely proportional to the square root of its molar mass.[3]

A milestone in membrane history was the application of the innovative concept of high-flux asymmetric reverse osmosis membranes in production of potable water from sea water[4]. Later, in 1980, Permea (now a division of Air Products) launched the first large scale gas separation "Prism" membrane system by adapting this technology. This membrane system can be used to separate and recover hydrogen gas from the purge gas streams of ammonia plants. A number of such plants were implemented in the 80s and 90s. The success of the Prism membrane gave a strong push to other companies to explore their own technologies for membrane gas separations. Later, cellulose acetate membrane systems for carbon dioxide separation[5] were introduced by Cynara (now part of Natco), Separex (now part of UOP), and GMS (now part of

Kvaerner). In 1990, nitrogen separation membranes were produced by Generon (now part of MG), Praxair, and Medal.[6] Several polymeric membrane systems were developed by companies for specific separations which are shown in Figure 1.1.

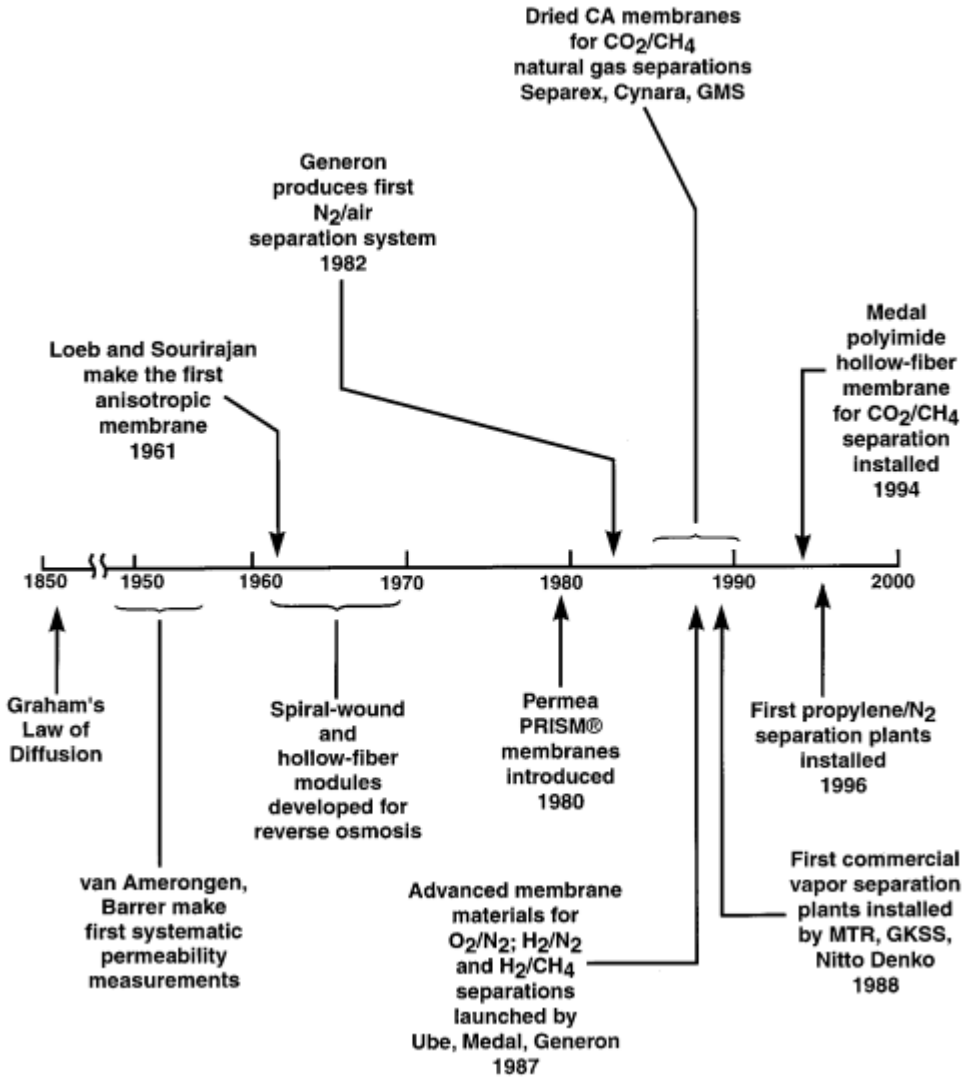

Figure 1.1 Milestones in the industrial application of membrane gas separation systems.[4]

Although the theories of gas diffusion through membranes have been investigated for more than 100 years, membrane gas separation was only applied in industry over the past 30 years. Baker[4] in 2002 estimated that the market scale of membrane gas separation technology in the year 2020 ($760 million per year) will be five times greater than that of the year 2000 ($150 million per year). Presently,

membrane gas separation has become the most robust of separation technologies in the industrial market.

1.1.2 Principles of Membrane Gas Separation

1.1.2.1 Overview

Membrane gas separations rely on different permeation rates for the gases to be separated. Two models are used to describe the permeation process. The pore-flow model is the early explanation for the gas permeation process. Gases can be separated by pressure-driven convective flow through micropores. A separation is achieved between different gases due to one of the gases being excluded from some of the pores in the membrane. This is often called sieving. Another model is the solution-diffusion model membranes without permanent pores. This has been widely used over the past 40 years as an explanation for transport in electrodialysis, reverse osmosis, and pervaporation. In this theory, gases will first dissolve in the membrane and then diffuse through it down a concentration gradient. A separation is achieved between different gases because of differences in the amount of material that dissolves in the membrane and the rate at which the material diffuses through the membrane.

1.1.2.2. Solution-Diffusion Model

The permeability through dense polymers is considered to be a solution-diffusion process. In the solution-diffusion model, transport occurs by diffusion. The component to be transported must first dissolve in the membrane. The general

approach of the solution-diffusion model is to assume that the chemical potential of the feed and permeate fluids are in equilibrium with the adjacent membrane surfaces such that appropriate expressions for the chemical potential in the fluid and membrane phases can be equated at the solution-membrane interface. This principle is more important for dense membranes without pores such as those used for reverse osmosis and in fuel cells.

Using the solution-diffusion model, the gas permeability coefficient[7] can be written as the product of a gas solubility coefficient, S, and a concentration-averaged, effective diffusion coefficient, D

$$P=DS \tag{1-1}$$

where P is the permeability coefficient, D is the diffusivity coefficient and S is the solubility coefficient. In the literature,[8-9] the widely employed units for P are cc(STP)-cm/(cm^2-sec-cmHg) describing the gas permeating a membrane at steady state (cc(STP)) with a thickness (cm), a membrane area (cm^2), a time interval (sec) with a pressure drop across the membrane (cmHg). The unit for D is cm^2/sec and S is cc(STP)/cm^3-cmHg. The permeability coefficient unit commonly reported in the literature is the Barrer defined by: 1 Barrer = 10^{-10}cc(STP)-cm /(cm^2-sec-cmHg).
The appropriate SI unit is kmol·m·m^{-2}·s^{-1}·kPa^{-1} or m^3(STP)·m·m^{-2}·s^{-1}·kPa^{-1}.

For a pure gas permeating through a polymer film or membrane, gas permeability, P, is defined as the trans-membrane pressure difference, p2-p1, and thickness normalized steady-state gas flux, N[7]

$$P=Nl/(p2-p1) \tag{1-2}$$

where l is the membrane thickness, p2 is the upstream pressure, and p1 is the downstream pressure. Unlike flux, which depends upon l and Δp (differential pressure), P is typically viewed, to a first approximation, as being a material property that is much less dependent than flux on membrane thickness and Δp. Each polymer has a different permeability coefficient for each gas, and the faster permeation of some gases relative to others provides the basis for the use of polymers to separate gas mixtures. The range over which permeability can vary in different polymers is enormous.

Diffusion is an activated energy process that can be expressed by an Arrhenius relationship:

$$D = D_0 \exp(-E_d / RT) \tag{1-3}$$

where E_d is the activation energy of diffusion and D_0 is the pre-exponential factor. The solubility coefficient can be expressed by the Van't Hoff relationship

$$S = S_0 \exp(-\Delta H_s / RT) \tag{1-4}$$

where ΔH_s is the heat of solution and S_0 is the pre-exponential factor. Combining these equations gives:

$$P = P_0 \exp(-E_p / RT) \tag{1-5}$$

where E_p is the activation energy of permeation and $E_p = E_d + \Delta H_s$. The value of E_d (and thus E_p) is different below and above the glass transition temperature.

A common parameter characterizing the ability of a polymer to separate two gases (e.g., A and B) is the ideal selectivity, $\alpha_{A/B}$[10]:

$$\alpha_{A/B} = P_A / P_B \tag{1-6}$$

$$\text{Since } P=DS, \quad \alpha_{A/B} = D_A S_A / D_B S_B \tag{1-7}$$

Like permeability, the ideal selectivity is often treated as a material property of a polymer.

1.1.2.3. Free Volume Concept

There are spaces between polymeric chains that are designated as free volume (i.e., unoccupied volume). [11] Free volume can vary as a function of temperature, chemical structure of the polymer, physical conformations, etc. Free volume is highly related to diffusivity and permeability, but hardly to solubility[12]. When it comes to membrane gas separation for different gases, free volume distribution turns out to be an important factor. Cohen and coworkers reported the relationship between free volume and diffusion co-efficiency, shown in the following equation[12-13]:

$$D = A\exp(-\frac{\gamma \upsilon^*}{FFV}) \tag{1-8}$$

In this equation, γ is an overlap factor which is introduced to prevent double counting of free volume elements, υ^* is the minimum required volume of the void that is related to the molecule size, and FFV is the fractional free volume of the polymer[14], and can be expressed as[15]

$$\text{FFV} = \frac{\upsilon_f}{\upsilon} = \frac{\upsilon - \upsilon_0}{\upsilon} = \frac{\upsilon - 1.3\sum \upsilon_w}{\upsilon} \tag{1-9}$$

where ν_f is the free volume of the polymer; ν (cm^3/g) is the experimental specific volume of the polymer; ν_0 (cm^3/g) is the theoretical occupied volume (volume of the polymer extrapolated to absolute zero) of the polymer chains. It is typically calculated by group contribution theory as described by Bondi[16] and ν_W is the *van der* Waal's

volume of groups comprising all polymer chains.

A continuous redistribution of free volume is allowed by polymer chain movement in the rubbery state (beyond T_g), and the redistribution of free volume can also occur at slower rates in the glassy state (below T_g). Figure 2 shows the relationship between temperature and free volume in amorphous polymers.

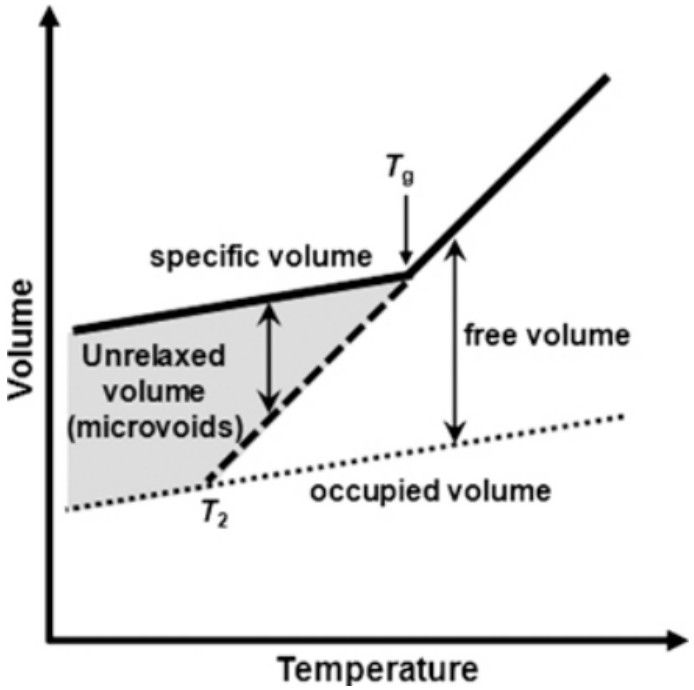

Figure 1.2 Specific volume (bold line) and occupied volume (dotted line) vs temperature curves for an amorphous polymer[17]

In Figure 1.2, the slope of specific volume versus temperature changes at the glass transition temperature as a rubbery polymer is cooled. As a result, a difference between the specific volume of the glass and extrapolated specific volume of the rubber at 0 ºK is yielded.

1.1.2.4. Trade-Off Relationship between Permeability and Selectivity

Polymeric membranes have been under development since the 1980s, and a significant research domain is structure-property relationships related to membrane

gas transport properties[5]. To achieve enhanced gas transport properties, a large number of polymers have been synthesized and modified, and this has led to the recognition of a trade-off relation between selectivity and permeability[18-21]. Polymers with higher selectivity are less permeable, while those that are more permeable have less selectivity (Figure 1.3).

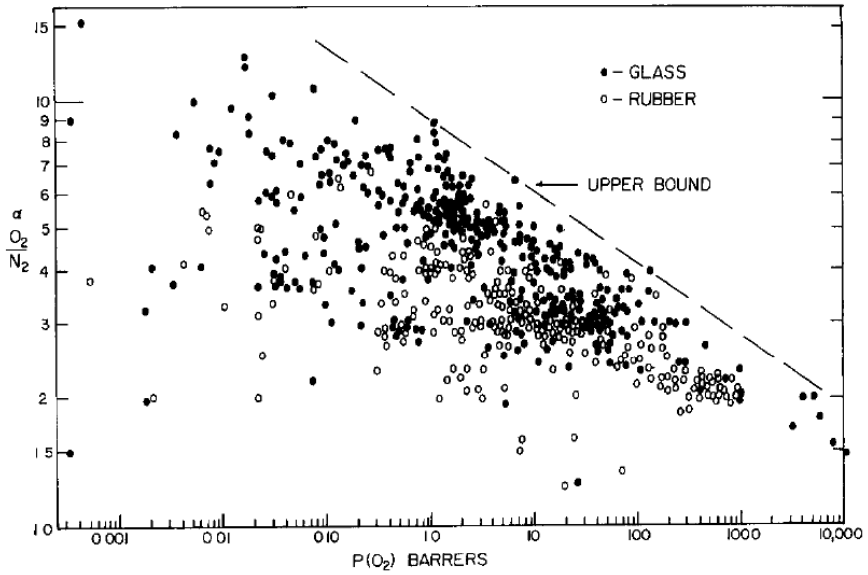

Figure 1.3 The 1991 upper bound correlation for O_2/N_2 separation

In 1991, this notion was explained by Robeson quantitatively[22]. The available published transport property data of a multitude of various rubbery and glassy polymers in the literature was plotted, and thus the term of "upper bound" relating to the limitations of gas separation membranes was coined. This upper bound is based on an empirical correlation between log-selectivity and log-permeability for the separation of oxygen and nitrogen (Figure 1.2). In the figure, a linear trend was observed, as the selectivity (α) increases as the permeability (P) decreases, and vice-versa. Equation 1-10 describes the "upper bound":

$$\alpha_{A/B} = \beta_{A/B} / P_A^{\lambda_{A/B}} \tag{1-10}$$

In equation 1-10, $\lambda_{A/B}$ and $\beta_{A/B}$ are the upper bound slope and front factor, respectively, and they are constants for gas pair A and B based on empirical observations initially reported by Robeson for common gas pairs. The equation expresses the linear relationship, as the permeability of an upper bound polymer gas A (P_A) increases, the selectivity of the polymer for gas A over gas B decreases, and vice versa.

Robeson's observed empirical upper bound relationship is based on experimental data, however, it was supported Freeman and coworkers[23] by theoretical analysis. The upper bound slope $\lambda_{A/B}$ was predicted using activation energy theory as

$$\lambda_{A/B} = (\frac{d_B}{d_A})^2 - 1 = (\frac{d_B + d_A}{d_A^2})(d_B - d_A) \tag{1-11}$$

d_A and d_B represent the penetrant diameter of polymer A and B. Comparing the value of the $(d_B+d_A)/d_A^2$ term, d_B-d_A dominates, and this yields an accurate agreement between theory and experimental observation. The front factor $\beta_{A/B}$ was further analyzed with the result of an upper bound slope $\lambda_{A/B}$, giving a relatively complicated relationship[24]:

$$\beta_{A/B} = \frac{S_A}{S_B} S_A^{\lambda A/B} exp\left\{-\lambda_{\frac{A}{B}}\left[b - f \times \left(\frac{1-a}{RT}\right)\right]\right\} \tag{1-12}$$

where S_A and S_B are the gas solubilities of A and B in the polymer, and the solubilities can be determined by the relationships with gas boiling point T_b, critical temperature T_c, or penetrant Lennard-Jones temperature (ε_A/k) by equations 1-13, 1-14 and 1-15[25]:

$$\ln S = m + 0.025T_b \quad (1\text{-}13)$$

$$\ln S = x + 0.016T_c \quad (1\text{-}14)$$

$$\ln S = y + 0.023(\varepsilon_A/k) \quad (1\text{-}15)$$

where m, x and y values vary for different polymers. These correlations apply for both aromatic and aliphatic polymers[26], with the exception of perfluorinated polymers where the slopes are different.

Equation 1-16 describes the linear relationship between the activation energy of diffusion E_d and diffusivity D_0, and from this equation, constants a and b (in equation 1-12) are determined[23]:

$$lnD_0 = a\frac{E_d}{RT} - b \quad (1\text{-}16)$$

Finally, the f parameter can be determined by Equation 1-17, which relates the activation energy of diffusion[27] E_d with the diameter of the penetrating molecule d. The values of c and f are constants and adaptable with respect to a specific polymer. Freeman found that the value of f to obtain a match between the empirical upper bound and his theory is approximately 12600 cal/mole.

$$E_d = cd^2 - f \quad (1\text{-}17)$$

To achieve better gas transport properties, novel polymers have been designed and synthesized for gas separation membranes, and this has provided access to more data and the appearance of more advanced materials such as “thermally rearranged”

(TR) polymers. As a result, the original upper bound was traversed as expected. In 2008, the tradeoff relationship between permeability and selectivity was re-addressed by Robeson to include new data, and the upper bound was shifted[26]. A significant contribution of the upper bound shift for He/H_2 separation was mostly made by perfluorinated polymers (Figure 1.4). The superior separation property of the perfluorinated polymer is due to the high solubility of the gas in the perfluorinated polymer. The permeability-selectivity tradeoff relationships were established based on membrane performance at 25–35°C, primarily because most permeability data in the literature were from measurements made in this temperature range. Recently, Rowe and coworkers developed a model that describes the predicted upper bound behavior shifts vertically with temperature[28], based on Freeman's theoretical framework of the trade-off relationship. The predicted upper bound shifts vertically with temperature, and the direction and magnitude of the shift depends on the sizes and condensabilities of the gases considered.

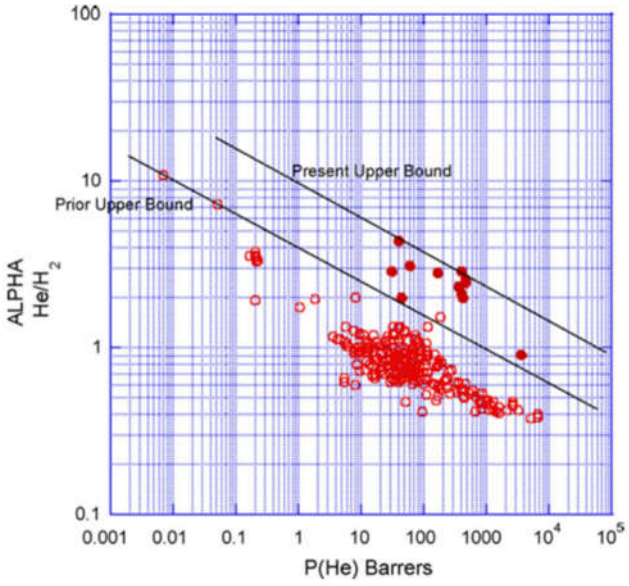

Figure 1.4 The 2008 upper bound correlation for He/H_2 separation[26]

1.2 Gas Separation Membranes

Since Permea built the first hydrogen separation Prism membrane plant in 1980, membrane-based gas separation has rapidly grown into a $1.9 billion business (2015), and is expected to reach close to $2.6 billion by 2020[29]. In the past few decades, hundreds of thousands of new polymer membrane materials have been reported[30-32], and many have substantially high permeabilities and selectivities. In this section, several classes of polymer membrane materials will be reviewed.

1.2.1 Polyimides(PI)

Polyimides are a class of polymer containing imide repeat units. They have been in mass production since 1955. Due to their high heat-resistance, polyimides have diverse applications in different areas, e.g. high temperature plastics, adhesives, dielectrics, photoresists, nonlinear optical materials, and membrane materials for separation[33]. Polyimide membranes can be extremely robust and can withstand prolonged use at temperatures around 200°C or short exposure to temperatures up to 400°C. Their remarkable thermal stability is closely dependent on the molecular structure of the repeat unit. Aromatic polyimides also tend to have good gas permeabilities with high selectivities, which makes them a good competitive gas separation membrane candidate. DuPont first applied polyimide membranes to separate helium from natural gas in 1962. In 1981, Ube Industries launched another

polyimide membrane production of Upilex-R. Since then, polyimide gas separation materials have been widely studied and still maintain interest[31].

Matrimid® is a thermoplastic polyimide based on 5-amino-1-(4-aminophenyl)-1,3,-trimethylindane and 6-amino-1-(4-aminophenyl) -1,3-trimethylindane[34]. It is a soluble fully imidized polyimide with excellent gas separation properties. Comparing with some other commercialized gas separation polymers such as Udel, cellulose acetate, etc., Matrimid has better gas separation properties, especially in CO_2/CH_4 separation. However, similar to all the linear polymer membranes, Matrimid membranes suffer significant plasticization under CO_2 exposure. As a result, the selectivity of CO_2/CH_4 decreases with time. As the concentration of gas inside the polymer increases, the polymer can swell, which increases free volume and chain motion that, in turn, increase gas diffusion coefficients and decrease diffusion selectivity. This phenomenon is known as plasticization[32]. To overcome plasticization in the linear polyimide membranes, some methods have been adopted by thermal treatment[34-35] and chemical crosslinking[36-38]. The plasticization can be reduced after thermal treatment or forming the crosslinked polymer structure, but at the same time, the permeability of these modified membranes usually decrease [39].

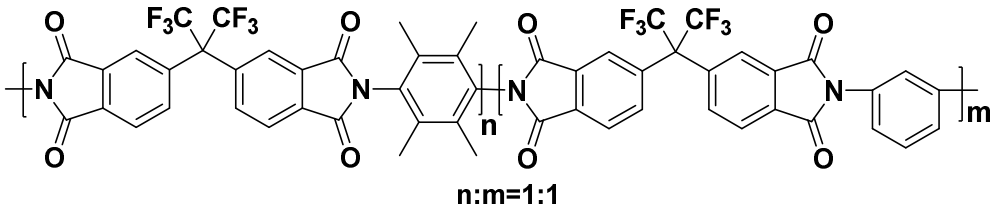

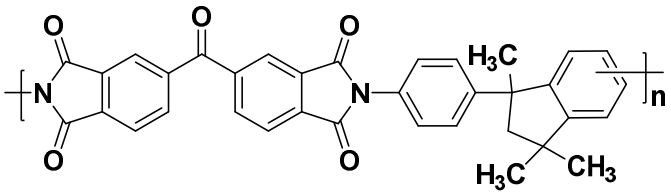

Matrimid

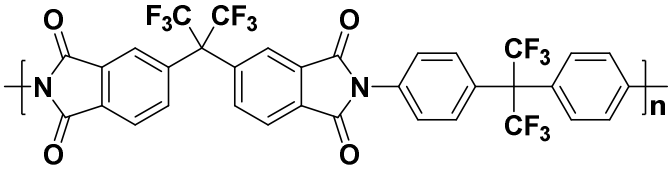

Fluorinated Polyimide

Figure 1.5 Structures of three commercial polyimides

Recently, fluorinated polyimides (Figure 1.5) have also been widely studied due to their excellent gas separation properties[40-41]. Fluorinated polyimides generally contain an aromatic imide moiety with hexafluoroisopropylidene linkages. The hexafluoroisopropylidene group increases the stiffness of polymer chain relative to an isopropylidene and decreases the chain packing efficiency due to steric hindrance. This creates more free volume and increases the permeability.

Recently, a series of soluble polyimides with high gas permeability have been reported[42-47]. All of these polyimides share some common characteristics, such as bulky side groups and non-coplanar spatial configuration. As a result of designing these structural features, polyimides can be highly permeable due to high free volume in the polymer structure. However, it is more difficult and less economical to obtain these polyimides than that of typical polyimides because multiple steps of synthesis

and purification are required.

1.2.2 Poly(Phenylene Oxide) (PPO)

In 1959, Hay and coworkers synthesized poly(2,6-dimethyl-1,4-phenylene oxide) (PPO)[48] shown in Figure 1.6. It was the first commercial poly(phenylene oxide) and was commercialized by General Electric[49] (now Sabic Innovative Plastics) and AKZO later[50]. The PPO polymer can be synthesized by various polymerization methods, including oxidative coupling polymerization of 6-xylenol (Figure 1.7) and aromatic nucleophilic substitution. Oxidative coupling polymerization is competitive because of the moderate reaction temperature, halogen-free monomers and environmentally friendly byproducts.[51]

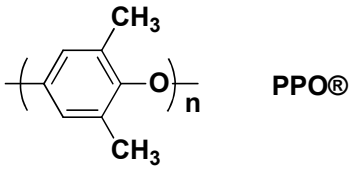

Figure 1.6 Poly(phenylene oxide)

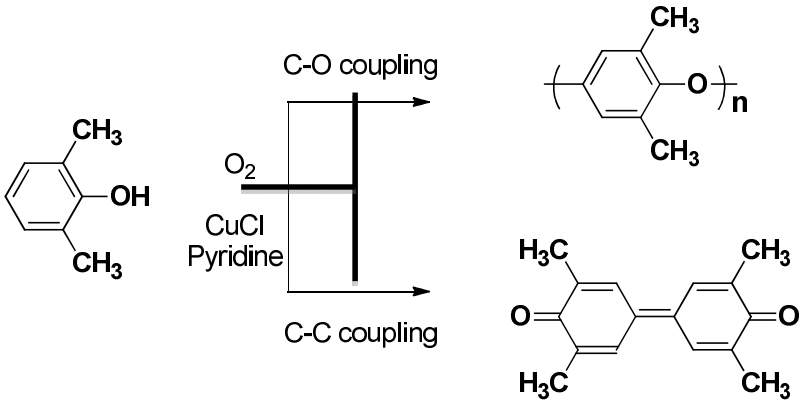

Figure 1.7 Oxidation coupling reaction

Like many glassy polymers, PPO and its derivatives are of interest for gas separation applications because of their excellent transport properties. They have been

extensively studied as potential membranes for CO_2/CH_4 separation systems. The methyl groups on the polymer backbone of PPO can disrupt of chain packing to increase free volume, which enhances gas diffusion and gives a high permeability to PPO. This high permeability makes it extremely attractive for gas separation applications, but unfortunately the selectivity of the PPO membrane is too low for many gas separation applications. Therefore, PPO and its derivatives such as brominated PPO, nitrated PPO, sulfonated PPO, etc. have been studied to improve its selectivity.

It has been reported that PPO and its carboxylated derivative (CPPO) can adsorb CO_2 and CH_4 and their binary mixtures[52]. The dual model sorption model predicts mixed gas sorption based on pure gas sorption parameters. Polymers with different chemical structures having a wide range of permeabilities have been included in in a paper to extend the mixed gas sorption database, and to confirm the accuracy of the accuracy of the model[53]. Therefore, those mixed gas dual mode sorption model with confirmed accuracy can be applied to any gas/polymer system.

It was found that the permeability of PPO varies with the degree of bromination, and the magnitude of the change is related to the nature of the gas[54-55]. For example, the percentage of increase is higher for a gas with lower condensability, and concentration-averaged diffusivities of CH_4 and CO_2 also show some variation with the extent of bromination. It is also worth noting that when the bromination was increased to 91%, the diffusivity of CO_2 increased notably, but CH_4 decreased slightly. These observations were interpreted in terms of changes in the average packing,

torsional mobility of the chain segments, and the cohesive energy density of the polymer. IR spectra of brominated high molecular weight PPO membranes revealed that brominating PPO at the phenyl ring results in decreasing both the in-plane C-H bending (1180 cm^{-1}) and the C-O-C torsional motion (1300 cm^{-1}). At 37.4% bromination and higher, splitting in the 1180 cm^{-1} band was observed due to different modes for C-H bending occurring, because a portion of the methyl groups were hindered by adjacent bromine substituents. Comparing with PPO, as the degree of bromination was increased to 37.4%, the permeability of gases in the brominated PPO membranes only increased slightly, while the permeability of gases almost doubled at 60% bromination[56]. In summary, both the IR spectral observations and the trend in gas permeability data confirmed the proposed mechanism that higher bromination degrees are needed to increase the rate of diffusional jumps by enhancing the permeability of gases through stiffening the PPO backbone.

Another PPO derivative membrane was prepared by chemical modification through sulfonation using chlorosulfonic acid[57]. The modified structure of PPO and its interactions with gaseous molecules were confirmed by FTIR and X-ray diffraction. It was tested for the separation of CO_2/CH_4 mixtures. Differential scanning calorimetry (DSC) and scanning electron microscopy (SEM) was used to investigate thermal stabilities of the modified polymers and membrane morphology, respectively, while the tensile strength was measured to evaluate their mechanical stabilities. The modified forms of PPO showed relatively lower mechanical property than the unmodified polymer membrane.

1.2.3 Cellulose Acetate (CA)

Cellulose esters (Figure 1.8) have been commercialized for over a century as natural polymers, because of their enhanced physical properties by esterification of cellulose into various useful forms. Cellulose esters can be applied as adhesives, coatings, liquid crystal displays, biodegradable plastics, and separation media[58]. In the 1980s, cellulose acetate was introduced for reverse osmosis membranes and commercialized later for gas separations, especially for natural gas separations[59-61].

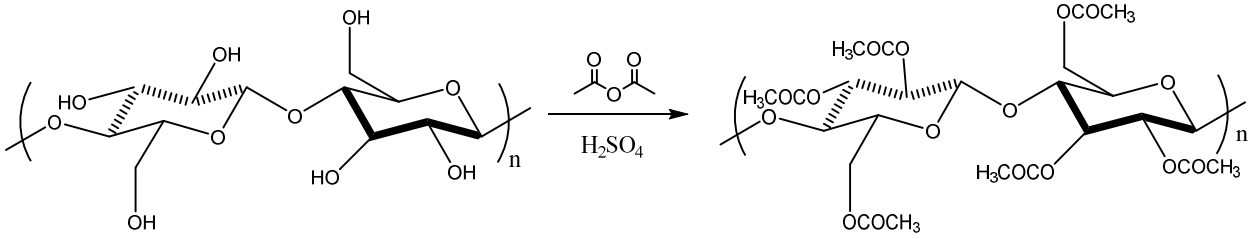

Cellulose **Cellulose Triacetate**

Figure 1.8 Acetylation of cellulose

Cellulose acetate can be produced by acetylation of cellulose using acetic anhydride or acetic acid[58]. The exchange of a hydroxyl group with acetate groups reduces crystallinity and hydrogen bonding to improve the solubility of cellulose acetate in common solvents and processibility via various methods. As only three functional groups of cellulose can be converted to acetate groups in one repeating unit, the degree of acetylation (degree of acetate substituents, DS) is generally from zero to three. DS has been shown to affect gas transport properties of cellulose acetate. As it increases, the permeability of cellulose for all common gases increases[60]. By replacing the polar hydroxyl group by the bulky acetate group, hydrogen bonding is

reduced, and this decreases the polymer density to provide a polymer structure with higher free volume.

Cellulose acetate membranes have been well developed and applied in industry, because of their low cost and abundance[62]. However, a crucial weakness of cellulose acetate membranes is that they can be plasticized by CO_2 and this decreases membrane selectivity. For CH_4/CO_2 separation, the reduction of membrane selectivity is undesirable because it decreases methane recovery in natural gas separations.

1.2.4 Polysulfone (PSF)

Polysulfones are a family of engineering thermoplastics with high chemical and thermal stability. In the backbone structure, the existence of electron withdrawing, kinked, sulfone groups (aryl-SO_2-aryl) and rigid phenylene rings restrict molecular mobility, resulting in a completely amorphous material with high Tg, high strength, good creep resistance, dimensional stability, and high heat deflection temperatures[30, 63]. A great number of polysulfones have been commercialized, such as Udel®, Victrex®, Radel®R and Radel®A (Figure 1.9). Most commercial polysulfones can be synthesized by nucleophilic aromatic substitution.

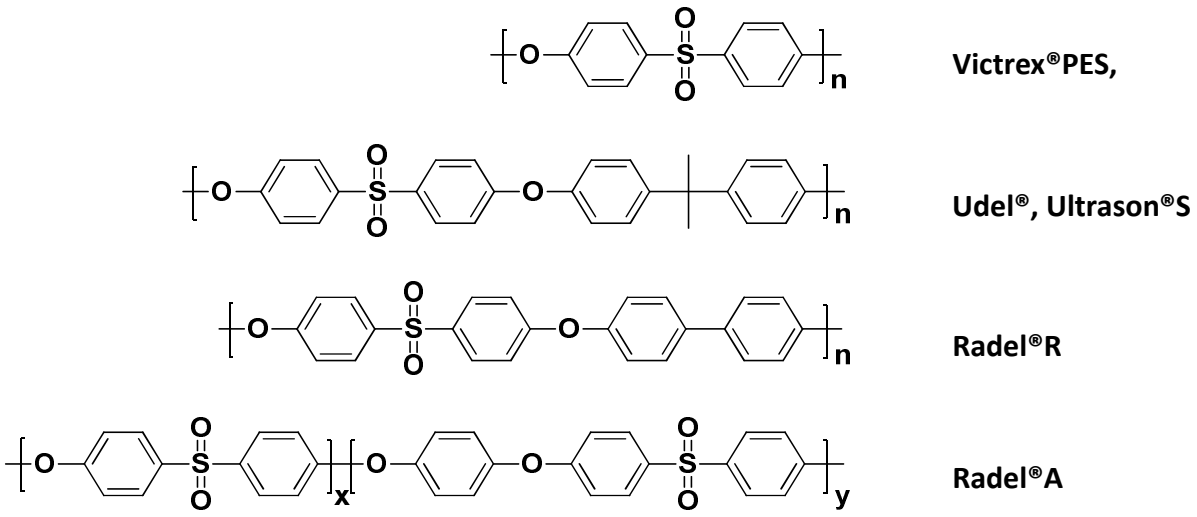

Figure 1.9 Structures of commercial polysulfones

The first polysulfone membrane used for gas separation, bisphenol A sulfone (Udel®), was developed by Monsanto in the late 1970s. Since then, the gas separation performance of these commercial polysulfones and their variants have been comprehensively studied. For commercial polysulfones, the permeability coefficient for all gases ranks in this order: Udel®≈ Radel®R> Radel®A> Victrex®.

Aguilar-Vega and coworkers assessed the effect of substitution of aromatic groups on the bisphenol connector unit of bisphenol-A based polysulfone materials on their gas transport properties[64]. Substitution of a methyl group by a phenyl ring results in a slight increase in permeability coefficients, and with similar to slightly higher selectivity for all gases comparined with polysulfone. The increases in permeability are related to the larger fractional free volume derived from aromatic substitution. Replacing the methyl groups in the polysulfone by two locked phenyl rings (fluorene bisphenol polysulfone) leads to doubling of permeability and solubility coefficients. The fluorene based polysulfone materials were shown to have the highest thermal and oxidative stability by thermal measurements, and they also have the largest fractional

free volume and the largest permeability coefficients. Therefore, such aromatic substitutions can be useful for developing gas separation membranes, which can be used in harsh thermal or oxidative environments.

A series of phenyl-substituted polysulfones were tested for their gas permeability, diffusivity, and solubility at 35 °C and pressures up to 20 atm[65]. Gas permeabilities and diffusivities were significantly lower for polysulfones bearing aryl substituents relative to those of unmodified polysulfones, and this was attributed to the increased restriction to sub-T_g torsional motion and decreased fractional free volume in the substituted polymers. Benzylic amine-substituted polysulfones exhibited higher CO_2 solubility and CO_2/CH_4 solubility selectivity compared with polysulfone, most probably because of the favorable interactions between basic CH_2-NH_2 groups and CO_2 molecules. However, CO_2 diffusivity in substituted polysulfones was not as high as expected considering free volume, which indicates that benzylic amine moieties and CO_2 interactions might be strong enough to block CO_2 mobility in the modified polymer. All the above results agree with infrared spectroscopy data that indicated the benzylic amino groups undergo a reversible reaction with CO_2 and form carbamate moieties.

Investigation were conducted to understand effects of the symmetrical structure of phenylene linkages and methyl group placement on the properties of polyether-polysulfones prepared from 4,4'-difluorodiphenyl sulfone and bisphenols[66]. The symmetrical polysulfones were found to have lower selectivity coefficients and higher gas permeabilities compared with the asymmetrical polymers. The

polysulfones that were di-methylated or with *m*-phenylene linkages on the bisphenol unit had lower fractional free volumes and glass transition temperatures, but higher sub-T_g relaxation temperatures. Generally, the chains of the asymmetrical polymers were more efficiently packed and appeared to have greater mobility constraints, stemming from both intramolecular and intermolecular origins, than their symmetric counterparts. All of these features influenced properties and especially their permeation behavior.

Unmodified and aryl-nitrated polysulfones have also been reported. Their gas permeabilities and permselectivities include CO_2, CH_4, O_2 and N_2[67]. Permeabilities for all gases decreased with aryl nitration, but permselectivity increased for CO_2/CH_4 and O_2/N_2 gas pairs. These results were attributed to changes in torsional mobility, packing density, and inter-chain attractions derived from the polar nitro group.

Polysulfone oligomers have have also been shown to be good toughening agents for epoxy thermosets to improve the mechanical prosperity of the systems. Yoon et al. investigated amine-terminated polysulfone modifiers that varied in molecular weights from 5000 to 20000 g $mole^{-1}$. Significant improvements in fracture toughness of thermoplastic-modified networks were achieved[68-70]. Varley examined the effect of addition of a reactive controlled molecular weight (M_n~8000 g/mole) polysulfone on the final properties and network structure of a Trisglycidyl-p-aminophenol (TGAP) / 4,4'-diamino-diphenyl-sulfone (DDS) system after cure and post-cure. The toughness was found to be related to morphology of this copolymer system, with relatively small increases in toughness observed when the morphology remained dispersed particulate

or co-continuous in nature. An obvious large increase in toughness was observed when the morphology became phase inverted[71-72].

Compared with other commercial polymers including polycarbonate, cellulose acetates and polyimides, polysulfones remain competitive for H_2/N_2 separations but not for CH_4/CO_2 separations.

1.3 Thermally-Rearranged (TR) Polymers

1.3.1 Overview of Thermal Rearrangement Technique

Recently, Park et al. introduced a new class of polymer membranes that he called "Thermally-Rearranged (TR) Polymers" with outstanding gas transport properties, especially for CO_2/CH_4 separations (Figure 1.10). These TR polymers can be prepared by a thermal rearrangement process in the solid state of thermally rearrangeable precursor ortho-hydroxy polyimides[73-76]. Synthesis of TR precursor polyimides and the thermal rearrangement process of precursor polyimides will be reviewed later in this chapter.

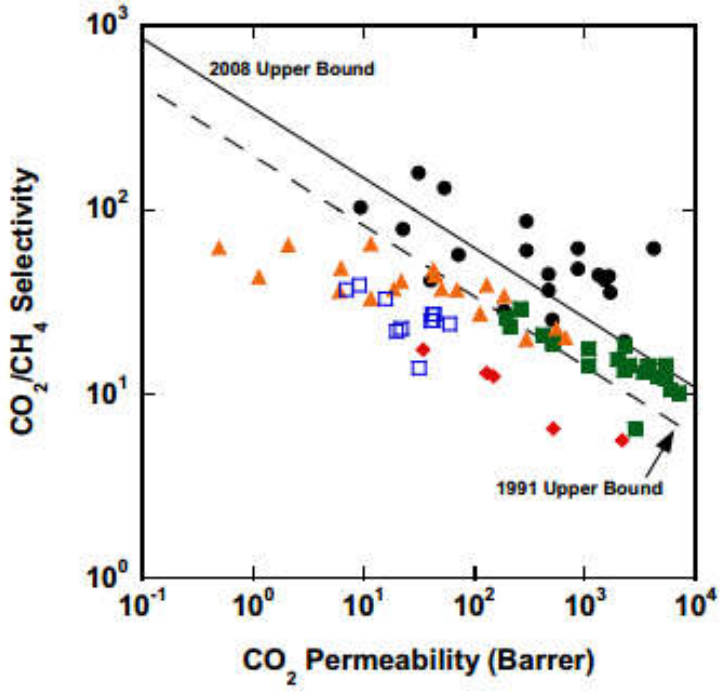

Figure 1.10 CO_2/CH_4 separation properties of various emerging polymer materials reported in the literature[32]. Black and red symbols represent TR polymers.

Thermally rearrangeable precursor polyimides are a family of polyimides with ortho-functional aromatic imide repeat units. The ortho-position functionality has been postulated to include -OR, -SR and –NR groups. In the thermal rearrangement process, soluble precursor polyimides partially or completely rearrange to insoluble polybenzoxazoles (PBOs) if OR or OH are in the ortho-position to the imide. Each mole of repeat unit is able to release two moles of CO_2 to form a new benzoxazole unit via either intramolecular or intermolecular routes. It is believed that the free volume increases after the thermal rearrangement is due to CO_2 molecules escaping from the original polymer matrix, and intermolecular rearrangement causes crosslinking of the polymer structure. This process provides excellent resistance to CO_2-induced plasticization of the TR polymers.

1.3.2 Synthesis of TR precursor polyimides

Aromatic TR precursor polyimides were synthesized by several different methods, and research revealed that synthetic routes can also affect the gas transport properties. In this section, three different synthetic strategies will be discussed. Technically, all these synthetic methods can be applied to produce TR precursor polyimides.

1.3.2.1 Two-step polyimide synthesis

Polyimides, as a class of high-performance polymer, often contain wholly aromatic backbones, with excellent thermal stability and chemical resistance, as well as good mechanical properties[77]. Most commonly, polyimides are prepared through condensation, or step polymerizations of organic diamines with organic tetracarboxylic acids or derivatives, such as dianhydrides or tetraacid chlorides. A general chemical structure of an aromatic or cycloaliphatic polyimide is given in Figure 1.11. Commonly used dianhydrides and diamines are provided in Figure 1.12, along with acronyms that will be used throughout this dissertation.

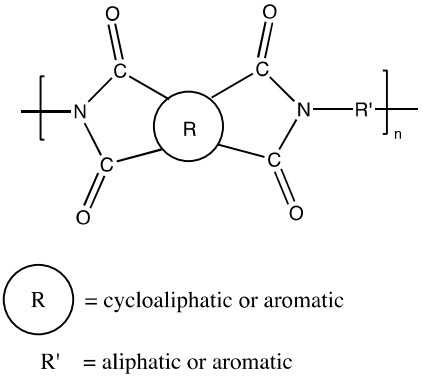

Figure 1.11 Generic structure of a polyimide

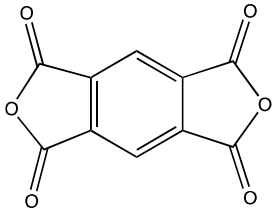

Pyromellitic Dianhydride (PMDA)

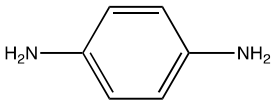

1,4-Phenylenediamine (*p*-PDA)

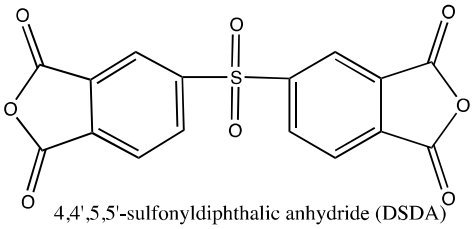

4,4',5,5'-sulfonyldiphthalic anhydride (DSDA)

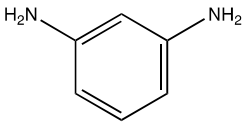

1,3-phenylenediamine *m*-PDA

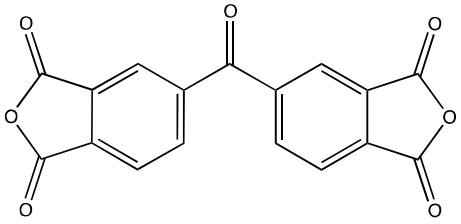

3,3'4,4'-benzophenonetetracarboxylic dianhydride (BTDA)

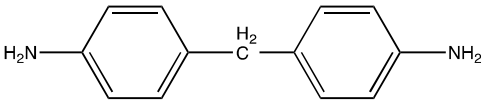

4,4'-methylene dianiline (MDA)

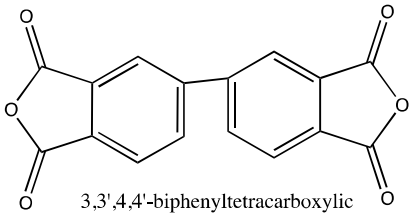

3,3',4,4'-biphenyltetracarboxylic dianhydride (BPDA)

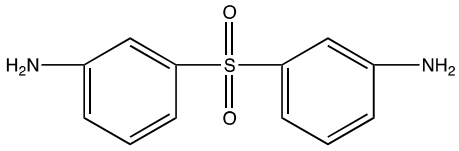

4,4'-diaminodiphenyl sulfone (*m*-DDS)

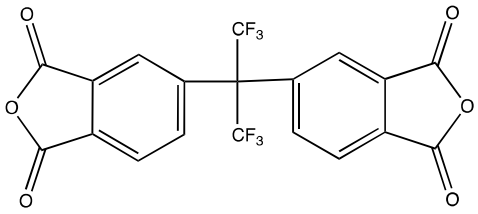

4,4'-hexafluoroisopropylidenebis(phthalic anhydride) (6FDA)

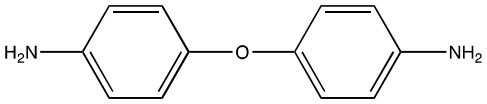

4,4'-diaminodiphenyl ether (ODA)

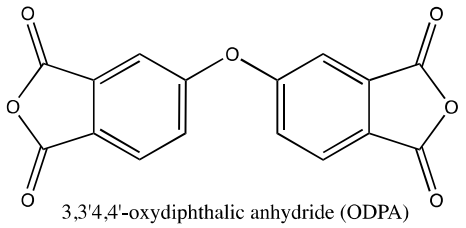

3,3'4,4'-oxydiphthalic anhydride (ODPA)

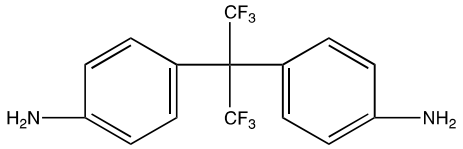

4,4'-hexafluoro(isopropylidene) dianiline

Figure 1.12 Commonly used aromatic dianhydrides and aromatic diamines in polyimide synthesis

The first report of polyimide synthesis was in 1908 by Marston Bogert[78]. However, it was nearly fifty years until high molecular weight polyimides were reported by DuPont in the 1950s[79]. The most common procedure for synthesizing polyimides is the classical two-step poly(amic-acid) method. The reaction proceeds first by combination of an aromatic diamine with a dianhydride at ambient temperature in a dry, polar aprotic solvent[80] such as *N*-methylpyrrolidinone (NMP), dimethylformamide (DMF), or *N,N*-dimethylacetamide (DMAc). The resultant poly(amic-acid) intermediate forms rapidly and is subsequently dehydrated (cyclized) by either thermal or chemical imidizations to the imide product, as shown in Figure 1.13. Kapton™(DuPont), was one of the first commercial polyimides developed in the 1950's and it is synthesized by the two step reaction of PMDA with 4,4'-diaminodiphenyl ether (ODA). In 1962, Endrey first achieved a high molecular weight polyimide using this synthetic route and it has received large attention over the past few decades due to its attractive soluble poly(amic-acid) intermediate[81].

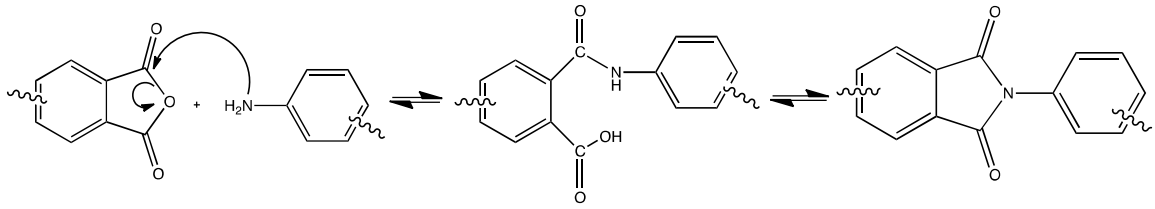

Figure 1.13 Formation of a polyimide via a poly(amic-acid) intermediate.

Many polyimides are infusible, intractable, and exhibit poor processability due to their planar, aromatic nature. Therefore, they must be processed or shaped into usable materials in the first stage prior to imidization in the second. The two-step method became popular because it allowed commercial processing of polyimides via the

soluble poly(amic-acid) pre-polymer. The following discussion will address issues relevant to the poly(amic acid) synthetic route such as solvent selection, reaction conditions and the mechanism of imidization.

In the classical two-step reaction, a suitable diamine can be combined with a dianhydride to generate a poly(amic-acid) in a polar aprotic solvent (NMP, DMAc, DMF, DMSO) at ambient temperature. Dry reaction conditions are critical to the attainment of high molecular weight poly(amic-acid)s. Nucleophilic attack by the amine nitrogen's lone electron pair onto the sp2 carbon of the carbonyl displaces the carboxylate functionality, and, following proton transfer, creates a polyimide intermediate with an *ortho*-substituted carboxylic acid (or an *o*-carboxycarboxyamide)[82]. Figure 1.14 shows the reversible formation of a poly(amic-acid), and the forward reaction rate constant is much larger than the reverse[83]. The figure illustrates a straightforward reaction of monomer to poly(amic-acid).

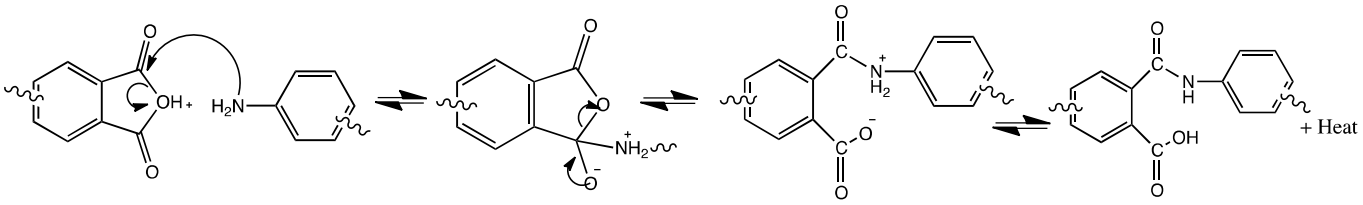

Figure 1.14 Mechanism of Poly(amic-acid) formation

Polyimide formation is a condensation reaction and therefore monomer purity and precise stoichiometry are vital for the formation of high molecular weight polymer. Being a second-order reaction, an increase in monomer concentration will form higher molecular weight polyimides as well as reduce the amount of impurities

from solvent degradation. Likewise, increasing the monomer concentration will result in higher amine/water ratios, diminishing the effect of water formed via cyclodehydration into the imide structure on the dianhydride monomers[84]. The two-step method is also sensitive to temperature. The reaction is exothermic and cooler temperatures are favored to drive the equilibrium. Typically, synthesis of poly(amic-acid)s is conducted at temperatures between -20 and 70 °C, and a viscosity increase is evident when equimolar amounts of monomer have reacted. Synthesis temperatures exceeding 70°C inhibit the attainment of high molecular weight due to the effect on the equilibrium of the poly(amic-acid) formation[85].

Side reactions have been historically elusive to quantify, as they are accompanied by inconsistent concentrations of impurities. They can be eliminated under rigorous conditions with carefully dried solvents and pure monomers. One side reaction that is unavoidable is the reverse equilibrium reaction to regenerate diamine and dianhydride. Because the equilibrium constant (Keq) for the reaction is so large, the reverse reaction does not prohibit producing high molecular weight polymer[86]. If this were the only side reaction present, the number-average degree of polymerization (X_n) calculated for most poly(amic-acids) would be greater than 300, as ($X_n \approx Keq^{1/2}$). Practically, poly(amic-acid)s typically have X_n values between 25 and 275, or a number-average molecular weight (M_n) of 10,000 to 100,000[86].

Dianhydride hydrolysis by traces of water remaining in the polar aprotic solvent (DMAc, NMP, etc.) or introduced with the monomers is the most significant side reaction in the polymerization and will prohibit high molecular weight by offsetting

stoichiometry due to hydrolysis of the dianhydride or amide linkage. Hydrolysis of the dianhydride with water results in a di-acid functionality[87-88], as shown in Figure 1.15. Water introduced from improperly dried solvent or monomer is not the only source of water in the reaction. Upon imide ring closure, water is produced and can effect hydrolysis reactions on other chains or react with nearby amide groups. It has been shown that the choice of dehydrating agent can play a role in forming an imide or imine structure in studies comparing the effect of tertiary amines in selecting for one structure or the other[89].

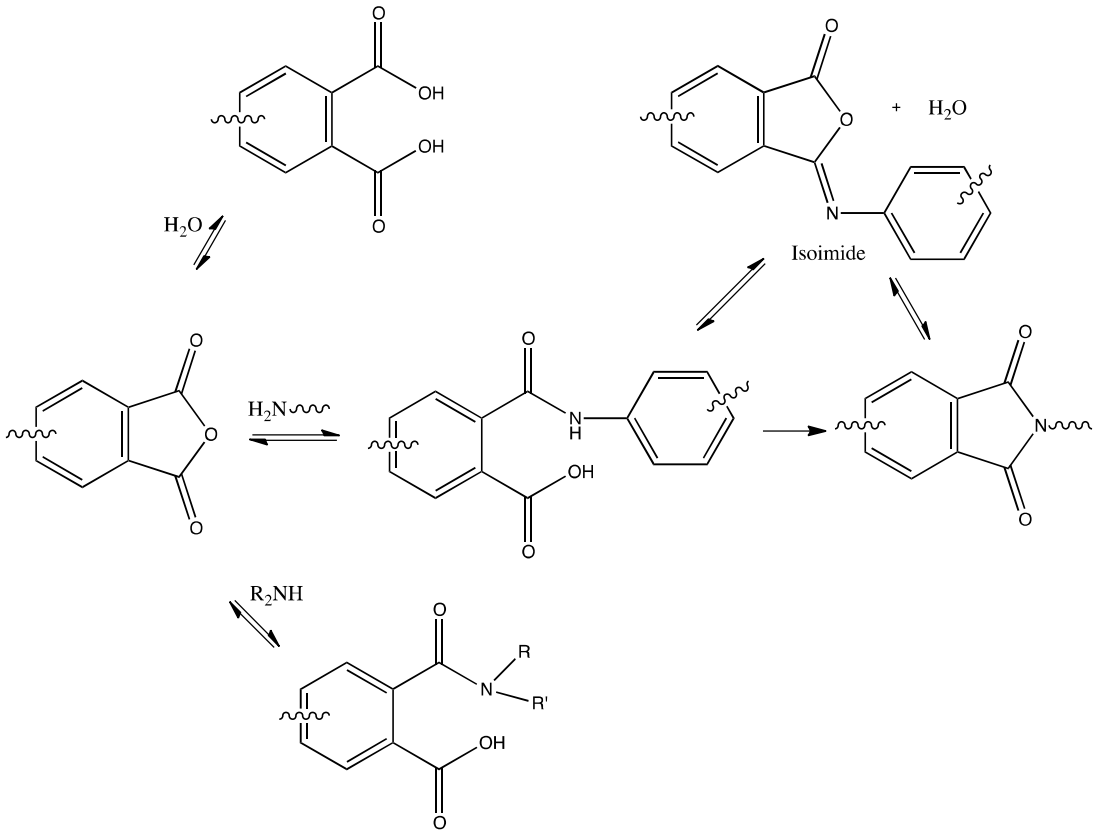

Figure 1.15 Possible reactions of the dianhydride route to imide formation

Solvent degradation to monofunctional amines is a common source of impurity in amide solvents[90]. Monofunctional amines will compete with a diamine in the reaction with a dianhydride, effectively capping one end of the polymer chain, and

upset the reaction stoichiometry.

The second step in the two-step method is conversion of the soluble poly(amic-acid) into the (usually) intractable polyimide. Thermal imidization is commonly used to form polyimides, usually after casting a film. The poly(amic-acid) is taken through a heating cycle, often step-wise, ranging in temperatures from 100-400°C under vacuum or inert atmosphere[80, 84, 91]. One of the most conventional heating cycles maintains a temperature of 100°C for one hour, within one-hour the system is heated to 200°C and maintained one hour, before finally heating to 300°C and holding for an hour. Final imidization temperatures vary due to the numerous molecular structure combinations possible, but the temperature should exceed the glass-transition temperature (T_g) of the polyimide to ensure adequate molecular mobility for the ring formation. As the conversion from poly(amic acid) to polyimide proceeds, the T_g increases and molecular mobility decreases. At a given temperature, the polymer transitions from a flexible rubber into a rigid glass. Although the exact mechanism is still not clear, it is proposed to go through a nucleophilic substitution type mechanism involving the amide nitrogen and the *ortho*-carboxylic acid. Two acceptable mechanisms proposed by Harris[90] are shown in Figure 1.16.

Mechanism 1

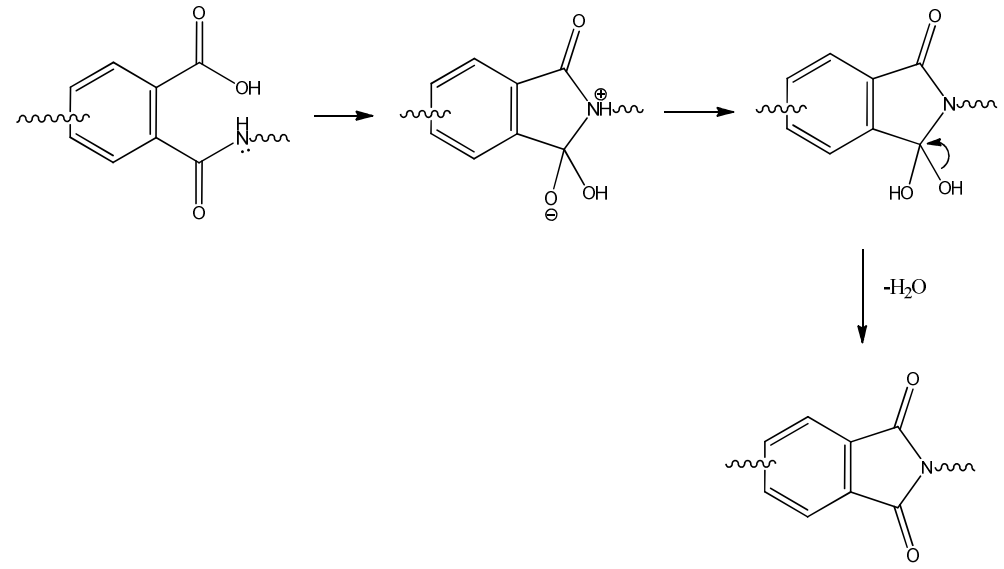

Mechanism 2

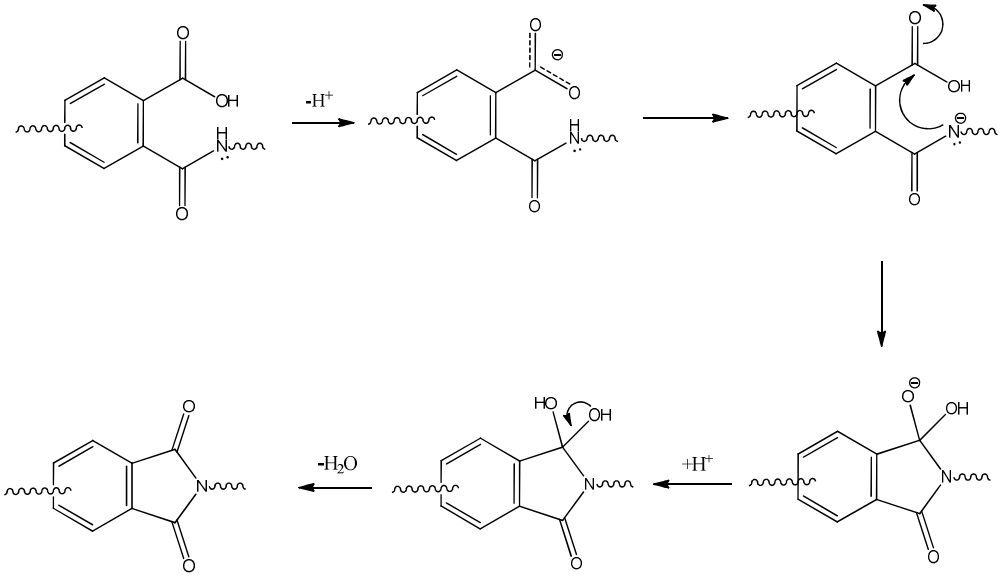

Figure 1.16 Two possible mechanisms of thermal imidization

The degree of imidization that ultimately occurs under thermal conditions is in itself variable and concerns over the completeness of reaction have been expressed[80, 92]. The extent of imidization is most notably a function of the heating cycle. Fourier-transform infrared spectroscopy (FTIR) is the primary method used to quantify the degree of imidization. Three characteristic absorption bands are primarily

used: 1780 cm^{-1} (C=O asymmetric stretch), 1380 cm^{-1}(C-N stretch), and 720 cm^{-1}(C=O symmetrical bending stretch)[91]. It has been postulated that films are the easiest to imidize, fibers are the hardest, and powders are intermediate. The degree of imidization in films ranges from 92-100%. However, for fibers, the degree of imidization is sometimes below 90%[90].

The chemical imidization of a poly(amic-acid) utilizes catalysts and chemical reagents to dehydrate the poly(amicacid) at ambient temperatures[81, 93-94]. While there is an economical benefit in reducing the amount of energy required to cyclodehydrate, the thermal route is often preferred industrially[90]. A benefit of chemical imidization is that the polymer is not exposed to harsh thermal conditions which could degrade the mechanical integrity and molecular weight of the polymer[95]. According to the patent literature[81, 93], the poly(amic-acid) is dehydrated by treatment with a lower molecular weight fatty "monobasic" acid anhydride, i.e. acetic anhydride. Endrey states that although cyclodehydration can occur solely in the presence of the carboxylic acid anhydride, it is beneficial to add a stoichiometric amount of a tertiary amine as a base catalyst to aid the cyclization. The most commonly used dehydrating reagents are equimolar mixtures of pyridine/acetic anhydride or acetic anhydride/triethylamine[80]. In the chemical imidization method, the polyimide may precipitate from the mixture depending on its solubility. Premature precipitation may indicate low molecular weight as polymerization will cease upon precipitation due to the heterogeneous conditions in the reaction.

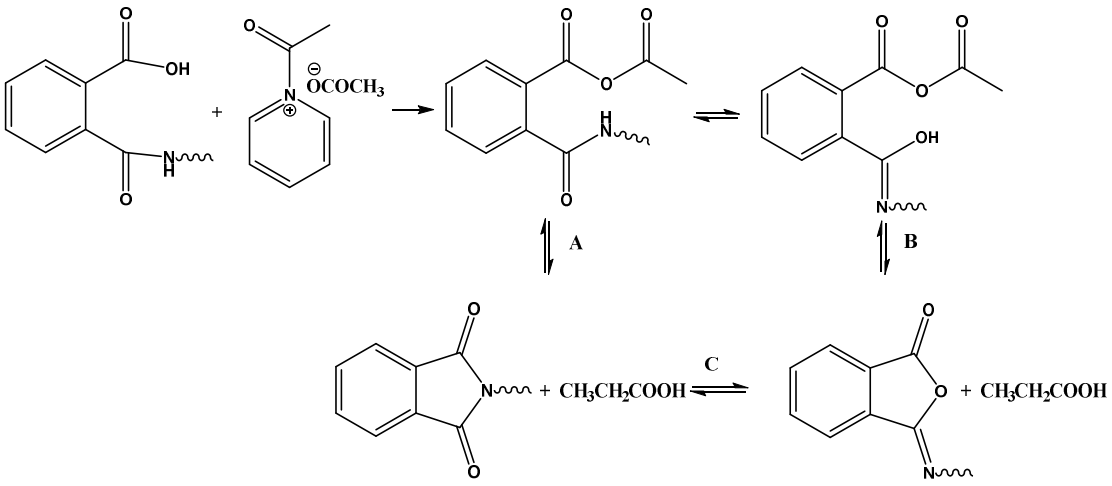

Figure 1.17 Mechanism of chemical imidization

Chemical imidization begins through formation of a complex between the pyridine and acetic anhydride, as seen in Figure 1.17, which leads to formation of two mixed anhydride structures through a nucleophilic substitution reaction. The tertiary amine (pyridine in this case) serves two important roles. First, it converts the anhydride into its ionic form, promoting its nucleophilicity. It also serves as the counter-ion in the salt that forms when the acetate deprotonates the carboxylic acid. The carboxylate is more nucleophilic than the acid and is thus more prone to nucleophilic attack to form the mixed anhydride. Note that the mixed anhydride formation in the first step eliminates the carboxylic acid proton and eliminates the reverse reaction. Reaction pathway A produces the imide from cyclization of the mixed anhydride and is thermodynamically favored.

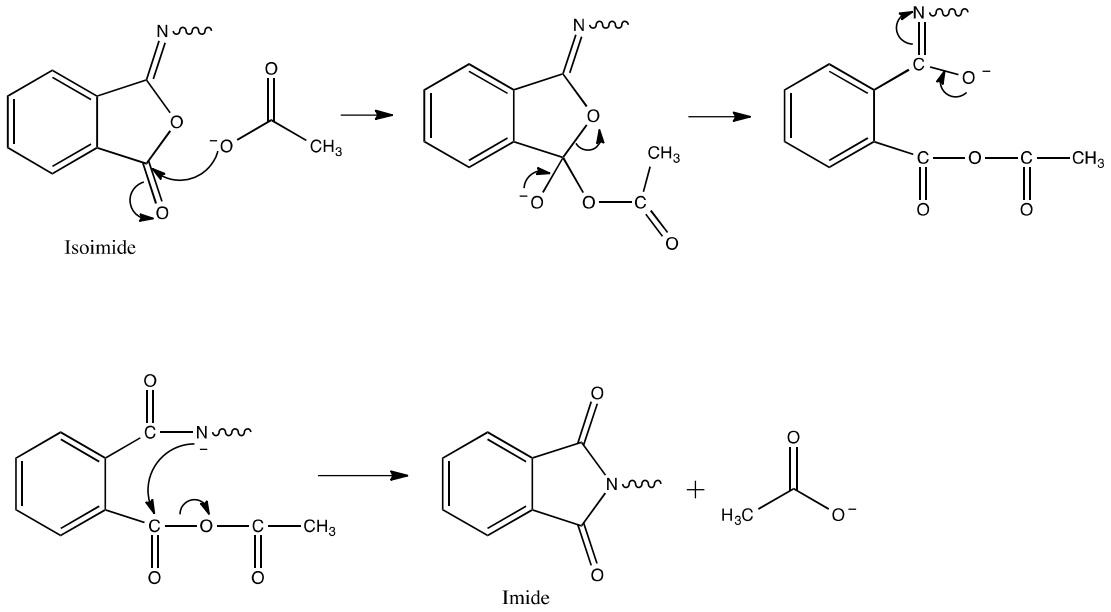

Figure 1.18 Mechanism of the rearrangement from isoimide to imide

The other possible mixed anhydride, the precursor to pathway B, can follow pathway B to form the isoimide structure, which under certain conditions can isomerize to form the desired imide product. A detailed mechanism[95] for isoimide to imide isomerization is shown in Figure 1.18.

Developments in the synthesis of polyimides improved the solubility of new wholly aromatic polyimides, driving investigations of a single-step solution imidization route. This method reacts an aromatic diamine and dianhydride in a stirred, high-boiling solvent at temperatures usually between 180-220°C and requires solubility of the final polyimide[96-97]. Unlike the two-step method, where the poly(amic-acid) is formed as a prepolymer and processed before a final imidization step, solution imidization reaction conditions cause chain extension and imidization to occur simultaneously. Commonly, solution imidization is performed using solvents in conjunction with a tertiary amine catalyst. The most commonly used solvents are nitrobenzene, α-chloronaphthalene, o-chlorophenol, m-methoxyphenol, and m-cresol

with an isoquinoline catalyst[98]. Occasionally, the polyimide will precipitate from the reaction due to crystallization. Harris et al. reasoned that higher temperatures allow excellent solvation of the polyimide and can be used to achieve conformations amenable to higher degrees of chain packing, which leads to crystallization and precipitation.

An important feature aside from polymer solubility in the solution imidization method is the use of an azeotropic distillation to remove the water produced upon cyclodehydration to the imide[99]. This is achieved by addition of a Dean-Stark condenser to the reaction vessel and performing the reaction at elevated temperatures (150-180°C). The azeotropic solvent is refluxed throughout the course of reaction to remove any traces of water during the polymerization. In such a system, traces of water produced upon imide ring closure will be less likely to disrupt the stoichiometry of the reaction due to the azeotropic distillation. Common azeotropic solvents utilized are *o*-dichlorobenzene (*o*-DCB), xylene, toluene or cyclohexylpyrrolidone.

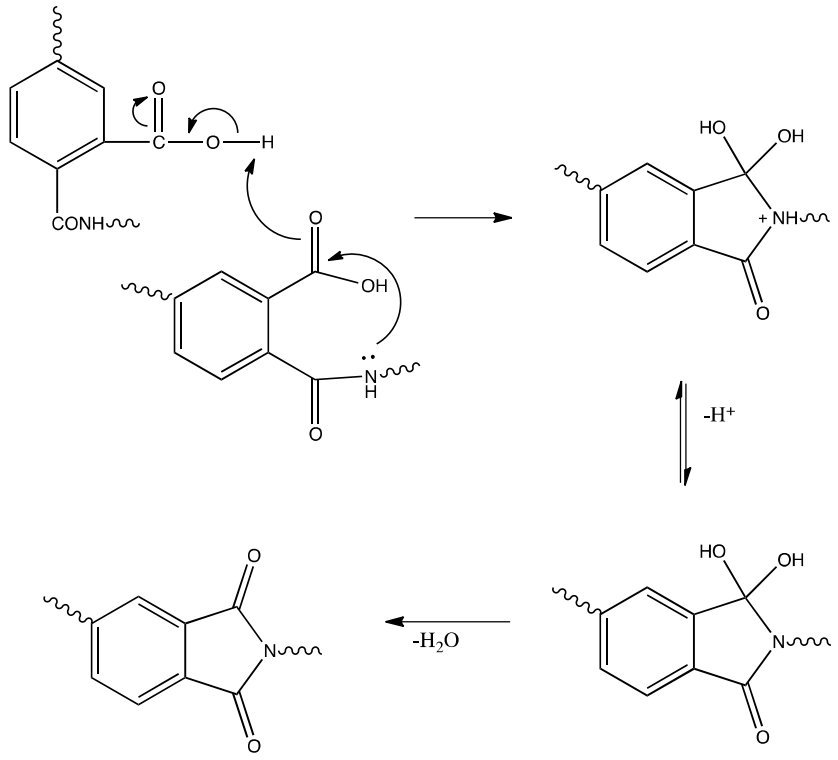

Figure 1.19 Possible imidization mechanism of the one-step, or solution imidization route

Kim et al. proposed a cyclization mechanism for one-step solution imidization[100], provided in Figure 1.19. It was shown that solution imidization occurs under unusual kinetics and followed an acid-catalyzed second order reaction, which could allow milder reaction conditions with lower temperatures and shorter times. Furthermore, the solution imidization process is not hindered by the increase in glass transition temperature that is observed in solvent cast film imidization.

1.3.2.2 Ester-Acid Method

In the 1970s, NASA termed the reaction PMR for polymerization of monomeric reagents[101]. The PMR method uses soluble, hydrolytically stable monomers that react at temperatures in excess of the polymer T_g to form a polyimide. The PMR-15 polyimide, an important aerospace composite matrix, is synthesized via this route by

combining the dimethyl ester of 3,3',4,4'-Benzophenone-tetracarboxylic dianhydride (BTDA) and 4,4'-Methylenedianiline (MDA). The reaction route to form a crosslinkable PMR resin is shown in Figure 1.20[102]. The polymer is endcapped with the ester-acid of norbornenedicarboxylic anhydride (NA) to allow post-imidization crosslinking.

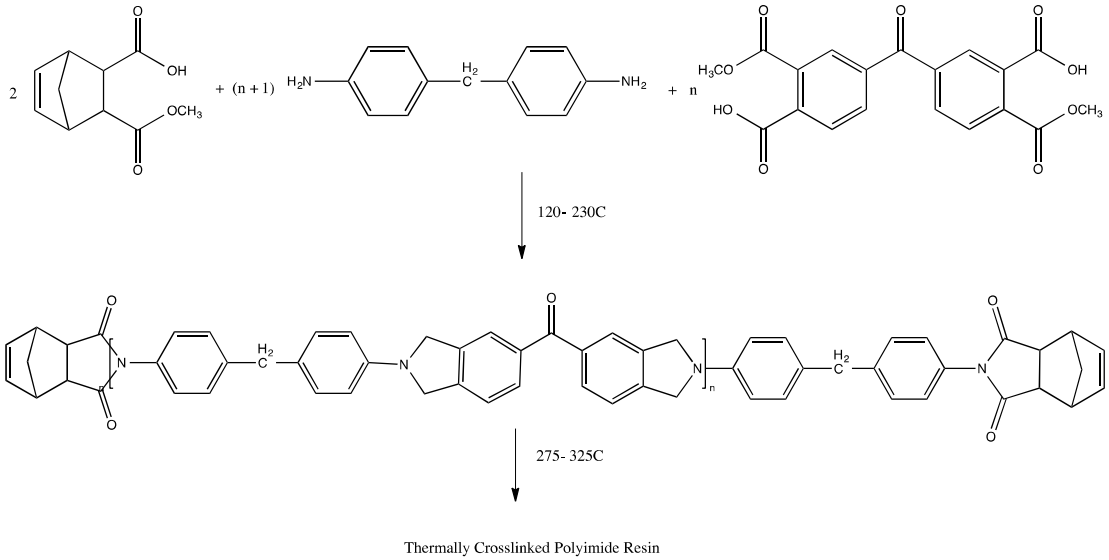

Figure 1.20 Proposed mechanism for polyimide formation via the ester acid route

This ester-acid method provides a few advantages over the two-step route. Any trace water present in the reaction will not hinder the formation of high molecular weight polyimide because the diester-acid, not the anhydride, is the monomeric reagent. In addition, the ester-acid is generally more soluble in polymerization solvents than the respective dianhydride or tetra-acid. Moy et al. proposed an anhydride formation mechanism for polyimide formation via the ester acid route[103] shown in Figure 1.21.

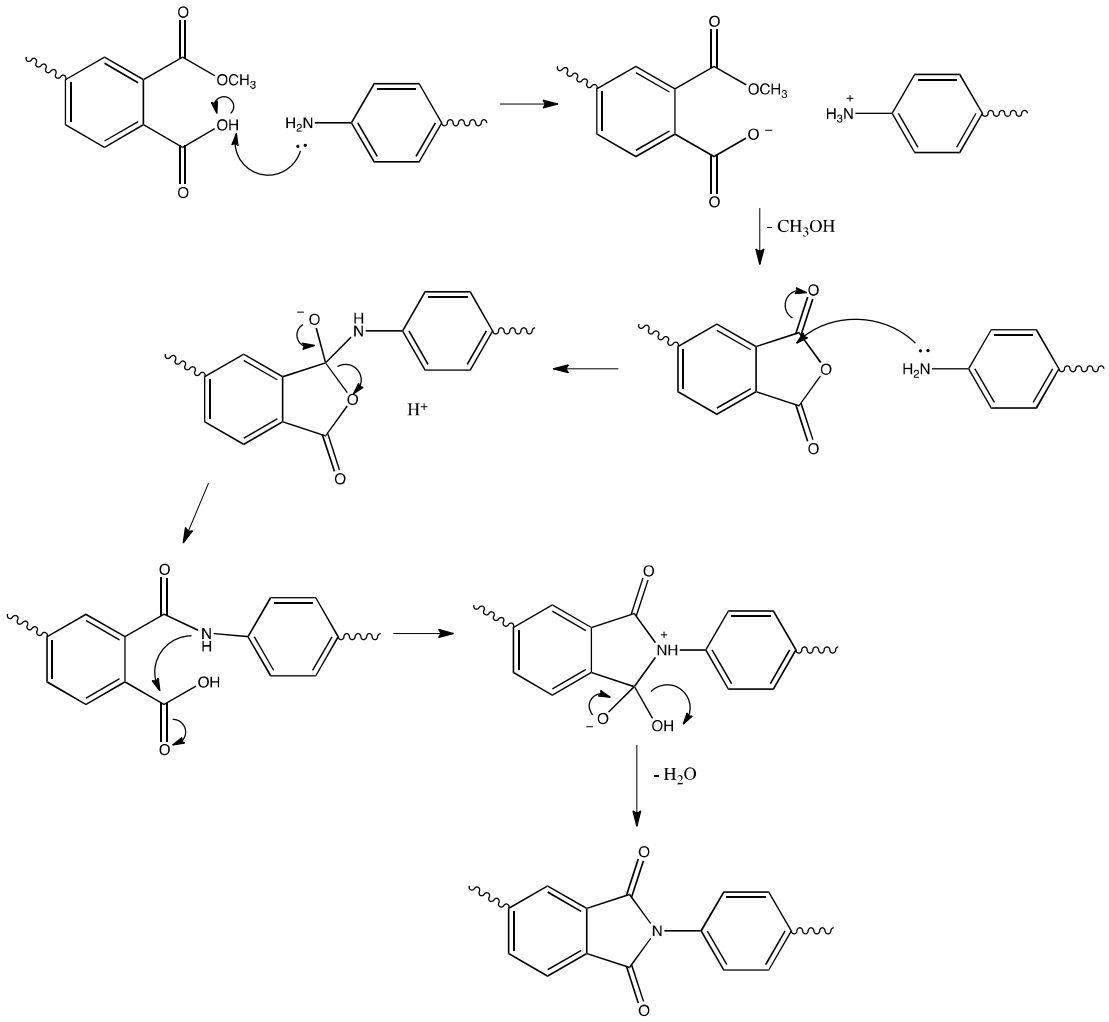

Figure 1.21 Proposed mechanism for polyimide formation via the ester acid route

1.3.2.3 Other Polyimide Synthetic Strategies

Springer et al. first reported the trans-imidization reaction where phthalimide was treated with methylamine at room temperature to yield *N*-methylphthalimide by stirring the intermediate in water[104]. The trans-imidization method is also known as the amine-imide exchange reaction. Using a system of difunctional monomers with increased reactivity, Imai et al. were able to obtain high molecular weight polyimides via trans-imidization[105]. The reaction is shown in Figure 1.22. The reaction is slow but formed high molecular weight poly(amic amide) in seven days at room temperature.

Heating to 240°C cyclized the poly(amic amide) to the polyimide. The byproduct, ethyl carbamate, was removed under vacuum. The interchange reaction requires that the exchanging diamine be as (or more) basic than the monoamine being displaced.

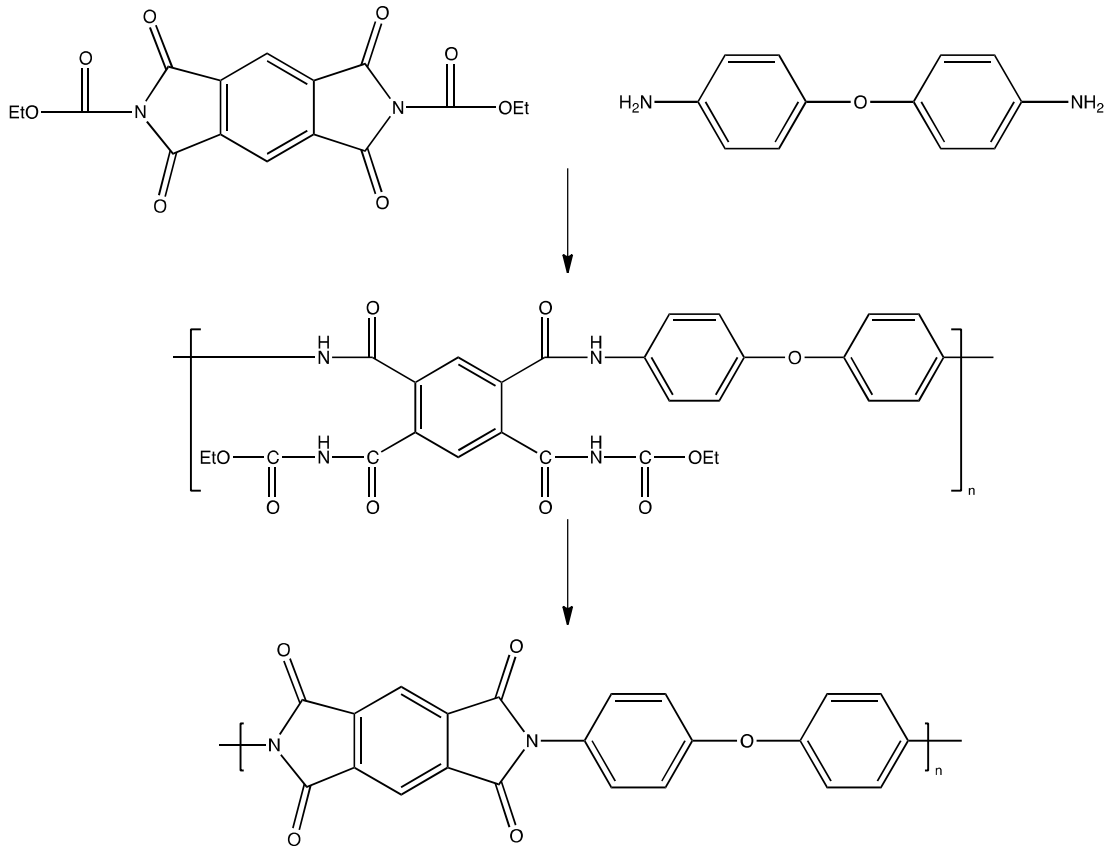

Figure 1.22 Synthesis of a polyimide via trans-imidization

1.3.3 Thermal Rearrangement Process

Figure 1.23 shows the TR conversion from a 6FAP-6FDA-EA TR precursor to a 6FAP-6FDA-EA TR polymer (EA stands for the synthetic route of the precursor polyimide as the Ester-Acid route). Generally, the thermal rearrangement process occurs as the temperature reaches the glass transition temperature of the precursor polyimides. Ideally, the potential range of the thermal rearrangement reaction is from near the glass transition temperature to the temperature where degradation begins to

occur on the polymer membrane. A TGA curve shown in Figure 1.24 of a 6FAP-6FDA-EA TR precursor shows the thermal rearrangement range highlighted[106]. The TR conversion of the membrane is controlled by the heat treatment time and the temperature. For example, low-conversion samples were held at 350°C for 60 minutes, and high-conversion samples were held at 450°C for 30 minutes.

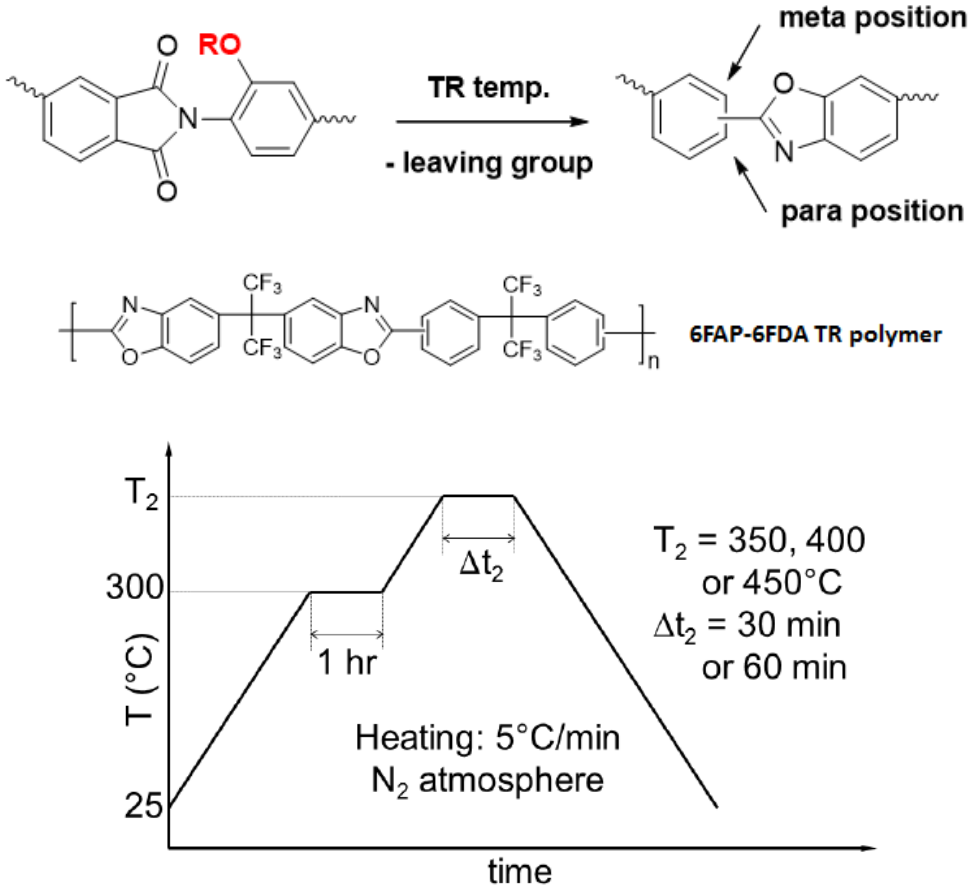

Figure 1.23 Thermal Rearrangement of 6FAP-6FDA-EA TR polymer and its protocol

The degree of thermal rearrangement conversion of the membranes was calculated by the weight difference between the precursors and the final TR polymer, since a significant weight loss occurs during the thermal treatment process. Therefore, the degree of conversion towards the final thermally rearranged product is usually defined as:

$$\%Conversion = \frac{Actual\ Mass\ Loss}{Theoretical\ Mass\ Loss} \times 100\% \qquad (1\text{-}18)$$

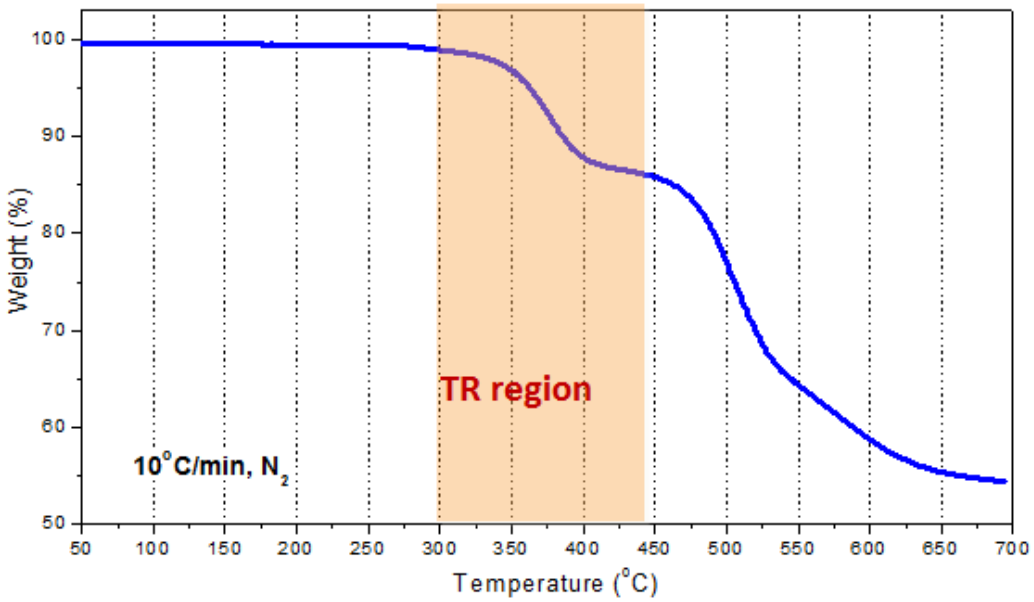

Figure 1.24 Thermal gravimetric analysis of TR precursor polyimides

The experimental mass loss is the weight loss measured after the thermal treatment and the theoretical mass loss is the expected weight loss assuming that the imide-to-benzoxazole conversion is fully achieved (release of two CO_2 per repeat unit when the *ortho* substituent is OH).

The assessment of conversion from Equation 1-18 assumes that the actual mass loss is exclusively due to the imide-to-benzoxazole rearrangement conversion. However, thermal degradation, particularly at high temperatures, may also contribute to weight loss simultaneously with the imide-to-benzoxazole rearrangement process [32]. Additionally, conversion of the polyimide to the TR polymer could proceed via an intermolecular reaction as well as through intramolecular conversion. Furthermore, during the thermal conversion, loss of pendant *ortho* substituents such as acetate groups, leaving a hydroxyl group in their place, would then undergo the thermal rearrangement to form the benzoxazole moieties. Thus, in those cases, the acetate

groups must also be accounted for in the weight loss[106-107].

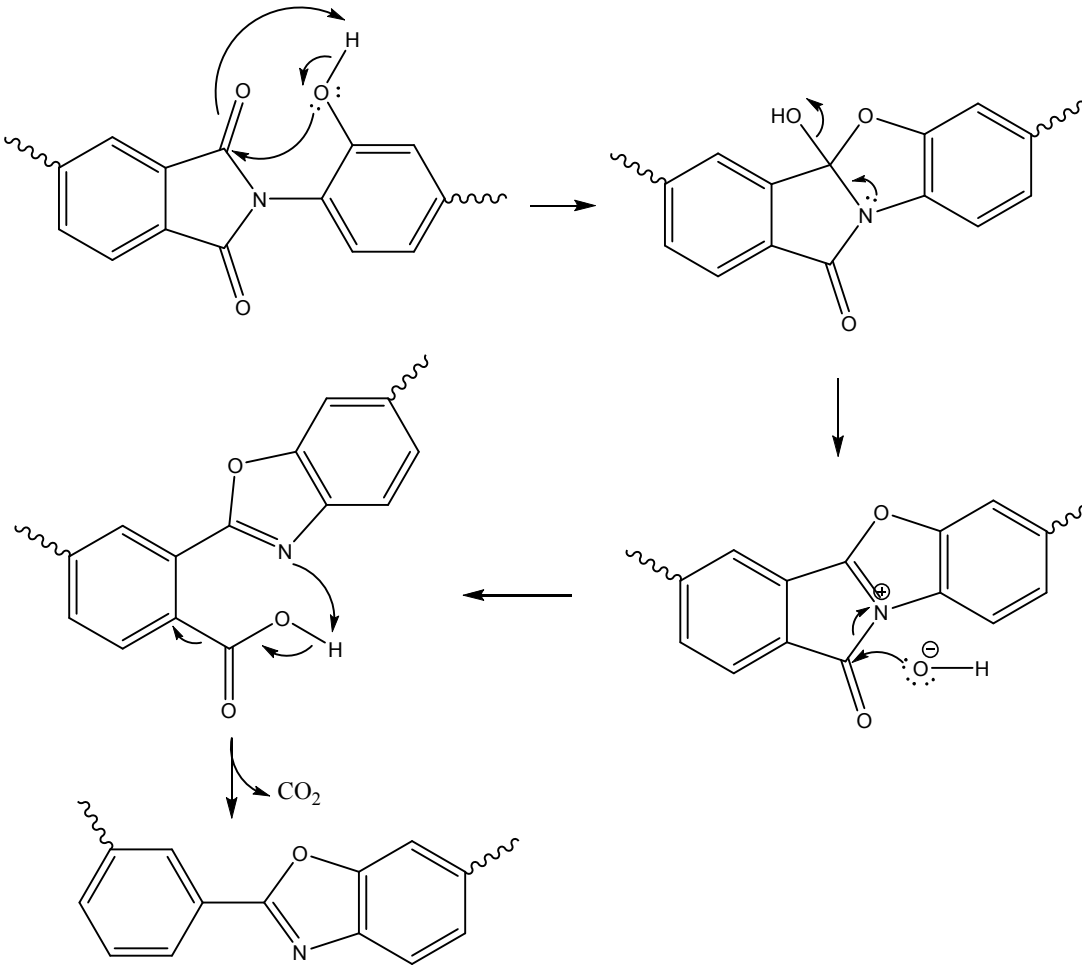

Figure 1.25 Proposed mechanism for imide to benzoxazole rearrangement

As a result of limited characterization methods, the mechanism of the thermal rearrangement process of *ortho*-functionalized polyimides is still under investigation. However, it is widely accepted that the TR process partially undergoes intermolecular as well as intramolecular rearrangement during the thermal treatment[108-109]. The resultant polybenzoxazoles are insoluble due to this crosslinking and they have enhanced CO_2 résistance against plasticization after the heat treatment. There is a commonly satisfied hypothesis that the mechanism involves intra- and inter-molecular cyclization, forming a benzoxazole structure from imide structures shown in Figure 1.25[110-111]. In this proposed mechanism, the starting material

ortho-hydroxyimide rearranges to a carboxyl-benzoxazole followed by decarboxylation in the range of 300–450 °C, and ends up with a fully aromatic benzoxazole repeat unit structure in the polymer backbone. After thermal rearrangement, the newly formed, crosslinked polybenzoxazole chains are much more rigid than the precursor chains, so that any physical changes such as relaxation after the TR conversion becomes less likely[108].

1.4 UV-Crosslinked Polymers

High permeability and high selectivity are two fundamental characteristics required of polymeric membranes to improve gas separation processes. The other key factor is maintaining this performance over the life of the membrane. A major issue is that of so-called physical aging, which is the densification of a glassy membrane over time. This is accelerated in these very thin membranes due the large amount of surface area. Membrane performance can be improved by the synthesis of new polymers, by modification of existing polymers, or by a combination of the two. There are some indications from the literature that crosslinking of polymeric membranes with high performance gas separation properties may be a useful way to change the balance between intrinsic permeability and selectivity in a beneficial manner[112-116]. Crosslinked polymer films offer obvious advantages as membranes, particularly in terms of stability. Without crosslinking the material will tend to swell when exposed to certain gas mixtures, and hence separation properties are affected[117-120].

The first reported UV-crosslinked polymer with improved gas separation performance was found in the patent literature[121]. Since then, many studies have been focused on the effect of UV crosslinking on the gas permeation properties of polymer films[122]. Kita and co-workers expressed that UV crosslinking can cause increasing of selectivity of thick polyimide films, but it was difficult to compare these data with the intrinsic properties of homogeneous polymers with curing because the degree of crosslinking in the film was not uniformly distributed. Wright et al. applied a UV crosslinking strategy to polyarylate films to improve their selectivity[123].

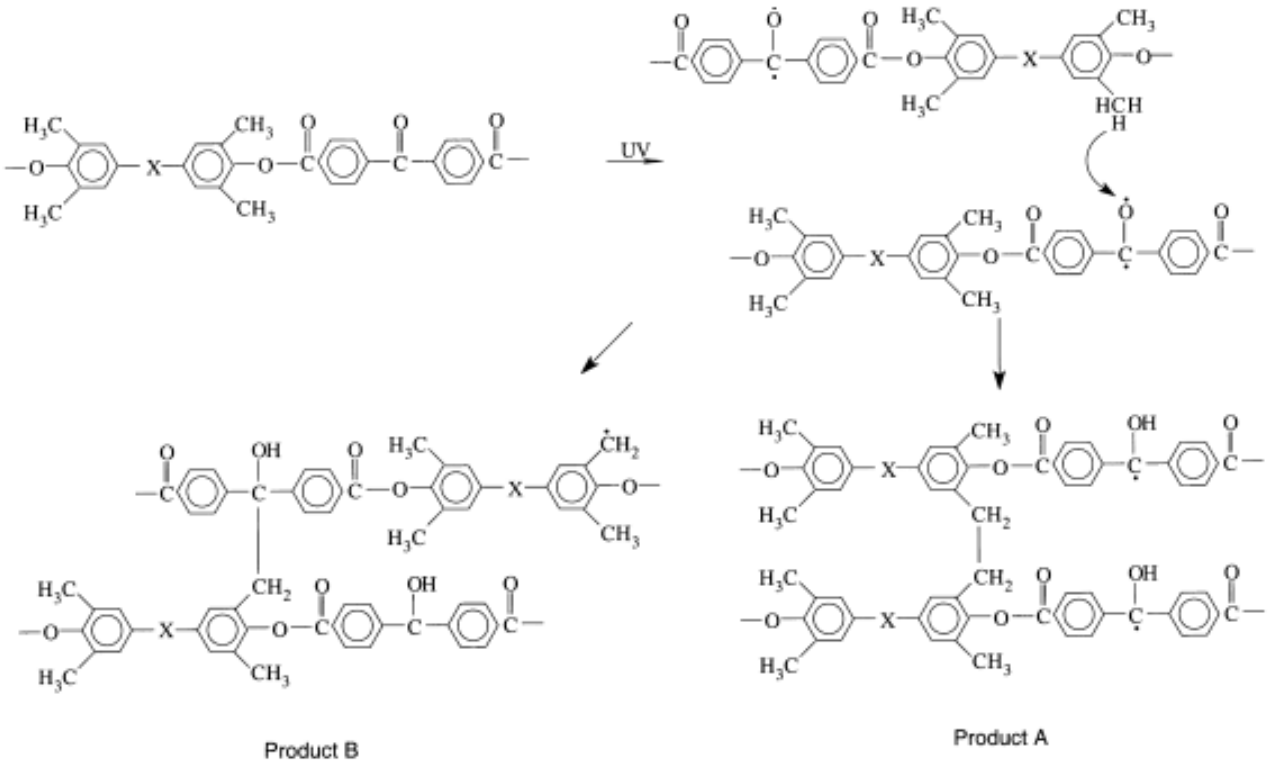

Figure 1.26 The proposed UV crosslinking mechanism for a benzophenone-based polyarylate where X is the connector group: $C(CH_3)_2$, $C(CF_3)_2$ or fluorene.

A mechanism for UV crosslinking of polymers with a benzophenone unit and a benzylic hydrogen donor group have been extensively studied. The widely accepted mechanism[112, 124-125] is shown in Figure 1.26. Under UV exposure, the benzophenone

carbonyl pi bond will be cleaved to provide a carbon radical and an oxygen radical. The oxygen radical trends to abstract a relatively labile benzylic hydrogen from a nearby source to form another carbon radical. At least two types of crosslinked products can form. The progress of this crosslinking reaction can be tracked by FTIR spectroscopy with the decay of the benzophenone carbonyl peak (1678 cm^{-1}).

CHAPTER 2: MONOMER PURIFICATION AND SYNTHESIS

2.1 Introduction

Step-growth polymerizations involve the stepwise, sequential condensation of difunctional monomers. To produce high molecular weight, linear polymers, several general criteria need to be met. These critical requirements include that (1) the monomers must have perfect difunctionality; (2) high monomer and reagent purity must be achieved to ensure one-to-one molar stoichiometry of monomers; (3) monomers need to have high reactivity towards one another, and not participate in any side reactions; and (4) very high (> 99%) conversion is also required. The following sections describe the careful purification and preparation of solvents and monomers required for these polymerizations.

2.2 Purification of Solvents and Reagents

Methanol

Chemical Structure: CH_3OH

Source: Spectrum Chemicals

Molecular Weight: 32.04 g/mole

Boiling Point: 64.7°C

Purification: Used as received for polymer precipitations.

Ethanol

Chemical Structure: CH_3CH_2OH

Source: Spectrum Chemicals

Molecular Weight: 46.07 g/mole

Boiling Point: 78.4°C

Purification: Used as received and as a solvent for recrystallization and the Ester-Acid polymerization reaction.

Isopropanol

Chemical Structure:

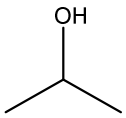

Source: Spectrum Chemicals

Molecular Weight: 60.10 g/mole

Boiling Point: 82.6°C

Purification: Used as received for polymer precipitations and recrystallization.

Chloroform

Chemical Structure: $CHCl_3$

Source: Spectrum Chemicals

Molecular Weight: 119.38 g/mole

Boiling Point: 61.2°C

Purification: It was stored over activated 3Å molecular sieves and used as a solvent for titration and film casting.

Toluene

Chemical Structure:

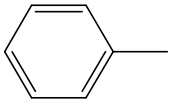

Source: Sigma Aldrich

Molecular Weight: 92.14 g/mole

Boiling Point: 110.6°C

Purification: Used as received and as an azeotropic solvent for polymerization reaction.

Pyridine

Chemical Structure:

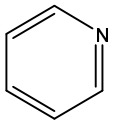

Source: Sigma Aldrich

Molecular Weight: 79.10 g/mole

Boiling Point: 115.6°C

Purification: Used as received and as a solvent for the synthesis of poly(phenylene oxide) oligomers.

Triethylamine (TEA)

Chemical Structure:

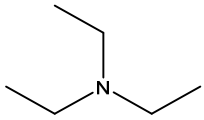

Source: Sigma Aldrich

Molecular Weight: 101.19 g/mole

Boiling Point: 89.5°C

Purification: Used as received and as a base for the Ester-Acid polymerization reaction.

1,2-Dichlorobenzene (o-DCB)

Chemical Structure:

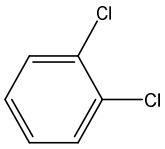

Source: Sigma Aldrich

Molecular Weight: 147.01 g/mole

Boiling Point: 180.5°C

Purification: Used as received and as an azeotropic solvent for Ester-Acid polymerization reaction.

N-Methyl-2-Pyrrolidone (NMP)

Chemical Structure:

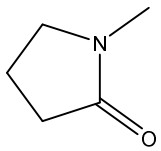

Source: Sigma Aldrich

Molecular Weight: 91.3 g/mole

Boiling Point: 202-204°C

Purification: NMP was vacuum distilled from calcium hydride and stored in a flask with activated 3Å molecular sieves.

N,N-Dimethylacetamide (DMAc)

Chemical Structure:

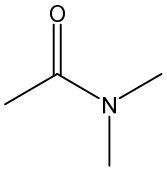

Source: Sigma Aldrich

Molecular Weight: 87.12 g/mole

Boiling Point: 165.1°C

Purification: DMAc was vacuum distilled from calcium hydride and stored in a flask with activated 3Å molecular sieves.

Potassium Carbonate

Chemical Structure:

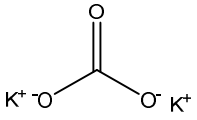

Source: Sigma Aldrich

Molecular Weight: 138.21 g/mole

Purification: Potassium carbonate was received as a white solid and if necessary ground by mortar and pestle. Potassium carbonate was dried under vacuum at 160°C for 12 hours before use as a base in polymerization reactions.

Copper (I) Chloride

Chemical Structure: CuCl

Source: Sigma Aldrich

Molecular Weight: 99.00 g/mole

Purification: Copper Chloride was reagent grade purity (97+%) and used as received.

Trifluoromethanesulfonic acid (Triflic Acid)

Chemical Structure:

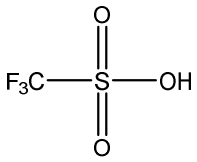

Source: Sigma Aldrich

Molecular Weight: 150.08 g/mole

Boiling Point: 162°C

Purification: Used as received.

Phenol

Chemical Structure:

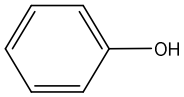

Source: Sigma Aldrich

Molecular Weight: 94.11 g/mole

Melting Point: 40.5 °C

Purification: Used was received.

2,2,2-Trifluoroacetophenone

Chemical Structure:

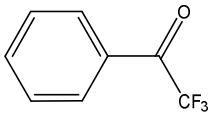

Source: Sigma Aldrich

Molecular Weight: 174.12 g/mole

Boiling Point: 165-166 °C

Purification: Used was received.

3-Aminophenol (m-AP)

Chemical Structure:

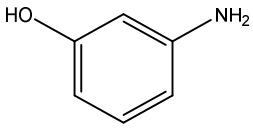

Source: Acros Organics

Molecular Weight: 109.13 g/mole

Melting Point: 120-124°C

Purification: m-AP was received as a light yellow solid and used as an end-capping reagent for oligomerizations.

2.3 Purification of Monomers

4,4'-Dichlorodiphenyl sulfone (DCDPS)

Chemical Structure:

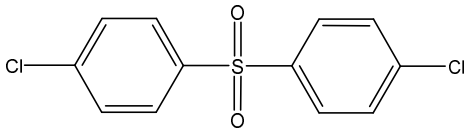

Source: Solvay

Molecular Weight: 287.15 g/mole

Melting Point: 145-147°C

Purification: DCDPS was recrystallized from toluene and produced large white crystals that were pulverized prior to drying. DCDPS was dried under vacuum at 100°C for 12 hours before use in polymerization reactions.

4,4'-Biphenol (BP)

Chemical Structure:

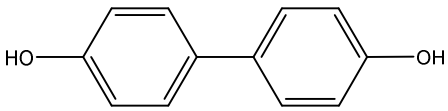

Source: Eastman Chemical

Molecular Weight: 186.21 g/mole

Melting Point: 282-284°C

Purification: BP was received as a sample in monomer grade purity and dried under vacuum at 100°C overnight before use in polymerization reactions.

2,2'-Bis-(3,4-dicarboxyphenyl)hexafluoropropane dianhydride (6FDA)

Chemical Structure:

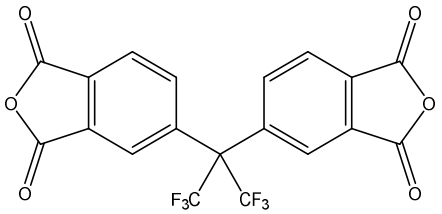

Source: Air Products & Chemicals

Molecular Weight: 444.24 g/mole

Melting Point: 244-247 °C

Purification: 6FDA was received as a white solid and dried under vacuum at 160°C for 24 hours before use in polymerization reactions.

3,3'-Dihydroxybenzidine (p-HAB)

Chemical Structure:

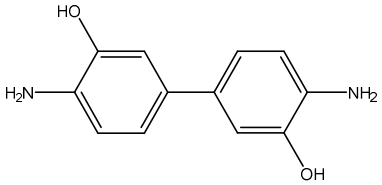

Source: TCI Chemicals

Molecular Weight: 216.24 g/mole

Melting Point: 292 °C

Purification: *p*-HAB was recrystallized from a mixture of DMAc and methanol, and

dried under vacuum at 80°C for 12 hours before use in polymerization reactions.

2, 6-Xylenol

Chemical Structure:

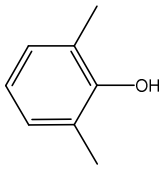

Source: Sigma Aldrich

Molecular Weight: 122.16 g/mole

Melting Point: 43-45°C

Purification: 2,6-Xylenol was received as a yellow solid with purity 99+%. It was heated at 80°C for 0.5 h to melt it before use in polymerization reactions.

4,4'-Difluorobenzophenone (DFB)

Chemical Structure:

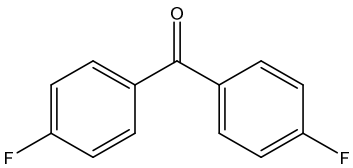

Source: TCI Chemicals

Molecular Weight: 218.20 g/mole

Melting Point: 102-105°C

Purification: DFB was received as a sample in monomer grade purity and dried under vacuum at 60°C for 12 h before use in polymerization reactions.

1,3-Bis(4-fluorobenzoyl)benzene

Chemical Structure:

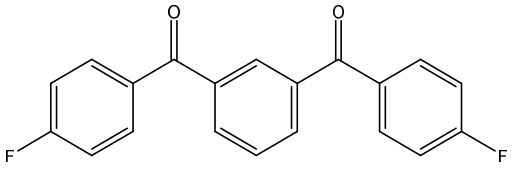

Source: Sigma Aldrich

Molecular Weight: 322.31 g/mole

Melting Point: 181-183°C

Purification: 1,3-Bis(4-fluorobenzoyl)benzene was received as a white solid with purity 98+%. It was dried under vacuum at 100°C for 12 h before use in polymerization reactions.

2.4 Synthesis of Monomers

1,1-bis(4-hydroxyphenyl)-1-phenyl-2,2,2-trifluoroethane (3F-Bisphenol)

3F-Bisphenol was used as a monomer to produce fluorinated poly(arylene ether ketone)s for high temperature dielectrics. This work was published[126] in 2016.

Chemical Structure:

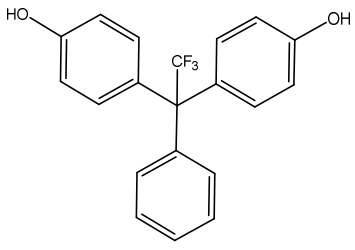

Molecular Weight: 344.33 g/mole

Procedure: To a 250 mL, three neck round bottom flask equipped with a magnetic stir bar, N_2 inlet and an addition funnel fitted with a drying tube, 41.32 g (0.44 mole) of

phenol, 19.32 g (0.11 mole) of 2,2,2-trifluoroacetophenone were added and heated to 45°C. Once a homogeneous solution was achieved, 3.8 mL ($4.2*10^{-2}$ mole) of triflic acid was introduced dropwise while maintaining the temperature at 45°C. After 1 hour, the slurry was treated with 200 mL of hot deionized water and the product was isolated by filtration. The pink solid was stirred in 200 mL of hot deionized water for 30 minutes, vacuum filtered, washed with hot water, methylene chloride and dried at 80°C with full vacuum applied for 24 hours before use in polymerization reactions. Yield is ~90%. The m.p. was 226°C, consistent with literature[127]. The proton NMR spectrum is provided in Figure 2.1.

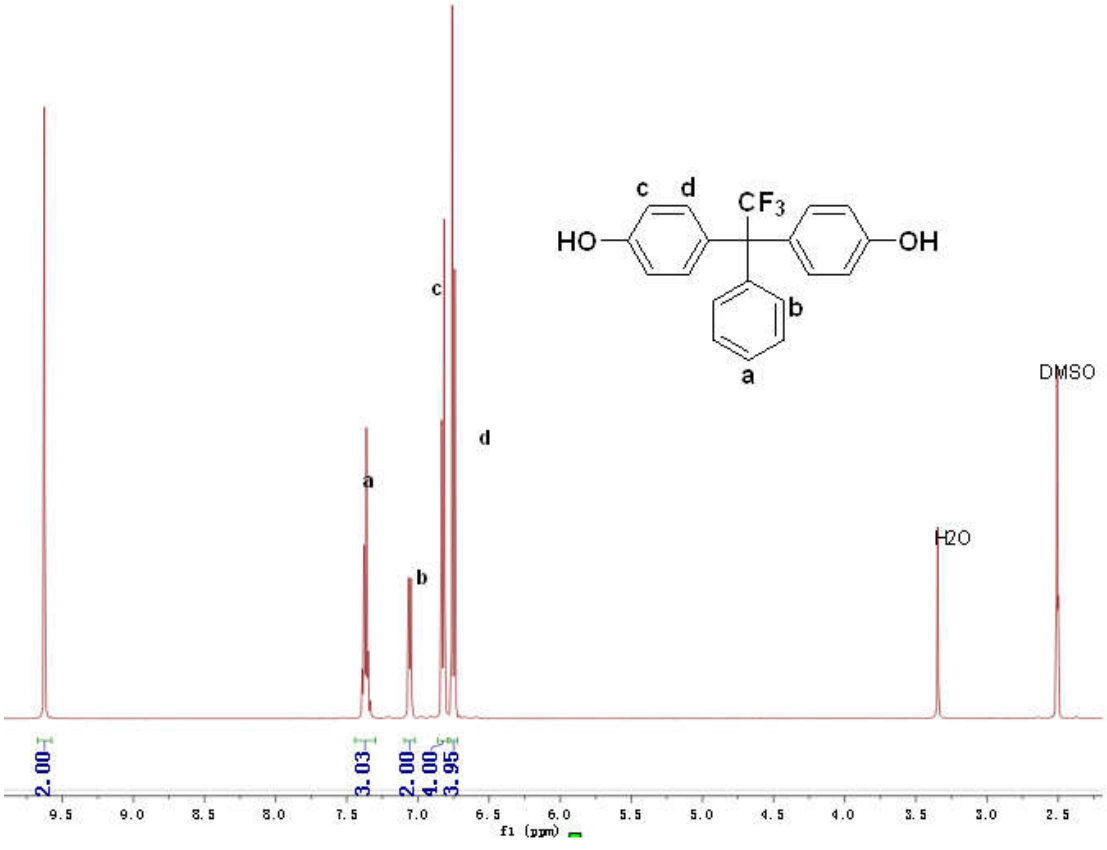

Figure 2.1 ^{1}H-NMR of 3F-bisphenol

1,1-Bis(3-amino-4-hydroxyphenyl)-1-phenyl-2,2,2-trifluoroethane (3FAP)

3FAP was used as a monomer to produce TR precursor polyhydroxyimide polymers with improved mechanical properties by replacing the $-CF_3$ group with the more rigid phenyl group in the monomer structure.

Chemical Structure:

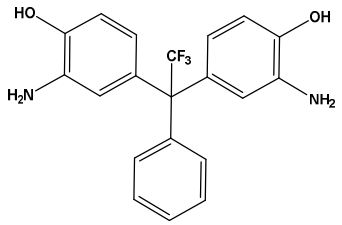

Molecular Weight: 374.36 g/mole

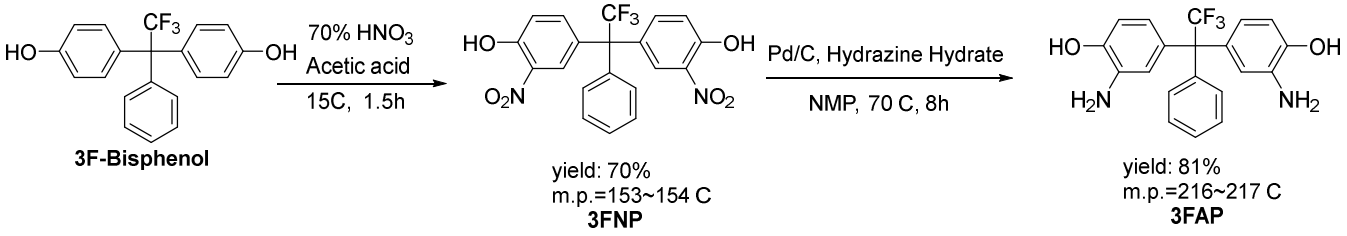

Figure 2.2 Synthesis of 3FAP

Procedure (Figure 2.2): Starting from 3F-bisphenol, it is a two-step reaction to make 3FAP. The first step is nitration of 3F-bisphenol to obtain 1,1-bis(3-nitro-4-hydroxyphenyl)-1-phenyl-2,2,2-trifluoroethane (3FNP). To a 500 mL, three neck round bottom flask equipped with a magnetic stir bar, N_2 inlet and an addition funnel fitted with a drying tube, 25.00 g (0.073 mole) of 3F-bisphenol and 120 mL of acetic acid were added and cooled to 15°C in a cold water bath. To the mixture, 15 g of concentrated nitric acid (70% HNO_3) in 80 mL of acetic acid was added dropwise. After 1.5 hours, the yellow product precipitated. About 500 mL of cold water was added, the product was filtered and washed multiple times with cold

water and dried under vacuum at 80°C for 12 hours. It was recrystallized in ethanol and dried under vacuum at 80°C for 24 hours to obtain a yellow crystal product with a yield of 70%. The proton NMR spectrum for this intermediate is shown in Figure 2.3.

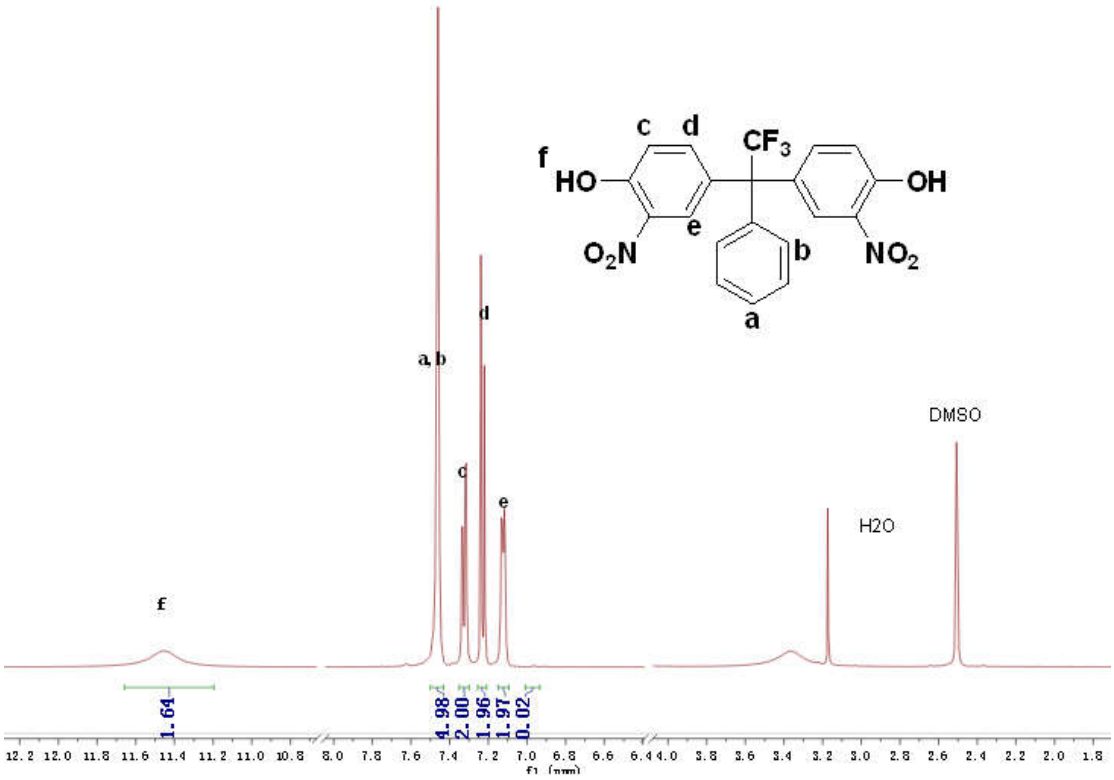

Figure 2.3 ^{1}H-NMR of 3FNP

The second step is to reduce the nitro groups to form amine groups on both sides. To a 250 mL, three neck round bottom flask equipped with a mechanical stirrer, N_2 inlet and an addition funnel fitted with a drying tube, 20.00 g (0.046 mole) of 3FNP, 1.00 g of Pd/C and 150 mL of NMP were added. The reaction mixture was heated in an oil bath at 70°C and stirred. Hydrazine hydrate[128] (15 mL, 0.322 mole) was added dropwise through the addition funnel. After addition, the mixture was stirred for 12 hours at 70°C. The reaction mixture was filtered through Celite and precipitated in 1000 mL of isopropanol. The gray solid was filtered, then dried under vacuum at

80°C for 24 hours. The yield was 81%. The m.p. was 216-217°C, consistent with literature[129]. The proton NMR spectrum is provided in Figure 2.4.

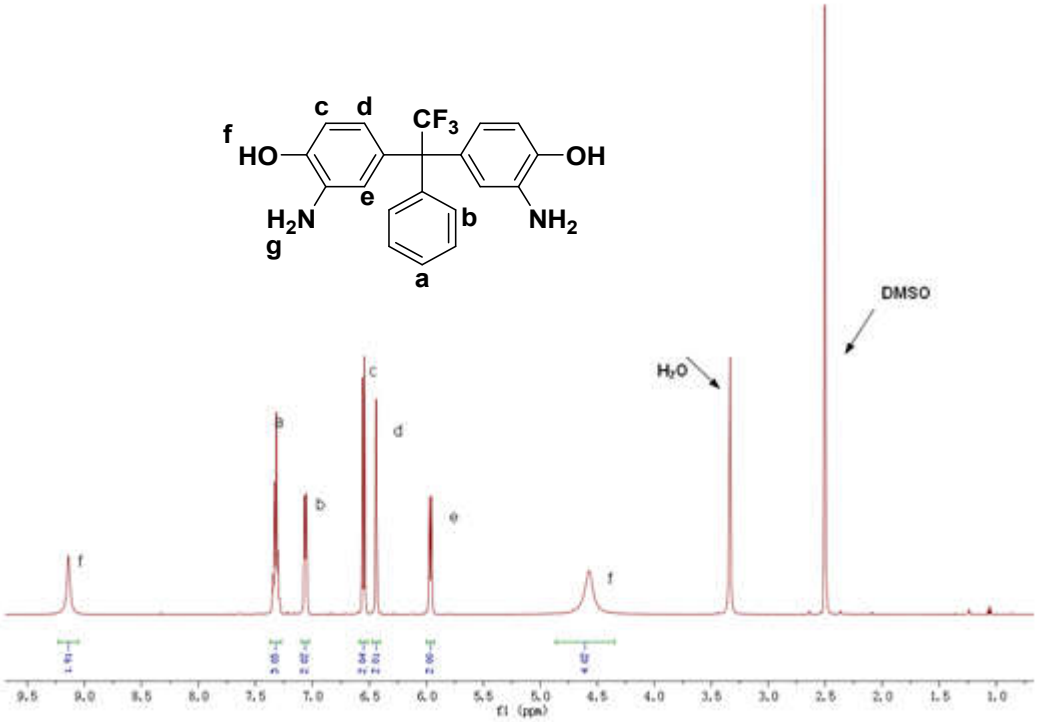

Figure 2.4 ^{1}H-NMR of 3FAP

Poly(Arylene Ether Sulfone) (PAES) Oligomer

PAES oligomers (Figure 2.7) were used as prepolymers to produce thermally rearrangeable polyhydroxyimide block copolymers with improved mechanical properties.

Chemical Structure:

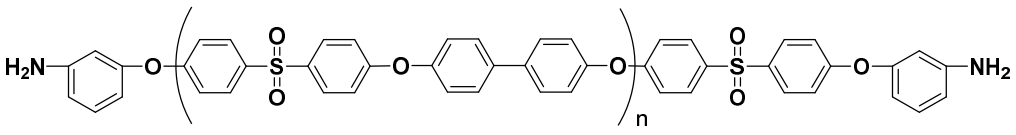

Molecular Weight: ~15,000 g/mole M_n

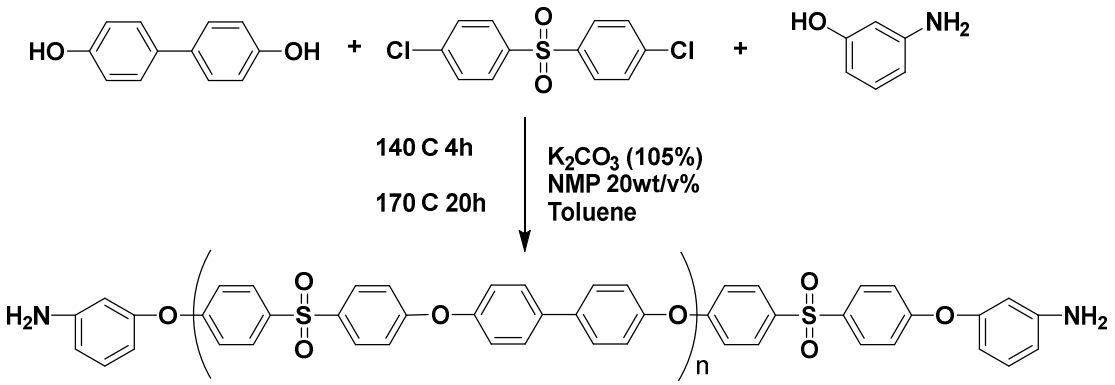

Figure 2.5 Synthesis of an amine terminated PAES oligomer with a targeted M_n of 15000 g/mol

Procedure: A targeted M_n of 15,000 g/mole M_n PAES oligomer was prepared via the synthetic route[130] shown in Figure 2.7. To a 500 mL, three neck round bottom flask equipped with a mechanical stirrer, N_2 inlet and toluene filled Dean Stark trap with condenser, 13.576 g (0.0729 mol) of biphenol, 21.537 g (0.075 mol) of DCDPS, 0.456 g (418 mmol) of *m*-AP, and 10.88 g (0.0788 mol) of K_2CO_3 (about 5% molar excess) were added, then 145 mL of DMAc and 70 mL of toluene were added. The reaction mixture was stirred at 140°C for 4 hours with N_2 passing through the flask. The temperature was then raised to 170°C. After 20 hours, the reaction mixture was removed from the oil bath and filtered to remove salt. The dark solution was then precipitated into isopropanol and stirred overnight. A white fibrous product was obtained after filtration, and it was then placed in an oven under vacuum at 100°C for 24 hours. ^{1}HNMR was used to confirm the structure and calculate the molecular weight. As shown in Figure 2.8, the M_n of the PAES oligomer was about 18,000 g/mole. Potentiometric titration with 0.01 N $HClO_4$ as a titrant was also used to verify the molecular weight, which was 14500 g/mole as a result.

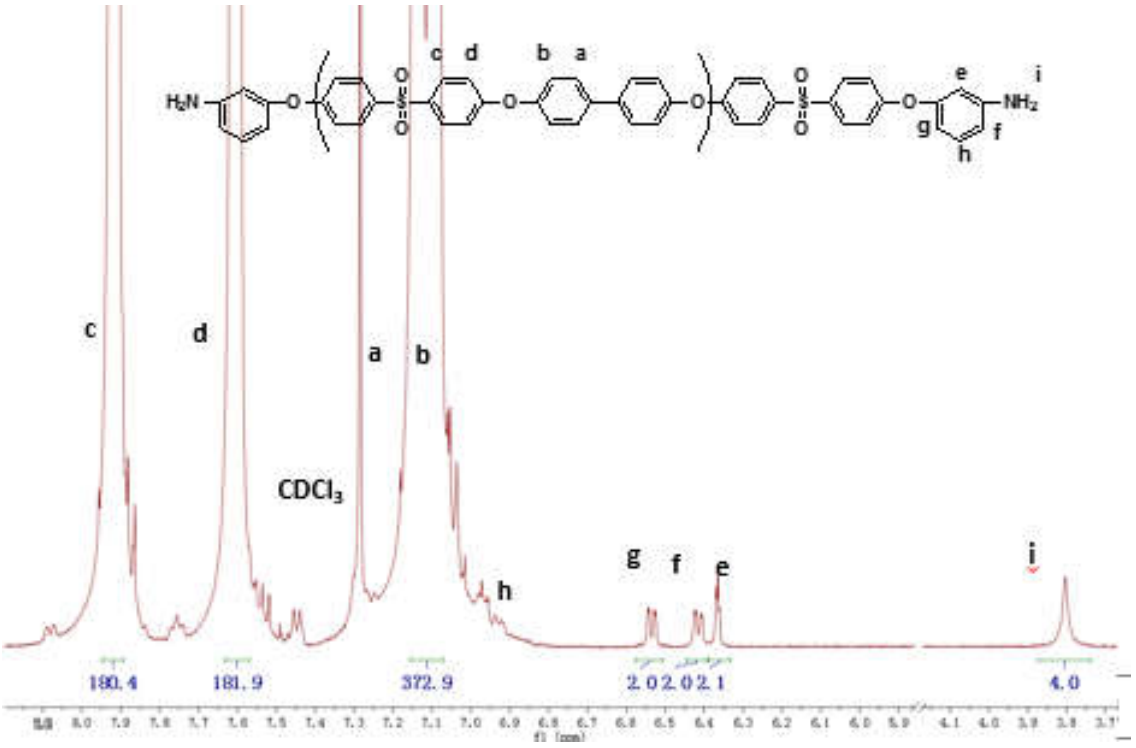

Figure 2.6 ^{1}H-NMR of PAES oligomer with a targeted M_n of 15,000 g/mole

PPO Oligomer

A series of PPO oligomers with systematically varied molecular weights were used to blend with a poly(arylene ether ketone) to produce UV-crosslinkable polymer blends.

Chemical Structure:

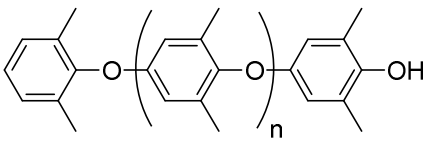

Molecular Weight: ~6000 g/mole M_n

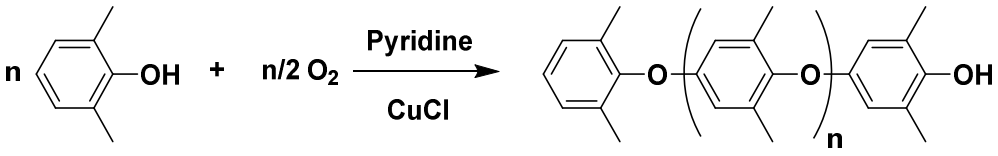

Figure 2.7 Synthesis of PPO oligomer

Procedure: PPO synthesis was adapted from Hay et al.[48-49], and the protocol for synthesizing an ~6,000 M_n oligomer is shown in Figure 2.9. Pyridine (250 mL) and 0.5 g (0.005 mol) of CuCl were charged to a 500-mL, 4-neck, round bottom flask equipped with an overhead stirrer, oxygen inlet tube, and condenser. Oxygen gas (0.1 SCFH) was passed through the stirred solution for 30 min, and the solution became dark green. Then, 10 g (0.082 mole) of 2,6-dimethylphenol was added. The reaction mixture became dark orange and the temperature was increased from 25 to 45 °C. The oxygen flow was terminated after 1 h and the reaction was stirred for 2 h. The solution became viscous and the color of the solution returned to dark green. The reaction mixture was cooled to room temperature and slowly added into 500 mL of methanol to precipitate the polymer, then the polymer was filtered and washed thoroughly with methanol containing a small amount of hydrochloric acid. The product was dissolved in chloroform, filtered and re-precipitated into methanol. After filtration, the faint yellow powder was dried at 110 °C for 24 h under vacuum. Yield was 71%. The structure was confirmed by ^{1}H-NMR. As shown in Figure 2.10, the M_n of the PPO oligomer was about 4100 g/mole. Size Exclusion Chromatography (SEC) was also used to measure molecular weights and distributions of the PPO oligomer. For this PPO oligomer, the M_n was 6000 g/mole with a PDI of 2.0 based on SEC data.

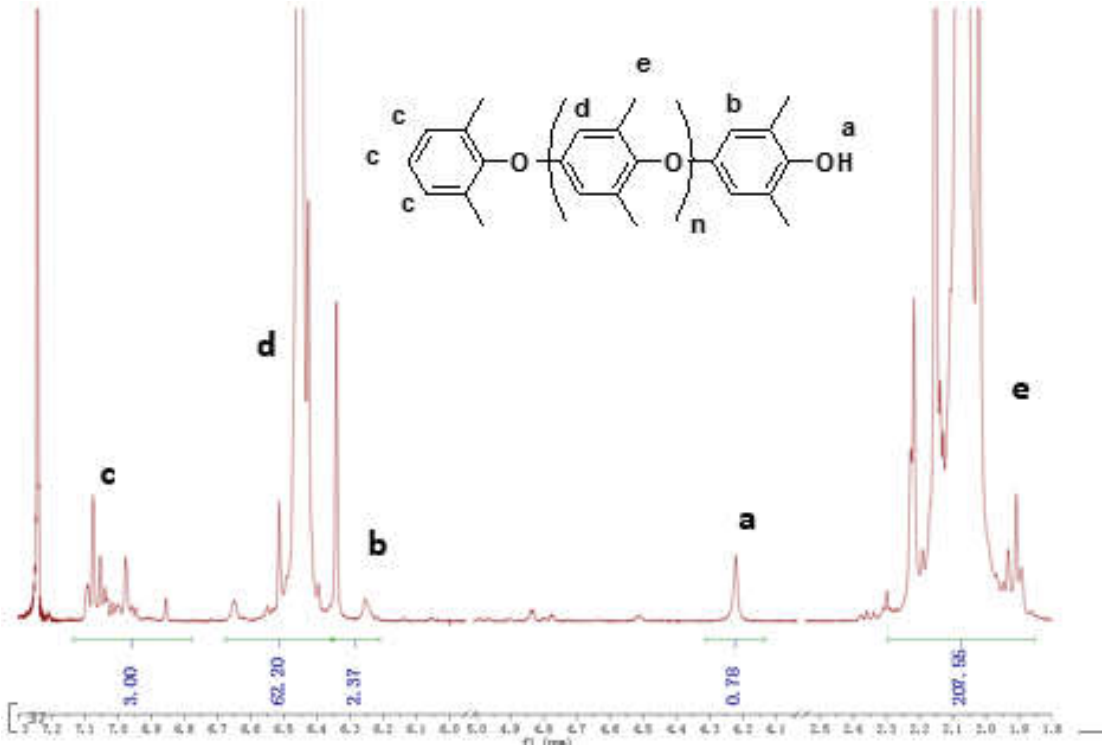

Figure 2.8 ^{1}H-NMR of a PPO oligomer with a targeted M_n of 6000 g/mole

CHAPTER 3: TOUGHENED THERMALLY REARRANGED POLYMERS FOR GAS SEPARATION MEMBRANES

Wenrui Zhang[a], Britannia Vondrasek[a], Gregory C. Miller[a], Shreya Roy Choudhury[a], Ran Liu[a], Sue J. Mecham[b], James E. McGrath[a], J. J. Lesko[1], Benny D. Freeman[c], Judy S. Riffle[c]*

[a]Macromolecules Innovation Institute, Department of Chemistry, Virginia Tech, 325 Stanger Street, 133 Kelly Hall, Blacksburg, VA 24061, USA

[b]Department of Chemistry, Lineberger Comprehensive Cancer Center, Eshelman School of Pharmacy, Carolina Center for Genome Sciences, and Institute for Nanomedicine, University of North Carolina, Chapel Hill, North Carolina 27599, United States

[c]Department of Chemical Engineering, Texas Materials Institute, Center for Energy and Environmental Research, The University of Texas at Austin, 10100 Burnet Road, Bldg. 133, Austin, TX 78758, USA

3.1 Abstract

Linear polyhydroxyimides can be rearranged to form crosslinked polybenzoxazoles upon heat treatment. Such thermally rearranged (TR) polymers have outstanding gas separation properties, but are limited in their industrial application due to their becoming mechanically brittle upon heat treatment.[73-74, 131-132] A low volume fraction of a poly(arylene ether sulfone) (PAES) block was introduced into the TR precursor polyhydroxyimide chain to improve mechanical properties. The PAES oligomeric

toughener was prepared from 4,4'-biphenol, 4,4'-dichlorodiphenylsulfone and endcapped with *m*-aminophenol. The multiblock copolyhydroxyimide incorporated the PAES in systematically varied amounts copolymerized with 4,4'-(hexafluoroisopropylidene)diphthalic anhydride and 3,3'-dihydroxy-4,4'-diamino biphenyl. The thermal rearrangement was carried out on the series of polyhydroxyimide-co-PAES copolymers to convert the polyhydroxyimide segments to the polybenzoxazoles. Before thermal rearrangement, the polyhydroxyimide-co-PAES precursors exhibited improved mechanical properties (tensile stress and strain at break) relative to the homopolyimide precursor. After thermal rearrangement, tensile stress and strain at break of all the TR copolymers decreased compared to their corresponding precursors, but the properties were improved relative to the homo TR control polymer.

3.2 Introduction

Membrane gas separation has become a fast-growing industrial technology because of its many advantages over traditional separation technologies including low capital cost and energy consumption relative to thermal distillation methods, and higher operational flexibility.[4, 8, 76, 133] Currently, membrane gas separation is widely used in processing raw natural gas to meet certain specifications before delivery to pipelines. Removal of CO_2 from natural gas is required in this process to minimize corrosion of the pipelines.[134] In order to achieve better separation productivity, several challenges need to be addressed including the trade-off between permeability and

selectivity, and the reduction of CO_2-induced plasticization. An ideal polymeric membrane for separation of CO_2 from CH_4 should achieve both high permeability and high selectivity, have good resistance to chemicals, plasticization, and thermo-oxidation, and have excellent mechanical properties.[18, 23]

Recently, Park et al. reported a family of gas separation membrane materials known as thermally rearranged (TR) polymers,[73-75] which are derived from aromatic polyhydroxyimide precursors via thermal treatments (350-450°C) in an inert atmosphere. In this process, the soluble polyimide precursors containing hydroxyl groups *ortho* to the imide ring undergo inter- and intra-molecular rearrangements and transform into insoluble polybenzoxazoles.[132] It has been demonstrated that dense membranes prepared from these TR polymers exhibited outstanding performance for CO_2/CH_4 separation with high gas permeability, high selectivity and excellent resistance to CO_2 induced plasticization.[131] Smith et al. investigated TR polymers prepared from 3,3'-dihydroxy-4,4'-diaminobiphenyl (HAB) and 2,2'-bis-(3,4-dicarboxyphenyl) hexafluoropropane dianhydride (6FDA), and showed that the thermally rearranged product exhibited good gas transport properties.[106] Guo et al. demonstrated that the glass transition temperatures of the polyhydroxyimide TR precursors played an important role in determining the optimum TR temperatures.[135] However, all of these TR polymers suffer a critical problem in that the membrane's mechanical properties dramatically decrease after undergoing the TR process, and this severely limits their potential utilities.[73-74, 131] To improve mechanical properties without sacrificing outstanding gas transport performance, the introduction of

toughening materials into the polymer may be a good solution. It has been reported that functional oligomeric poly(arylene ether sulfones) (PAES) can be good toughening agents for high performance composite materials.[68-72, 130]

In this chapter, a series of toughened thermally rearrangeable copolymers based on PAESs, polyhydroxyimides (HAB and 6FDA) and their corresponding TR polymers are presented. Synthesis, chemical characterization, membrane preparation, mechanical properties and single gas permeability/selectivity of TR precursors and TR copolymers are discussed.

3.3 Experimental

Materials

3-Aminophenol, triethylamine, acetic anhydride, calcium hydride (CaH_2), potassium carbonate (K_2CO_3), and anhydrous 1,2-dichlorobenzene (*o*-DCB, anhydrous) were purchased from Sigma-Aldrich and used as received. Nitric acid, acetone, toluene, isopropanol, methanol and ethanol were purchased from Spectrum Chemicals and used as received. Dimethylacetamide (DMAc) and N-methyl-2-pyrrolidone (NMP) were purchased from Fisher. DMAc and NMP were used as reaction solvent and were dried over CaH_2, distilled under reduced pressure and stored over 3 Å molecular sieves before use. *p*-HAB was purchased from TCI. 6FDA was kindly provided by Air Products and dried in a vacuum oven at 160°C before use. 4,4'-Dichlorodiphenylsulfone (DCDPS, 99%) and 4,4'-biphenol were kindly provided by Solvay and DCDPS was recrystallized from toluene before use.

Synthesis of a Controlled 15,000 Molecular Weight (Mn) Amine-End-Capped PAES.

4,4'-Biphenol (13.5765 g, 72.91 mmol), DCDPS (21.5370 g, 75.00 mmol), 3-aminophenol (0.4563 g, 4.18 mmol), K_2CO_3 (10.88 g, 78.80 mmol) (about 5% molar excess), 145 mL of DMAc and 70 mL of toluene were introduced into a 3-neck, 500-mL round bottom flask equipped with an overhead stirrer, toluene filled Dean-Stark trap, with condenser, and nitrogen inlet. A stirring, thermocouple regulated, oil bath was used to heat the reaction mixture to 140°C. The reaction was stirred at 140°C until all water was azeotropically removed with toluene. The temperature was then increased to 170°C, and the water and toluene were drained from the Dean-Stark trap. After 20 h, the amber opaque solution was cooled to room temperature and filtered. The resulting transparent solution was precipitated into 2 L of IPA as a white solid. The oligomer was filtered, washed with IPA, and dried under vacuum at 90°C for one day. Yield was 95%.

Synthesis of a series of PAES based HAB-6FDA polyhydroxyimide copolymers (PAES-HAB-6FDA) via an ester acid method.

Aromatic polyhydroxyimides containing PAES segments were synthesized via the ester-acid method.[136] The synthesis of a 5 wt% amine-end-capped PAES based HAB-6FDA polyhydroxyimide copolymer (5%PAES-HAB-6FDA) is illustrated as a representative example of synthesis.

6FDA (10.000 g, 22.51 mmol) was introduced into a 3-neck flask equipped with an overhead stirrer, absolute ethanol filled Dean-Stark trap, with a condenser, and a

nitrogen inlet. Then, 60 mL of absolute ethanol and 6.58 mL of triethylamine (47.27 mmol) were introduced. A stirring, thermocouple-regulated, oil bath was used to heat the reaction to 100°C. The mixture was refluxed with stirring for 1 h, then the trap was drained. When distillation of ethanol ceased, the trap was again drained and refilled with *o*-DCB. *p*-HAB (4.8563 g, 22.46 mmol) and PAES (0.7819 g, 0.0521 mmol) were dissolved in 36 mL of DMAc and then introduced to the reaction flask followed by 11 mL of *o*-DCB (~4/1, v/v) to produce a solids content of ~30% wt/v. The mixture was heated at 160°C for 24 h, and then at 180°C for 48 h. The reaction solution was allowed to cool and then precipitated in IPA. The product was dried under vacuum at 180°C for one day. Yield was 95%.

Synthesis of PAES-HAB-6FDA based polyacetylimide (PAES-HAB-6FDA-Ac)

Acetylation of PAES-HAB-6FDA polyhydroxyimides were carried out by following a modified literature method.[137] The acetylated PAES-HAB-6FDA polyacetylimide is hereafter referred to as PAES-HAB-6FDA-Ac. The synthesis of a 5%PAES-HAB-6FDA-Ac is provided as a representative example of synthesis. To a 100-mL, three-neck round bottom flask equipped with a mechanical stirrer, a N_2 inlet and a condenser, 5%PAES-HAB-6FDA polyhydroxyimide (5.00 g, 7.5 eq hydroxyl units), 7 mL of acetic anhydride (75 mmol, 10 M excess per hydroxyl unit) and 6 mL of pyridine (75 mmol) were added in 50 mL of anhydrous NMP. The solution was heated to 50°C and maintained at that temperature for 24 h with continuous stirring and a N_2 purge. The resulting viscous solution was cooled to room temperature and precipitated in an excess amount of stirred methanol. The acetylated polyacetylimide

(5%PAES-HAB-6FDA-Ac) was filtered and dried under vacuum at 180°C overnight. Yield was 99%.

Film Casting

One g of PAES-HAB-6FDA was dissolved in 40 mL of DMAc (~2.5%, w/v). The mixture was stirred until a homogeneous solution was obtained. The solution was filtered with a pressure filter through Whatman™ qualitative filter paper and then through a 0.45 μm filter to remove any dust and particulates. This solution was sonicated for 60 min to remove dissolved gases. A 5 x 5 inch glass plate was cleaned with acetone and dried before use. The solution was cast on the glass plate on a leveled casting surface in a vacuum oven following the protocol below. It was heated at 25 – 100ºC for 2 h without vacuum; then at 100 – 120°C for 2 h without vacuum; 120 – 140°C for 2 h without vacuum; 140 – 160°C for 4 h without vacuum; then at 160°C for 8 h in a vacuum oven under full vacuum. The film was soaked in DI water overnight while covered with a glass plate to avoid curling. The surface water was removed with a Kimwipe and the film was dried at 100°C for 2 h and then the temperature was raised to 160°C under vacuum for 12 h.

Thermal Rearrangement of PAES-HAB-6FDA films

The PAES-HAB-6FDA films were converted to their corresponding polybenzoxazole films via thermal rearrangement (TR) using a Thermolyne 47900 muffle furnace in air. In the TR process, the polymer films were first pre-heated at 300°C for 1 h in air before being heated at the desired TR temperature. The TR films were obtained by holding them at the TR temperature of 400°C for 1 or 2 h. The

percent TR conversion, as presented in equation 3-1, is defined as 100 times the ratio of the actual mass loss upon thermal rearrangement relative to the theoretical mass loss:

%TR Conversion = Measured Weight Loss/Theoretical Weight Loss×100% (3-1)

Characterization

^{1}H nuclear magnetic resonance (^{1}H NMR) experiments were conducted on a Varian INOVA 400 MHz NMR spectrometer operating at 400 MHz to confirm the chemical structures of the polyhydroxyimides and the oligomeric modifiers. All spectra were obtained from ~10% (w/v) polymer solutions in deuterated dimethylsulfoxide (DMSO-d_6) at room temperature.

Potentiometric titration was used to determine the number average molecular weight of Amine-End-Capped PAES. A 0.001 N $HClO_4$ solution was used as a titrant to react with amine end groups. The potential change was monitored with a potentiometer (Fisher Scientific Accumat Model 910) equipped with a pH probe (Orion 9272BN PerpHect Sure Flow). PAES (0.1 g) was dissolved in 50 mL of chloroform. Then the PAES solution was titrated with the 0.001 N $HClO_4$ solution. The equivalence point was determined by the change of conductance (potential change). This process was repeated three times and the amount of consumed $HClO_4$ solution was used to calculate the M_n of the PAES oligomers based on equation 3-2.

$$<M_n>= \frac{Mass_{PAES}}{Volume_{HCLO4}\times 0.001\times 0.5} \quad (3\text{-}2)$$

Fourier Transform Infrared spectroscopy with Attenuated Total Reflectance (FTIR-ATR) was used to follow the structural changes of the polyhydroxyimides

during the TR process. The FTIR-ATR spectra were recorded on an FTIR spectrometer (Bruker Tensor 27) equipped with an ATR attachment with a horizontal diamond crystal. The resolutions of the spectra were 4 cm^{-1} and 64 background scans were collected. A small amount of polymer film was placed on the diamond crystal and the FTIR spectrum was measured with 64 scans. All measurements were performed at ambient temperature.

Thermogravimetric analysis (TGA) was performed with a TA Instruments TGA Q500. Fully dried samples were evaluated over the range of 50–700°C at a heating rate of 10°C min^{-1} in a N_2 atmosphere and in air. Differential scanning calorimetry (DSC) was performed with a TA Instruments DSC Q1000 in a nitrogen atmosphere at a heating rate of 10°C min^{-1} to determine the thermal transitions of the polymer films. The glass transition temperature was taken as the midpoint of the change in slope of the baseline.

Size exclusion chromatography (SEC) was conducted on the HAB-6FDA-Ac polyacetylimides to measure molecular weight distributions. The solvent was DMAc that was distilled from CaH_2 and that contained dry LiCl (0.1 M). The column set consisted of 3 Agilent PLgel 10-μm Mixed B-LS columns 300×7.5 mm (polystyrene/divinylbenzene) connected in series with a guard column having the same stationary phase. The column set and detectors were maintained at 50°C. An isocratic pump (Agilent 1260 infinity, Agilent Technologies) with an online degasser (Agilent 1260), autosampler and column heater was used for mobile phase delivery and sample injection. A system of multiple detectors connected in series was used for

the analyses. A multi-angle laser light scattering (MALLS) detector (DAWN-HELEOS II, Wyatt Technology Corp.), operating at a wavelength of 658 nm, a viscometer detector (Viscostar, Wyatt Technology Corp.), and a refractive index detector operating at a wavelength of 658 nm (Optilab T-rEX, Wyatt Technology Corp.) provided online results. The system was corrected for interdetector delay and band broadening and the light scattering detectors were normalized using a (?21K g/mole polystyrene standard obtained from Agilent?). Data acquisition and analysis were conducted using Astra 6 software from Wyatt Technology Corp. Validation of the system was performed by monitoring the molar mass of a known molecular weight polystyrene sample by light scattering. The accepted variance of the 21,000 g/mol polystyrene standard was defined as 2 standard deviations (11.5% for M_n and 9% for M_w) from a set of 34 runs. The Astra software was used to calculate the dn/dc of the known concentration samples based on an assumption of 100% recovery of the injected sample. The calculated dn/dc for each sample was used to measure the molecular weight averages using the light scattering and refractive index results from the SEC experiments.

Gel Fraction Measurements

Gel fractions are the weight percents of the cross-linked/insoluble portion of the films. Sample films were dried at 120°C under vacuum overnight. Then 0.1−0.2 g (W_0) of the initial film sample was placed in a 20-mL scintillation vial filled with DMAc and stirred at 100°C overnight. The remaining solid was filtered, transferred to a pre-weighed vial, and dried in vacuum oven at 120°C overnight. The final weight (W_f)

was taken the next day. Gel fraction values (wt%) were calculated by dividing the weight of the dried gel portion (W_f) by the initial mass of the film (W_o) as shown in equation 3-3.

$$\text{Gel Fraction\%} = \frac{W_f}{W_o} \times 100 \quad (3\text{-}3)$$

Mechanical Property Measurements

Mechanical properties were measured using an Instron Elecropuls E1000 fitted with a 250 N load cell. The film thickness was measured based on the average of 5 points at the narrow section of dogbones using a Mitutoyo digimatic micrometer model MDC-1"SXF. Thin films used for tensile testing in this study ranged in thicknesses between 20 and 40 μm. Dogbone-shaped thin film specimens (sample Type V of ASTM D638-14) were cut using a Cricut Explore One™ computer controlled cutting machine. After a sample was mounted in the grips, it was pulled at 3 mm/min until it failed. A stress-strain plot was prepared for each sample, and tensile stress and elongation at break were recorded. At least three samples were tested for each material. The Young's modulus was estimated by taking the ratio of stress to strain in the initial linear region of each stress/strain plot.

Pure Gas Permeability Measurements

Pure-gas permeability coefficients were measured using a constant volume-variable pressure method.[138] A gas at a feed pressure of p_o was applied to the upstream side of the film, and gas permeated through the film into a calibrated downstream chamber of volume, V. Permeabilities of H_2, CH_4, N_2, O_2, and CO_2 were measured in that order at 35 °C and feed pressures ranging from 3 to 17 atm for the

polyhydroxyimides and their TR analogs. The permeability of gas A, P_A, was calculated as follows in equation 3-4:

$$P_A = \frac{Vl}{p_o TRA}\left[\left(\frac{dp}{dt}\right)_{ss} - \left(\frac{dp}{dt}\right)_{leak}\right] \quad (3\text{-}4)$$

where l is film thickness, R is the gas constant, T is absolute temperature, A is the film area, and $(dp/dt)_{leak}$ and $(dp/dt)_{ss}$ are the rates of pressure rise in the downstream volume during the leak test and when the gas permeation through the film was at pseudo-steady state, respectively. The leak test was conducted by isolating the downstream and upstream sections of the permeation system and monitoring changes in the downstream pressure for about 1 h. Permeabilities are reported in units of Barrer, where 1 Barrer is 10^{-10}10 cm^3(STP) cm/cm^2 s cmHg. Pure-gas selectivity, $\alpha_{A/B}$, is defined as the ratio of pure-gas permeabilities in equation 3-5:

$$\alpha_{A/B} = \frac{P_A}{P_B} \quad (3\text{-}5)$$

where P_A is the permeability coefficient of the more permeable gas, and P_B is the permeability of the less permeable gas.

3.4 Results and Discussion

Synthesis and structural characterization of the amine-endcapped polysulfone oligomers (PAES)

In our group's previous work, mechanical properties and morphologies of reactive polysulfone toughened epoxy networks were invesitgated.[69, 139-140] Ductile polysulfone was suggested as a good toughening agent and this was highly dependent of the excellent adhesion developed between the polysulfone and epoxy phases due to

the chemical bonds.[68] In these studies, bisphenol A was used as the monomer to produce polysulfone oligomers as toughening agents because it is molecularly miscible with the epoxy precursors. Bisphenol A also contains the 2,2'-isopropylidene moiety which leads to polymers with higher fractional free volume and thus higher gas permeabilities for gas separation.[22, 26, 141] However, in this work, 4,4'-biphenol was used instead of bisphenol A (Figure 3.1) for synthesis of the PAES oligomers to be copolymerized into the polyhydroxyimides and then thermally rearranged to toughened polybenzoxazole copolymers. The primary reason for incorporating biphenol rather than bisphenol A is the instability of the aliphatic isopropylidene unit under the required high TR temperature.

Figure 3.1 4,4'-biphenol (left) and Bisphenol A (right)

The effect of molecular weights of the polysulfone on mechanical properties was also studied. Based on their results, a number average molecular weight of 15,000 g/mole of PAES was selected as a good toughening segment. This provides good mechanical properties as well as reactivity and processability.[68-70, 140] The synthesis of amine-endcapped polysulfone oligomeric toughening agents shown in Figure 3.2 was performed using nucleophilic aromatic substitution step polymerization with a weak base.[142-143] A monofunctional amine *m*-AP was added in amounts calculated by the modified Carothers equation to target a number average molecular weight of 15,000 g/mole and to provide functional aromatic amine groups to afford covalent

incorporation into the polyhydroxyimide copolymers on both chain ends. This allows the oligomers to further react with a dianhydride to form polyimides. The commercial monomer DCDPS was used to form sulfone linkages in this PAES oligomer. Relatively high reaction concentration (25 wt/v%) was used to ensure high monomer conversion to obtain good control over molecular weight as required for step-growth polymerizations. Toluene was used as the azeotropic solvent to remove water both from monomers and K_2CO_3 decomposition. The water appeared as a cloudy layer in the bottom of the Dean-Stark trap. Refluxing was continued until no more water was observed in the distillate. The temperature was raised slowly to the final reaction temperature by heating the oil bath to 170°C, and then toluene was slowly removed until the initial charged volume was collected. The reaction viscosity appeared unchanged after 24 hours. Since the molecular weight of these polymers was targeted at 15,000 g/mol, no obvious change in viscosity was anticipated or observed. The solution was brown near the end of the reaction.

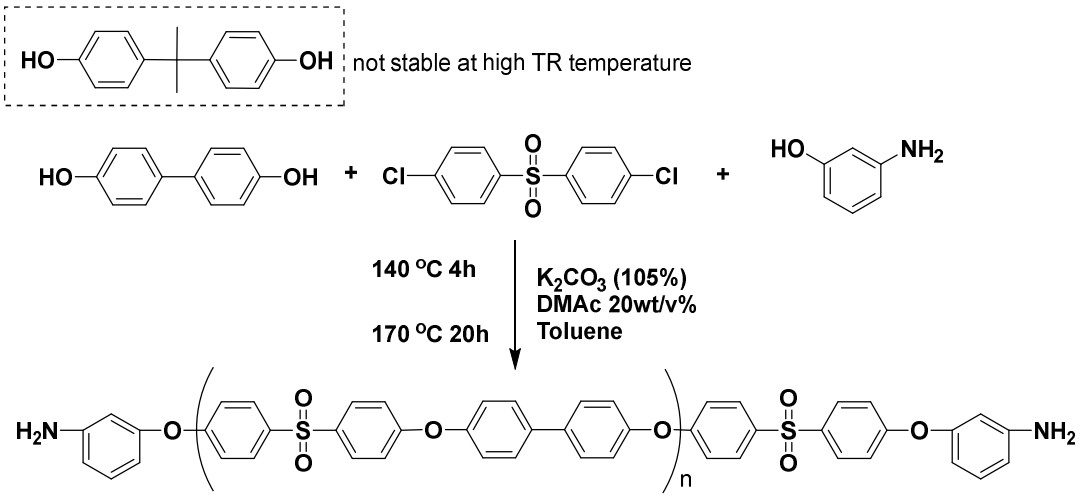

Figure 3.2 Synthetic scheme for amine-endcapped polysulfone oligomers (PAES)

After a total of 24 hours reaction time, the reaction mixture was removed from

the oil bath and filtered to remove salt. The brown solution was precipitated into 2 liters of a mixed solution (isopropanol:water =1:1) and stirred overnight to remove residual water soluble salt. A white fibrous product was obtained after filtration that was then dried in the oven under vacuum at 90°C for 24 hours.

One method that was utilized to confirm the chemical structure and determine the molecular weight of the Amine-End-Capped PAES oligomers was by ^{1}H-NMR as shown in Figure 3.3. No residual starting materials were observed in the ^{1}H-NMR spectra. All of the proton signals were assigned (Figure 3.3). Three peaks (g, f, e) in the range 6.3-6.5 ppm are aromatic signals from the *m*-AP endgroups. The upfield signal i corresponds to the active amine protons. Four peaks (a, b, c, d) in the downfield region are aromatic resonances from the polysulfone backbone structure. A $<M_n>$ of 19,500 g/mole was calculated (Figure 3.4) by comparing the integration values of the *m*-AP endgroups (g) to the aromatic DCDPS (c+d) or BP (a+b) peaks in the oligomer backbone.

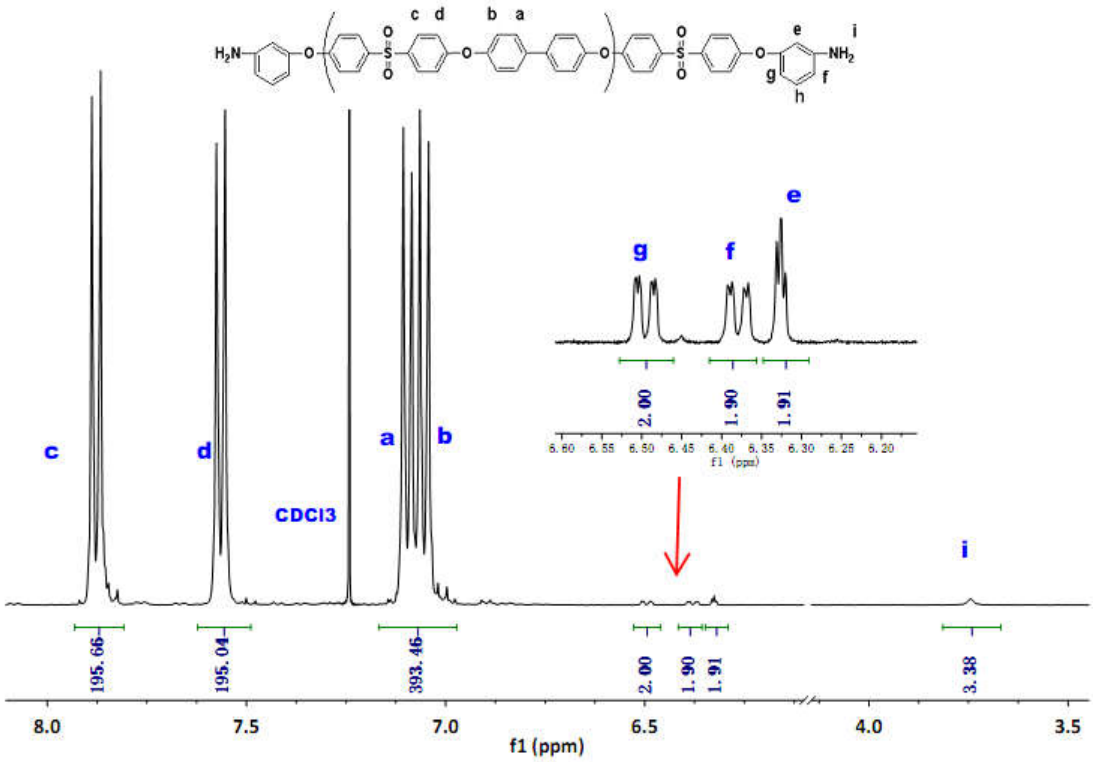

Figure 3.3 ^{1}H NMR confirms the structures of Amine-End-Capped PAES

Sum of the peak areas due to 2 *m*-AP endgroup protons (g)

Number of oligomer chains= **(g)/2**

Area due to DCDPS (c+d) or BP (a+b) protons

Number of repeat units (RU) = **(c+d)/8**

$$\mathbf{<M_n>=\frac{c+d}{4\times g}\times 400+43=\frac{195+195}{4\times 2}\times 400+43\sim 19500\ g/mol}$$

Figure 3.4 Sample calculation of the molecular weight using ^{1}H NMR for a PAES oligomer with a targeted <Mn> of 15,000 g/mol. EG, RU, and MW represent endgroup, repeat unit, and molecular weight, respectively

Potentiometric titration of the amine endgroups was also conducted to determine the molecular weights of the Amine-End-Capped PAES oligomers since titrations are inherently more accurate than NMR data. A non-aqueous titration process was utilized by using a strong acid solution (0.001 N perchloric acid $HClO_4$ dissolved in acetic

acid) to titrate the weakly basic aromatic amine endgroups. Three parallel trials of titration were carried out, and a $<M_n>$ of 14,500 g/mol was calculated by equation 3-2 based on the titration data in Table 3.1.

Table 3.1 Summary of titration results

	Trial 1	Trial 2	Trial 3	Average
Mass of PAES (g)	0.0955	0.1020	0.1040	0.1005±0.0036
Volume of $HClO_4$ (L)	0.01378	0.01390	0.01390	0.01386±0.00001
M_n of PAES (g/mol)	13860	14676	14964	14500±467

Comparing the above two results, the molecular weight obtained from NMR is less reliable since the peak corresponding to the repeating unit is too broad to integrate accurately. Therefore, the titration values were used in the subsequent block copolymer calculations.

Synthesis of a series of PAES based HAB-6FDA polyhydroxyimide copolymers (PAES-HAB-6FDA)

A series of PAES-HAB-6FDA charged with different weight percentages of PAES were synthesized from dianhydride and diamine monomers via an ester-acid method.[135, 144] In this process (Figure 3.5), a hydrolytically unstable dianhydride monomer was first placed into the reaction flask and reacted with ethanol to form a hydrolytically stable intermediate with ester and acid groups on both sides. Next, the macromonomer Amine-End-Capped PAES and the diamine monomer HAB were dissolved in the reaction solvent and then introduced to the system with the intermediate from the first step. After 48 hours, high molecular weight block

copolymer products were obtained.

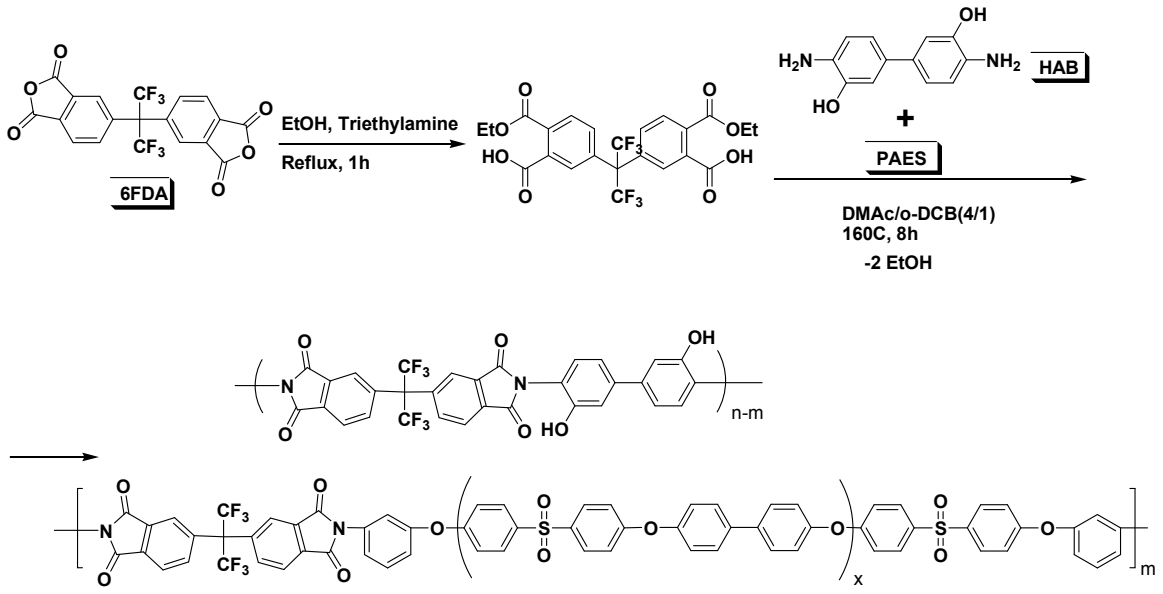

Figure 3.5 Synthesis of PAES-HAB-6FDA

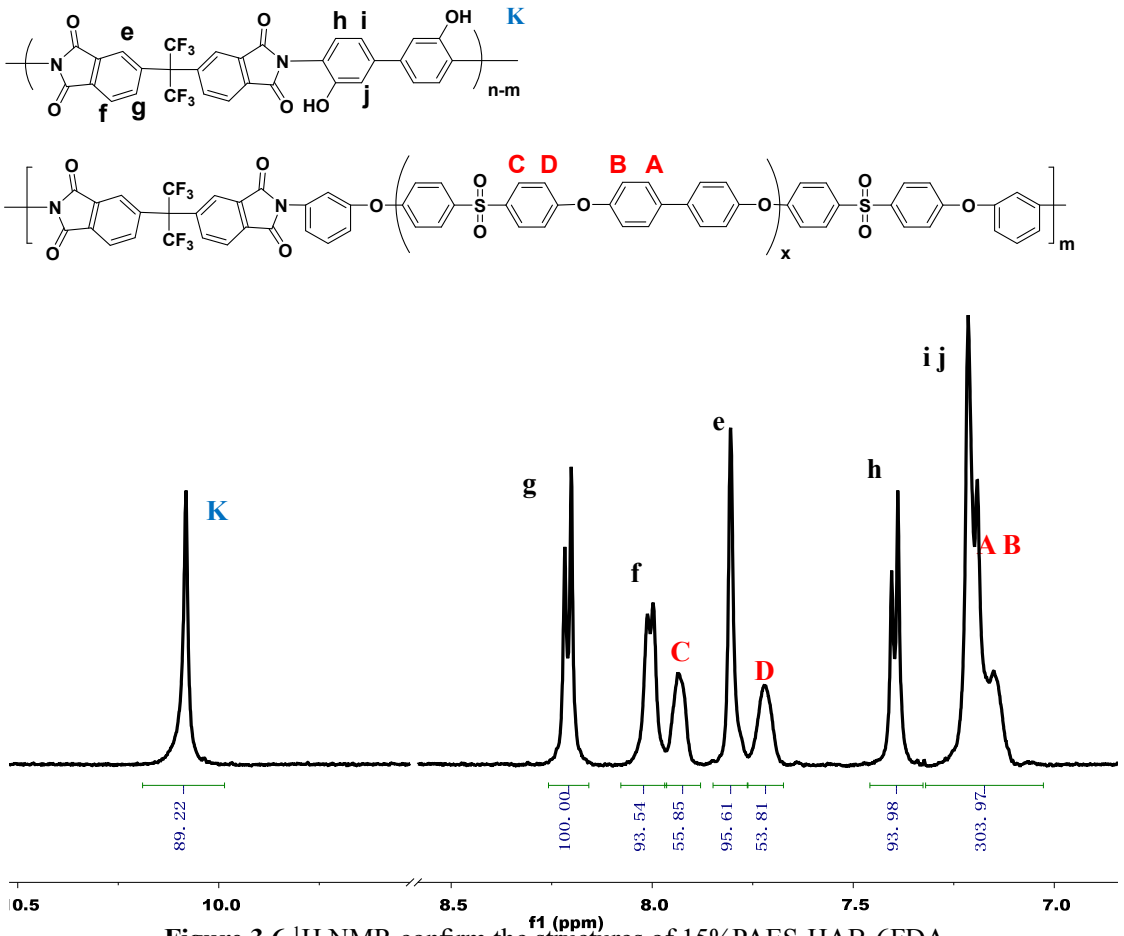

Figure 3.6 ^{1}H NMR confirm the structures of 15%PAES-HAB-6FDA

The concentrations of PAES in the PAES-HAB-6FDA copolymers were confirmed by ^{1}H-NMR. The copolymer with 15 wt% of PAES is referred to as 15% PAES-HAB-6FDA and its ^{1}H-NMR spectrum is shown in Figure 3.6. Comparing the ^{1}H-NMR spectra of the copolymer products with those of three starting materials, it was found that all of the resonances had shifted, thus indicating that all of the monomers were chemically linked to form block copolymers instead of blends. No end group peak signals of PAES were observed in the ^{1}H-NMR spectra, which suggested that high conversion from PAES to copolymers had been achieved. Four signals (C, D, A and B) are aromatic protons from the PAES segments, and the remaining peaks correspond to the HAB-6FDA polyhydroxyimide segments.

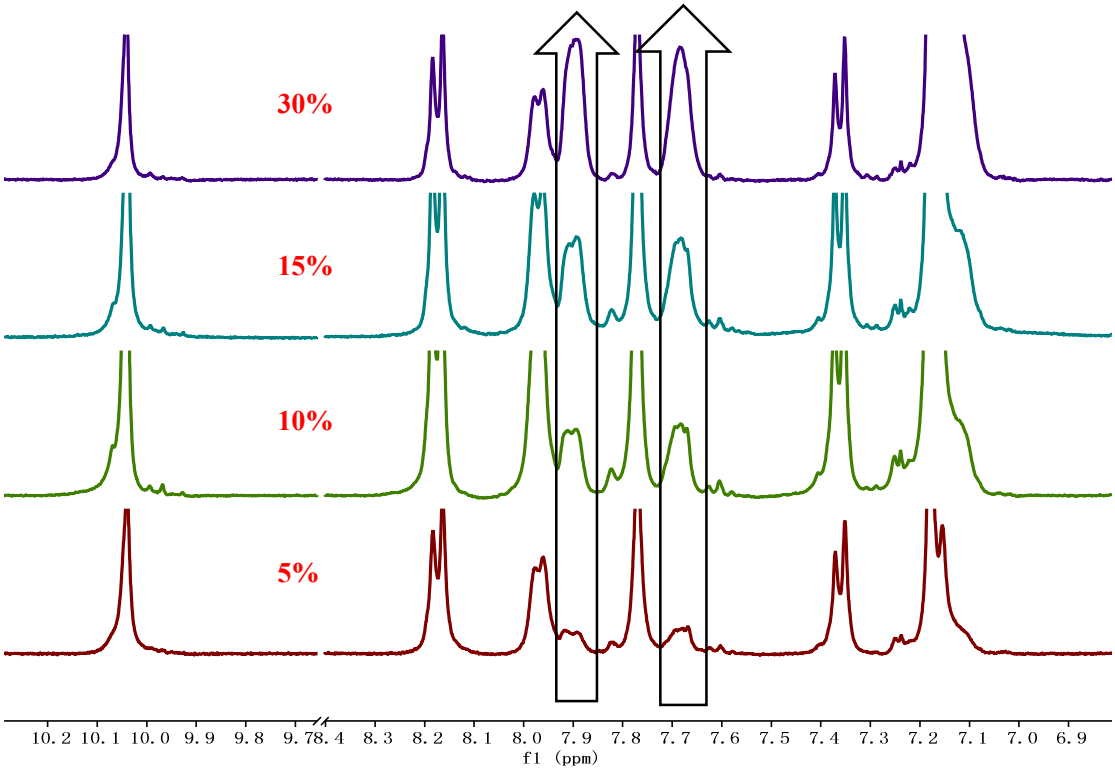

Figure 3.7 ^{1}H-NMR spectra comparison of copolymers with different amounts of PAES (from bottom to top is 5%, 10%, 15%, and 30% PAES-HAB-6FDA, respectively)

An overlay of ^{1}H-NMR spectra is shown in Figure 3.7. In these spectra, it can be

clearly seen that integration values of the protons from the PAES increase with increasing amount of PAES charged into the system. Each weight percentage of PAES in the block copolymers was calculated based on the corresponding ^{1}H-NMR spectrum. The results for each block copolymer are shown in Table 3.2, and the theoretical results are very close to the experimental values.

Table 3.2 Summary of different composition of PAES-HAB-6FDA copolymers

PAES Charged (wt%)	5%	10%	15%	30%
Calculated PAES (wt%)	(5.97±0.82)%	(10.23±0.83)%	(14.63±0.85)%	(30.90±0.85)%

Synthesis of PAES-HAB-6FDA based polyacetylimide (PAES-HAB-6FDA-Ac)

Previous studies have demonstrated that polyhydroxyimides have higher viscosities than their polyacetylimide substituents due to the effect of hydrogen bonding interactions in polyhydroxyimides.[111, 137] The polyhydroxyimides also interact with SEC column to yield low mass recovery and inaccurate molecular weight results. In order to obtain reproducible and acceptable molecular weight information from SEC, acetylation reactions of PAES-HAB-6FDA block copolymers were conducted to reduce the hydrogen bonding interactions (Figure 3.8). In the acetylation reaction, an excess of acetic anhydride was used to ensure full replacement of hydroxyl groups. The polyacetylimide products were easily purified by precipitation and filtration. After acetylation, ^{1}H-NMR was used to characterize the reaction conversion.

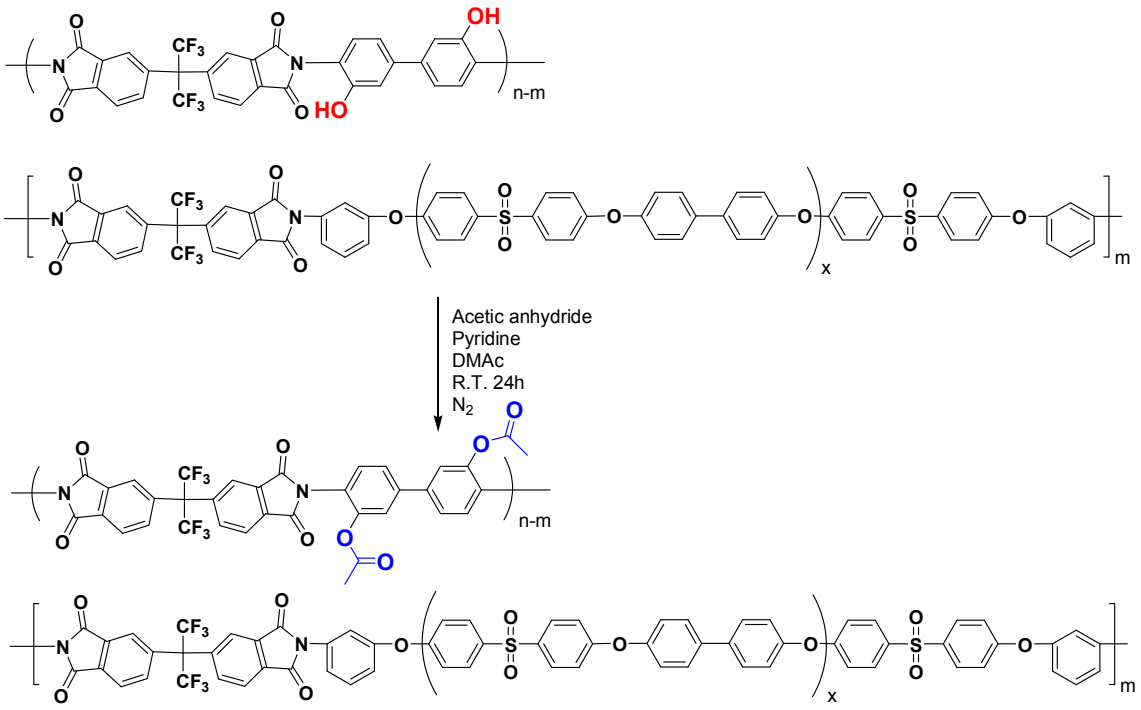

Figure 3.8 Acetylation from PAES-HAB-6FDA to polyacetylimides

In Figure 3.9, the top spectrum is based on the 15%PAES-HAB-6FDA polyhydroxyimide and the signal k corresponds to the active proton in the hydroxyl group. In the bottom spectrum, the active proton signal is no longer present in the downfield area but a proton signal from the acetyl methyl group appeared upfield. All the other signals were observed with slightly different chemical shifts in the polyhydroxyimide and polyacetylimide spectra (Figure 3.9). A comparison of the spectra before and after acetylation indicated that full conversion had been achieved and that all of the hydroxyl groups had been converted to acetyl groups.

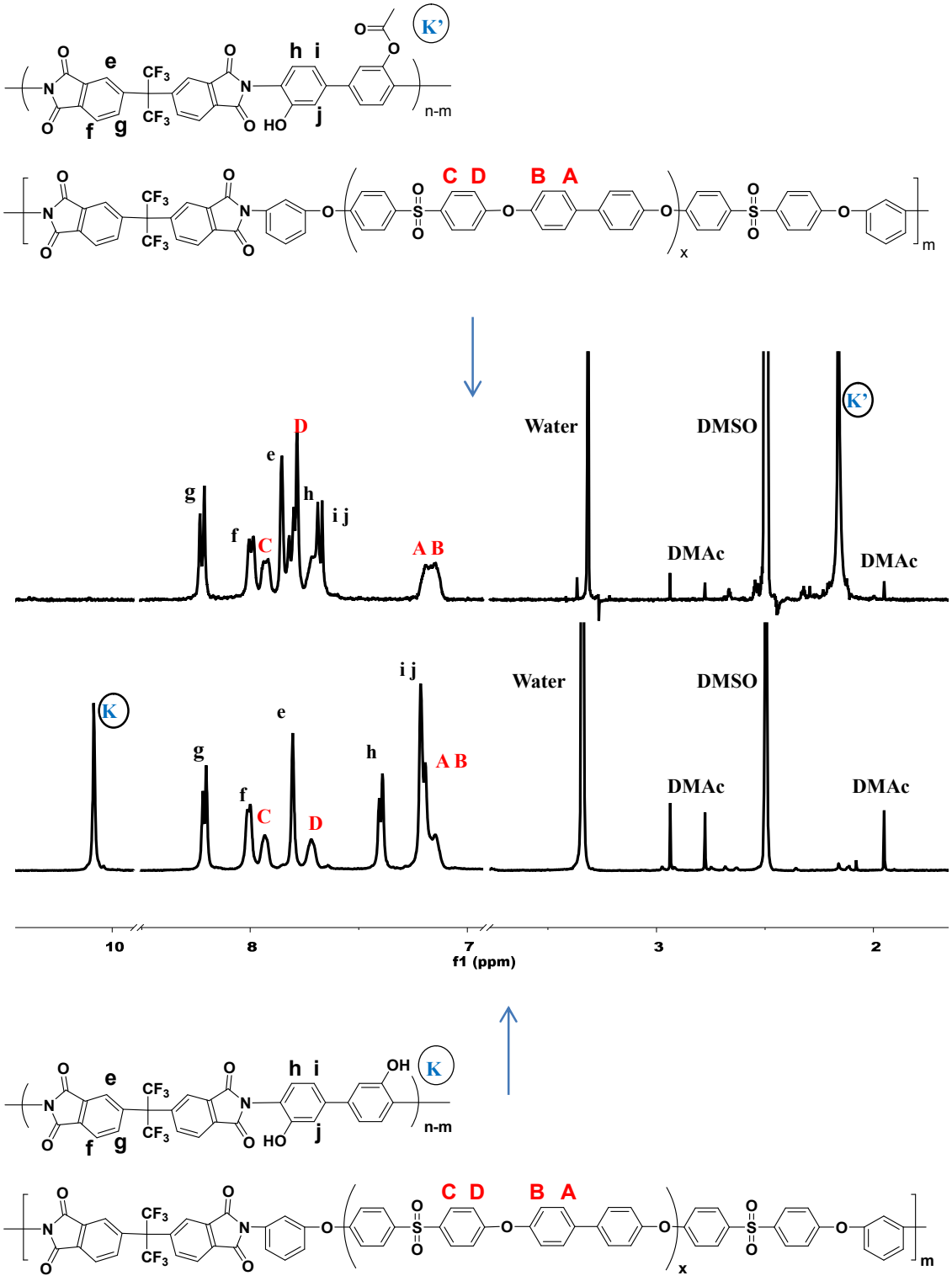

Figure 3.9 ^{1}H NMR confirms acetylation from polyacetylimides (top) to PAES-HAB-6FDA (bottom)

Molecular weights of the polyacetylimides containing 0, 5, 10, 15 and 30 wt% of

PAES-HAB-6FDA-Ac were characterized by SEC (Table 3.3). High molecular weights were obtained for all of these block copolymers. The high molecular weights may contribute to the improved mechanical properties. Higher contents of PAES in the block copolymers tend to yield lower molecular weights. This could be a consequence of a larger deviation from stoichiometry when a higher amount of PAES is charged. Although the number average molecular weight of the Amine-End-Capped PAES oligomers was based on titration, the $<M_n>$ of the macromonomer is still an average of the molecular weight of the individual chains and therefore the PAES molecular weight is not as consistent and accurate as the molecular weights of the pure low molar mass monomers HAB and 6FDA. When more PAES was introduced to obtain a higher wt% of PAES in the product, a greater deviation of stoichiometry could result in lower molecular weight of the final block copolymer.

Table 3.3 Summary of molecular weights of PAES-HAB-6FDA copolymers from SEC

	PAES	PI (6FDA-HAB)	5% PAES-PI-Ac	10% PAES-PI-Ac	15% PAES-PI-Ac	30% PAES-PI-Ac
M_n(kDa)	18.6	41.1	94.3	88.8	62.6	59.9
M_w(kDa)	29.4	81.7	282.0	300.9	205.1	207.1
PDI	1.6	2.0	3.0	3.4	3.3	3.5
dn/dc (mL/g)	0.2084	0.1309	0.1009	0.1499	0.1514	0.1639

In Figure 3.10, SEC light scattering (red) and refractive index (blue) chromatograms of 5%PAES-PI-Ac are shown as representative for all block copolymers. The polymer peak is highlighted from 19 min to 31 min showing the range in which the molecular weight was measured. The distribution appears to be

bimodal or to have a shoulder but this is not believed to be the case for these copolymers. Due to the significant difference in the refractive index increment between the PAES and the polyimide blocks (0.21 and 0.13 respectively) and the fact that the PAES block is of significant molecular weight, it is anticipated that the incorporation of the large PAES block is not constant across the molecular weight distribution. PAES has a higher refractive index than the polyhydroxyimide because sulfur content usually leads to significant shifts in refractive index toward the high RI side. The intensity of the light scattering signal is proportional to the refractive index increment squared as well as the molar mass and concentration based on Eq 3-6. The shoulders in both the light scattering and refractive index signals at low elution volume indicate that the high molecular weight fraction has more of the high refractive index component (PAES) when compared to the low molecular weight fraction. Intuitively this makes sense as the inclusion of a 15K g/mole PAES-diamine rather than a low molecular HAB diamine automatically increases the chain molecular weight by approximately 15K g/mole meaning that the chains that incorporate PAES are more likely to be on the higher molecular weight end of the distribution and those that do not incorporate the PAES are automatically more likely to be on the low end of the molecular weight distribution.

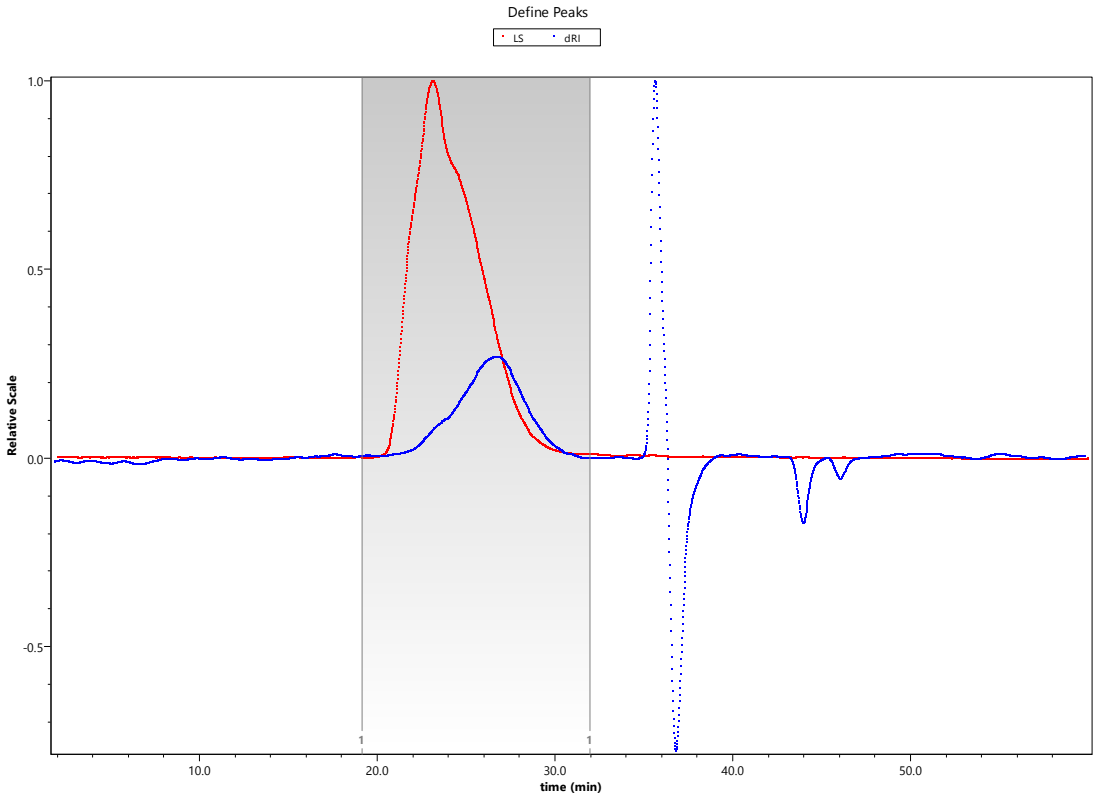

Figure 3.10 SEC chromatograms of 5%PAES-PI-Ac. The red one is from light scattering (LS) detector, while the blue one is from differential refractive index (dRI) detector.

$$R_\theta = M_w \times K \times \left(\frac{d_n}{d_c}\right)^2 \times c \qquad \text{Eq 3-6}$$

In this equation, the intensity of scattered light is measured as the Raleigh ratio R_θ, Mw is weight average molecular weight, K is a constant and c is concentration. (dn/dc) is the refractive index increment of any polymer and solvent combination.

Thermal properties of TR precursors and their TR copolymers

Thermal conversion of the polyhydroxyimides to their corresponding polybenzoxazoles produces carbon dioxide as a by-product and also results in crosslinked products. TGA scans can provide an estimate of the temperature/time regime that is needed to convert the polymers and evolve the by-product. Figure 3.10 presents TGA scans for the 5%PAES-HAB-6FDA block copolymer and the TR

conversion. Typically, TGA scans of the TR polymers derived from the polyhydroxyimides display a two-stage weight loss.[73, 107, 145] The first stage, between 300 and 500°C, is the so called TR region and the weight loss is primarily related to the thermal rearrangement with evolution of carbon dioxide. The second stage, starting after the TR region, is attributed mainly to thermal degradation of the TR polymer backbone. The observed TR region weight losses of the PAES-modified PAES-HAB-6FDA block copolymers containing 5, 10, 15 and 30 wt% PAES matched their corresponding theoretical weight losses with complete TR conversion from polyhydroxyimide precursors to polybenzoxazole TR polymers.

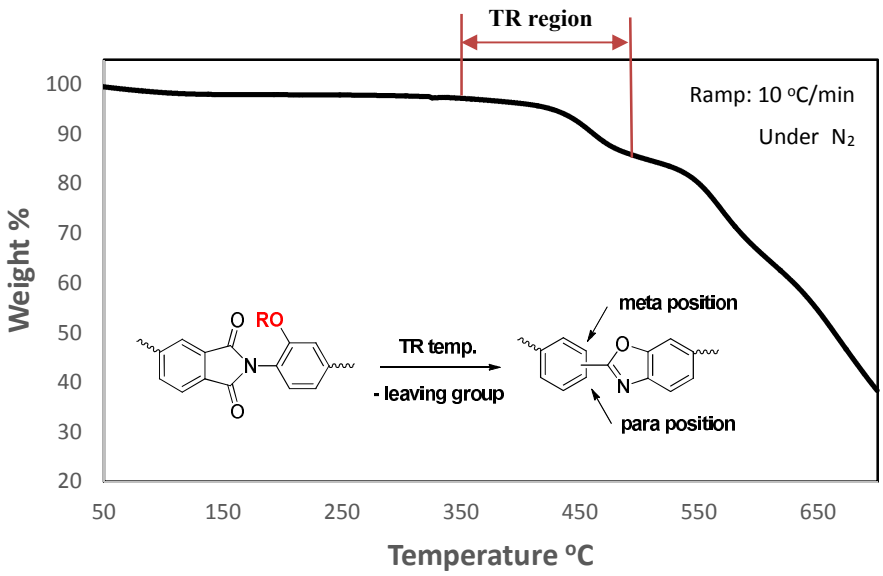

Figure 3.11 Thermogravimetric analysis of 5%PAES-HAB-6FDA TR polymers

Table 3.4 Summary of TR conversion and gel fraction of TR films

	Weight loss after TR at 400°C 1 h			
Precursors	Measured	Theoretical	TR Conversion	Gel fraction
0%PAES-6FDA-HAB	3.8%	14.1%	27.0%	95%
5%PAES-6FDA-HAB	6.9%	13.4%	51.5%	100%
10%PAES-6FDA-HAB	8.3%	12.7%	65.2%	100%
15%PAES-6FDA-HAB	9.3%	12.0%	78.0%	100%
30%PAES-6FDA-HAB	8.6%	9.9%	87.7%	100%

In Table 3.4, the %TR conversions and gel fractions of block copolymers containing different amounts of PAES are presented. The gel fractions are a measurement of the weight fraction of the cross-linked/insoluble portion in a film sample. In the case of the TR process, the insoluble fraction of the TR film originates from both intramolecular rearrangements (formation of possibly insoluble PBOs) and intermolecular rearrangements or cross-linking (formation of insoluble networks)[135]. In this study, all TR films achieved high gel fractions due to the formation of either insoluble PBOs or crosslinked structures. The %TR conversion indicates the amount of polyhydroxyimide segments that were converted to polybenzoxazole segments. It was found that higher contents of PAES in the precursor block copolymer resulted in

higher %TR conversions. A possible explanation is that the PAES provides better chain mobility due to its lower T_g, which facilitates the thermal rearrangements. Compared with the 0%PAES control polymer film, the polymer film that contains 30%PAES undergoes thermal rearrangement to achieve higher %TR conversion under the same heat treatment conditions.

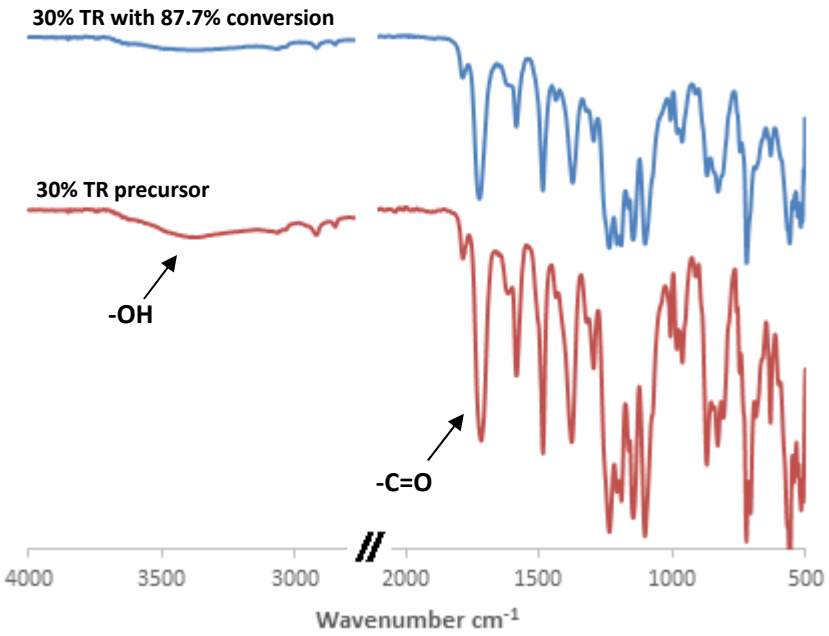

Figure 3.12 Comparison of FTIR-ATR spectra betweem 30% PAES-HAB-6FDA TR precursor polymers (bottom) and 30% PAES-HAB-6FDA TR polymers with a 87.7% TR conversion (top)

The structural changes upon conversion from HAB-6FDA polyhydroxyimide to polybenzoxazole during thermal rearrangements were tracked with FTIR-ATR by qualitatively observing the decreased absorbance of –OH group (~3400 cm^{-1}) and imide peaks C=O (~1720 cm^{-1}).[135, 137, 144] Taking 30% PAES-HAB-6FDA TR copolymers as an example, comparison of FTIR-ATR spectra between the precursor copolymers (bottom) and TR copolymers with a 87.7% TR conversion (top) is shown in Figure 3.11. Thermal rearrangement of polyhydroxyimide TR precursors to

polybenzoxazoles reduced the amount of hydroxyl and ketone groups and thus declined peak intensities at ~3400 cm^{-1} and ~1720 cm^{-1} in FTIR spectrum.

Mechanical properties

Mechanical properties are one of most important performance parameters for a gas membrane material. Poor mechanical properties are a major obstacle against commercialization of the polybenzoxazole thermally rearranged membranes.[146] Good mechanical strength is required to withstand high pressure during operation and also for the films to be sufficiently robust for membrane fabrication. Mechanical properties of TR polymer films depend on many factors including the casting procedure, TR protocol, molecular weight, rate of tensile deformation, and extent of any crosslinking or branching.[147] In this study, mechanical properties of PAES-HAB-6FDA copolymers with various compositions of TR precursor films and their corresponding TR polybenzoxazole analogs were investigated. Stress, strain and toughness value (area under the curve) at break as well as Young's moduli are shown in Table 3.5. Overlay curves from Instron tests are shown in Figure 3.13.All of the precursor films were heated in a TR process at 400°C for 1 hour except the 0%PAES precursor control film, which was prepared by TR450°C for 2 hours to ensure high TR conversion.

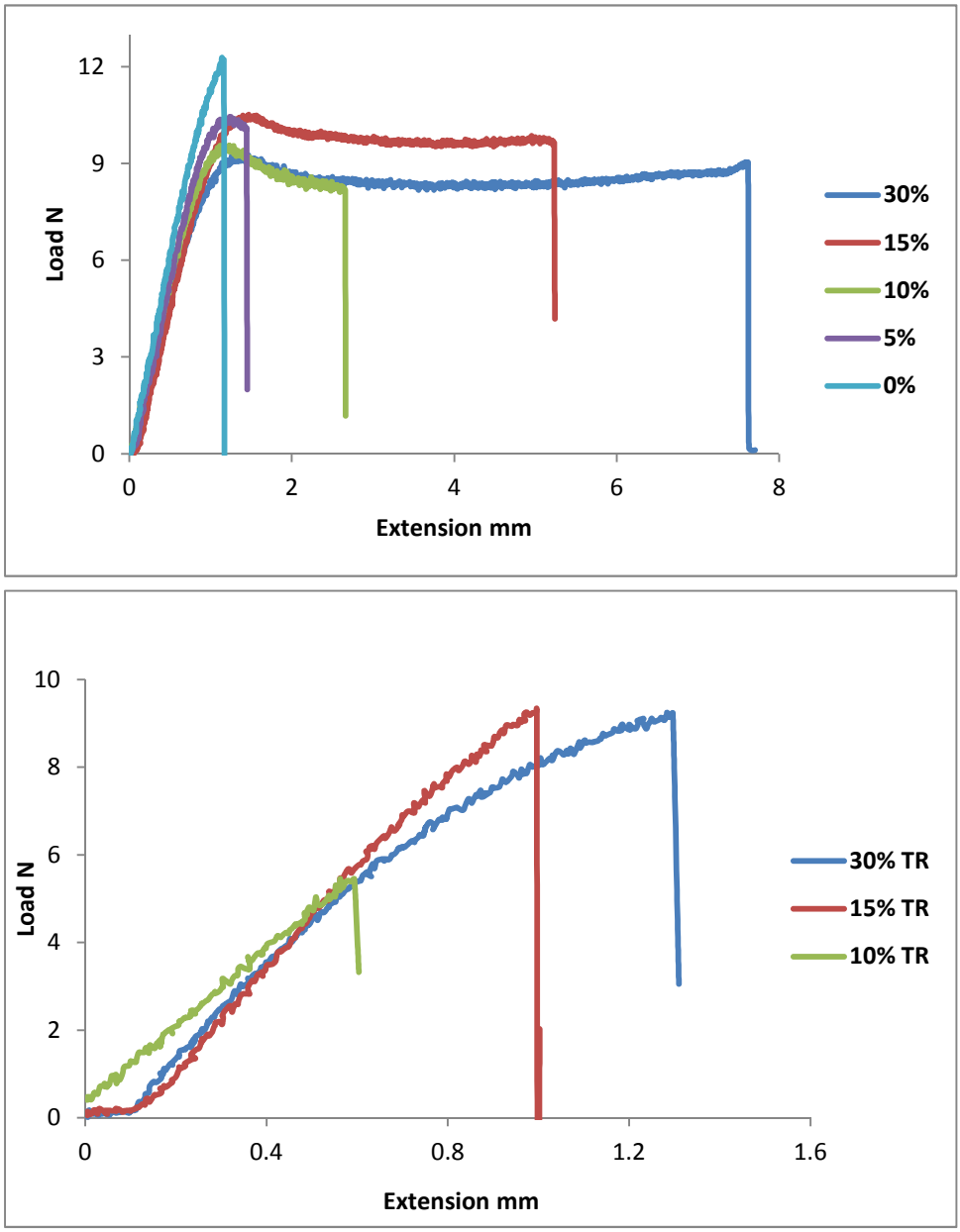

Figure 3.13 Instron data curves. Top one is for TR precursor films (non-TR) and bottom one is for TR films

The weight average molecular weights of different precursor polymers are labeled in the brackets. All of the PAES-HAB-6FDA precursors exhibit high tensile strength (stress) at break (>100 MPa). Meanwhile, the elongation (strain) at break increases from 6% to 31% by incorporating PAES contents up to 30%. The tensile stress of pure PAES is ~54 MPa, and the elongation at break is ~48%.[148] The

improvement of elongation with slightly lower stress in a block copolymer with higher PAES content is mainly caused by introducing the PAES oligomer toughening agent segments into the homo TR polymer (HAB-6FDA). After the TR process, the TR films are not as tough as the TR precursor films, since both the tensile strength and elongation decrease significantly. Compared with the homo TR polymer film of 0%PAES-HAB-6FDA-TR, 30%PAES-HAB-6FDA-TR exhibits much better mechanical properties with doubled tensile strength and elongation, almost four times toughness value at break.

It is well-known that deterioration of the mechanical properties of these TR membranes is largely due to the decomposition that occurs during the thermal rearrangement process at high temperatures.[135, 149] In order to demonstrate the effect of molecular weight on mechanical properties, two 15% PAES block copolymers, low (M_w~45kDa) and high (M_w~205kDa) molecular weights, were measured. Before the TR process, the low and high MW films showed similar mechanical properties. After the TR process, the high MW film maintained relatively good mechanical properties while the stress and strain of the low MW film dropped dramatically to only half of those properties of the high MW film.

Table 3.5 Summary of tensile properties of PAES-HAB-6FDA copolymers

	Stress (MPa) @ break	Strain % @ break	Modulus (GPa)	Toughness** (MPa)	TR conversion %
0% (81.7kDa)*	101±6	6.4±0.8	2.06±0.09	4.70±1.70	NA
0% TR (81.7kDa)	59±10	2.3±0.4	2.61±0.16	0.91±0.34	80.0
5% (282kDa)	126±2	6.1±0.7	3.51±0.07	6.35±1.31	NA
5% TR (282kDa)	99±6	3.3±0.5	3.19±0.25	2.33±0.59	51.5
10% (300kDa)	123±5	7.6±0.2	3.27±0.12	8.33±2.64	NA
10% TR (300kDa)	60±10	2.0±0.3	3.13±0.11	0.72±0.27	54.2
15% (205kDa)	122±2	13.5±0.7	3.10± 0.19	22.90±5.95	NA
15% TR (205kDa)	88±8	3.3±0.3	2.90±0.26	1.82±0.35	78.0
30% (207kDa)	108±1	31.0±0.3	2.82±0.11	30.91±3.40	NA
30% TR (207kDa)	105±16	4.7±0.3	2.55±0.33	3.30±0.51	87.7

Note: *the weight average molecular weights are included in brackets.

** Toughness is value of the area under the stress/strain curve.

Recently, some studies showed that mechanical properties of the thermally rearranged polymers can be improved by combining TR polymers with other materials. Li et al. reported that TR polymers derived from spirobisindane-containing polyhydroxyimides yielded good tensile stress (70-95 MPa) with very high elongations at break (15%-20%), which were about four times higher than those of the TR polymers from this study.[150] Scholes et al. blended a thermally rearrangable polyhydroxyimide (HAB-6FDA) with a "non-TRable" polyimide (4MPD-6FDA) (2,3,5,6-tetramethyl-1,4-phenylene diamine (4MPD)) that provided additional flexibility. For example, with 25 wt% of 4MPD-6FDA in the blend, tensile stress and elongation at break increased by 40% and 190%, respectively, relative to those of HAB-6FDA TR polymers.[151] Zhuang et al. reported mechanically tough, TR random/block poly(benzoxazole-co-imide)s with tensile strengths of 72−114 MPa and elongations at break of 5−16%, with a ~40% increase of tensile strengths and ~60% increase of elongation, relative to those of HAB-6FDA TR polymers.[146, 152] Liu et al. demonstrated the effect of 2,2'-bis(3-amino-4-hydroxyphenyl)-hexafluoropropane (APAF) content on the mechanical property change of random copolyimides of APAF/HAB-6FDA. These APAF/HAB-6FDA TR copolymers had tensile strengths of 65-77 MPa and elongations at break of 2.5−3.7% while HAB-6FDA TR homopolymers had a tensile strength of 85 MPa and elongations at break of 4.0%.[149] It is difficult to directly compare the mechanical property data among different systems due to different methods and conditions utilized, including synthesis, film casting, TR process, and tensile test, etc. However, it is feasible to evaluate the

improvement of mechanical properties by comparing strengths and elongations of the toughened polymers with those of corresponding non-toughened polymers. Take 30%PAES-HAB-6FDA as an example, doubled tensile strength and elongation at break were obtained after PAES toughening, while in previous studies about enhancement of 0-40% in tensile strength and 0-300% in elongation. Therefore, the above discussion demonstrate that our PAES toughened TR polymer films have some advantages over other toughened TR systems, especially in improving tensile strength.

3.5 Conclusions

Thermally rearranged (TR) block copolymers were prepared from a series of PAES oligomers based on HAB-6FDA polyhydroxyimide precursors. Potentiometric titration was used to determine the number average molecular weight of the PAES oligomer to ensure a perfect stoichiometry for step-growth polymerization of high molecular weight block copolymers. Structures of the PAES oligomers and block copolymers were confirmed by ^{1}HNMR. FTIR-ATR was used to confirm the structural changes of the polyhydroxyimides during the TR process. Thermogravimetric analysis (TGA) showed similar thermal stability and rearrangements (weight loss in TR region) for all precursor film samples. As the PAES toughening agent content was increased, TR conversion increased due to better chain mobility provided by PAES structures. In addition, mechanical properties of the

membranes increased after introducing PAES. The 30%PAES-HAB-6FDA block copolymers exhibited the best mechanical properties with doubled tensile strength and elongation at break compared with the homo TR polymer 0%PAES-HAB-6FDA.

CHAPTER 4: POLY(PHENYLENE-OXIDE) BASED COPOLYMERS FOR GAS SEPARATION MEMBRANES

Jarrett R. Rowlett,[a] Qiang Liu,[b] Wenrui Zhang,[a] Joshua D. Moon,[b] Michelle E. Dose,[b] Judy S. Riffle,*[a] Benny D. Freeman,[b] James E. McGrath[a]

[a] Macromolecules Innovation Institute, Department of Chemistry, Virginia Tech, 325 Stanger Street, 133 Kelly Hall, Blacksburg, VA 24061, USA

[b] Department of Chemical Engineering, Texas Materials Institute, Center for Energy and Environmental Research, The University of Texas at Austin, 10100 Burnet Road, Bldg. 133, Austin, TX 78758, USA

From J. Mater. Chem. A, 2016,4, 16047-16056. Used with permission of Royal Society of Chemistry, 2017.

4.1 Abstract

Poly(phenylene oxide)-poly(arylene ether ketone) (PPO-PAEK and PPO-PAEKK) copolymers were prepared by polycondensation of a difunctional poly(2,6-dimethylphenylene oxide) oligomer with 4,4'-difluorobenzophenone or 1,3-bis(4-fluorobenzoyl)benzene respectively and their properties were compared to a homopolymer from 2,2-bis(4-hydroxy-3,5-dimethylphenyl)propane (tetramethylbisphenol A, TMBPA) and difluorobenzophenone. The polymers were cast into films, then crosslinked in the solid state with UV light with the wavelength of 365-nm at room temperature to form asymmetrically crosslinked thermoset membranes with high gel fractions. This approach offers a means for fabrication of

membrane films, fibers or composites, as well as tuning of gas transport properties through crosslinking in the solid state. Structural analysis via NMR, IR, and UV-vis spectroscopy confirmed the expected copolymer compositions and provided support for a free radical crosslinking reaction involving coupling between the aromatic ketone and labile benzylic methyl groups. Introduction of the ketone group resulted in a decrease in permeabilities, but an increase in selectivities for O_2/N_2 and CO_2/CH_4 gas pairs over unmodified PPO. Additionally upon crosslinking a large shift was seen in the gas properties of all the membranes, with permeability decreasing and the selectivity increasing for the O_2/N_2 and CO_2/CH_4 gas pairs.

4.2 Introduction

Poly(2,6-dimethylphenylene oxide) (PPO) and its derivatives have been extensively studied as potential membranes for CO_2/CH_4 separation systems.[4, 153] These polymers, like many other glassy polymers, are of interest for gas separation applications because of their excellent transport properties, and specifically PPO due to its high permeability.[22-23, 26] The high permeability of PPO is primarily attributed to enhanced gas diffusion through increased free volume induced by the disruption of chain packing by the methyl groups on the polymer backbone.[154] This high permeability makes it extremely attractive for gas separation applications, unfortunately the selectivity of the PPO membrane is too low for many gas separation applications.

Derivatives of PPO have included modifications of the polymer by electrophilic

aromatic substitution with bromo, nitro, sulfonic acid, and other various groups on the open ortho positions on the aromatic backbone.[55-57, 67, 155] Additionally, effects of side chain substitution have been investigated with carboxylation and esterification of the methyl substituent, and also replacement of the methyl group with aromatic rings.[156-159] Bromination of PPO causes a stark increase in permeability over that of the unmodified PPO, with relatively little decrease in gas selectivity, resulting in highly permeable PPO membranes.[56, 155] The addition of the bromine groups increase the free volume and disrupt the packing density of the PPO polymer chains. In contrast for nitrated PPO copolymers, relative to untreated PPO, selectivity increases and permeability decreases.[67] Nitrile and other polar groups seem to have a minimal effect on the density of PPO membranes, with the polarity of the groups resulting in a decrease in torsional motion of the polymer chains which results in higher selectivity and lower permeability. Thus depending on the nature of the groups added to PPO, gas properties can be significantly changed in either direction. However even with modification, all PPO systems, including PPO homopolymer, have potential issues with insufficient thermal and oxidative stability due to the presence of the aromatic methyl substituents present in the backbone of the PPO polymer. Removal of these groups with derivatives such as poly(2,6-diphenylphenylene oxide), which uses the aromatic ring in place of the methyl groups, results in higher stability membranes.[154, 156-157, 160] However, the methyl groups seem essential to the strong gas properties as these deviates perform very poorly and permeability is significantly reduced.

While significant work has been done on PPO modifications, relatively little

research has focused on synthesis of copolymers containing PPO.[161-163] This would seem to be a great option as the PPO and methyl group structure would be maintain, while allowing for altering of polymer and gas transport properties with selection of a comonomer or secondary phase. Though, one primary obstacle has been that PPO is synthesized by a conventional oxidative polymerization process, which produces monofunctional polymers.[48, 164-166] This is problematic as traditional copolymerization cannot be easily performed for PPO using the oxidative polymerization process, and with monofunctional polymers, only diblock copolymers can be synthesized. To obtain difunctionality in the PPO polymer, the 2,6-dimethylphenol monomer needs to be polymerized with a difunctional/dihydroxyl compound such as a tetramethyl-substituted bisphenol derivative, e.g. 2,2',6,6'-tetramethyl-4,4'-biphenol, 4,4'-methylenebis(2,6-dimethylphenol), or 2,2-bis(4-hydroxy-3,5-dimethylphenyl)propane). These compounds allow the PPO to grow off the hydroxyl groups which builds the polymer chain, with the molecular weight being controlled by the amount of the difunctional compound used.24-26 These reactions require precise conditions with low oxygen flow rates and longer reaction times to ensure inclusion of the difunctional comonomer. These strict reaction conditions may be due to reduced reactivity of the ortho-substituted bisphenol moiety over the 2,6-dimethylphenol monomer. Difunctionality can also be achieved by using a quinone coupling reaction with low molecular weight PPO to produce difunctional oligomers.[167] Once synthesized however, the difunctional oligomers can be used to produce copolymers in various step-growth polymerization

reactions.[161-162]

Thus, the authors aim to create copolymers in this study utilizing a difunctional PPO oligomer and difluoroketones to produce ketone containing PPO copolymers. The inclusion of the ketone attempts to increase the selectivity of PPO, along with providing a source for possible UV crosslinking. Crosslinking could potentially further increase selectivity and stability, along with resistance to CO_2 plasticization, which has been seen in aromatic polyimides after crosslinking.[32, 168-171] Additionally, the authors could find very few reports of gas transport properties of PPO copolymers.[172-173] Therefore, a study of the effect of copolymerization of PPO on its gas transport properties represents an important addition to the gas separation membrane field. With the designing of crosslinked PPO copolymers potentially providing a new class of membranes with outstanding and variable gas transport properties.

This chapter reports the synthesis, characterization, crosslinking, and gas transport properties of novel poly(2,6-dimethylphenylene oxide)-poly(arylene ether ketone) (PPO-PAEK) and poly(2,6-dimethylphenylene oxide)-poly(arylene ether ketone ketone) (PPO-PAEKK) copolymers. These were cast into films (15-25 microns thick), then crosslinked via UV irradiation. The copolymers were synthesized by polycondensation of a difunctional PPO oligomer with difluorobenzophenone or bis(4-fluorobenzoyl)benzene. The PPO copolymers were compared to PPO, industrial standards, and a poly(arylene ether ketone) prepared from tetramethylbisphenol A and difluorobenzophenone to elicit effects of polymer structure on the membrane and

transport properties. In addition, effects of crosslinking and ketone concentration in these membranes on gas transport properties have been investigated.

4.3 Experimental

Materials

Difunctional poly(phenylene oxide) (PPO) oligomers were purchased from Sabic and had a number average molecular weight of ~1,650 g/mol. 2,6-Dimethylphenol (2,6-xylenol, 99+%), 1,3-bis(4-fluorobenzoyl)benzene, and N,N-dimethylacetamide (DMAc) were purchased from Sigma-Aldrich. DMAc was distilled from calcium hydride before use. 4,4'-Difluorobenzophenone and 2,2-bis(4-hydroxy-3,5-dimethylphenyl)propane (tetramethylbisphenol A, TMBPA, 99+%) were purchased from TCI America. Reagent grade potassium carbonate (K2CO3) was purchased from Fisher Scientific and dried under vacuum at 180oC prior to use. Toluene, isopropanol, ethanol, acetic acid, and chloroform were obtained from various sources and used as received.

Synthesis of poly(phenylene oxide)-poly(arylene ether ketone) copolymers (PPO-PAEK, PPO-PAEKK) and the tetramethylbisphenol A-based poly(arylene ether ketone) homopolymer (TMBPA-BP)

The copolymers were synthesized via nucleophilic aromatic substitution and was performed as follows: a difunctional PPO oligomer of ~1,650 g/mol (8.70 g, 5.27 mmol), difluorobenzophenone (1.15 g, 5.27 mmol), and DMAc (50 mL) were charged

into a 100-mL, 3-neck, round-bottom flask equipped with a mechanical stirrer, nitrogen inlet and Dean-Stark trap. The mixture was heated to 140oC and stirred until the monomers were completely dissolved. Once dissolved, K_2CO_3 (1.10 g, 7.96 mmol) and toluene (25 mL) were added into the flask. The reaction was allowed to reflux at 140^{o}C for 4 h to azeotropically remove water from the system and then it was slowly heated to 160^{o}C to remove the toluene. The reaction was allowed to proceed at 160^{o}C for 12 h and then cooled to room temperature. After 12 h the solution was very viscous, and was diluted with 50 mL of DMAc. Filtration of the solution to remove the by-product salt was difficult. Therefore, the product was precipitated into boiling DI water to afford a white fibrous product. Afterwards, the copolymer was stirred in DI water (~80^{o}C) overnight to remove any residual salt or solvent, filtered, and then dried in vacuum at 180^{o}C for 24 h. Yield was nearly 90% or higher for all of the polymers. The PPO copolymer utilizing 1,3-bis(4-fluorobenzoyl)benzene was synthesized in the same fashion.

The tetramethylbisphenol A-containing poly(arylene ether ketone) (TMBPA-BP) was synthesized by dissolving tetramethylbisphenol A (7.1098 g, 25 mmol) and difluorobenzophenone (5.4550 g, 25 mmol) in DMAc (90 mL) with excess K2CO3 (8.3 g, 60 mmol) and toluene (25 mL). After the monomers and base fully dissolved, the solution was gradually heated to 155°C over 3 h. The polymerization was allowed to proceed for 20 h and then cooled to 90°C. While still at 90°C, the synthesis solution was precipitated in 20 vol% acetic acid in DI water. To remove residual solvent and impurities, the polymer was extracted in pure DI water for 24 h, filtered,

boiled in ethanol for 3 h, filtered and washed with fresh ethanol, and dried under vacuum at room temperature for 18 h.

Membrane preparation

PPO copolymers were dissolved in DMAc (~4% w/v) and filtered using a high-pressure, 0.45-μm filter with a nitrogen pressure of 1500 psi. The resultant solution was cast onto a clean glass substrate, dried in vacuum at 80ºC for 12 h, and then in vacuum at 150ºC for an additional 12 h. Membranes were removed from the glass substrates by immersion into a DI water bath. Films with thicknesses ranging between 12-26 microns were dried at 150ºC overnight in vacuum prior to testing to remove any absorbed water or residual solvent. TMBPA-BP films were prepared via solution casting using chloroform as the solvent. After about 0.5 g of polymer was dissolved in 10-15 mL of chloroform, the solution was filtered through a 1.0 μm polytetrafluoroethylene (PTFE) syringe filter. The solution was then cast onto a clean, leveled glass plate, heated at 80 ºC under partial vacuum for 24 h, and then heated at 100 ºC at full vacuum for 24 h. After the film was peeled off the glass plate, the films was heated again at 100 ºC for 24 h. DMAc was chosen for the PPO copolymers as they had limited solubility in chloroform. Additionally, the TMBPA-BP polymer was cast using chloroform rather than DMAc since its lower boiling point allowed the solvent to be removed at lower temperatures, which was desirable due to concerns over the thermal stability of the homopolymer. Film thickness were between 14 – 20 microns.

UV crosslinking

UV crosslinking was performed via a mercury longwave UV lamp (UVP, Model B-100) equipped with a 365-nm light filter at room temperature with an intensity of 17 mW/cm^2. Each sample was irradiated in air at a distance of 3.5 cm from the UV lamp for 1 h per side.

UV-vis Spectroscopy

The Beer-Lambert law can be used to estimate the UV intensity, I, at any point in a film:

$$I = I_0 \times 10^{-ECD} = I_0 \times 10^{-A} \quad (4\text{-}1)$$

where I_0 is the UV incident intensity, E is the extinction coefficient, C is the concentration of the photoactive species, D is the path length, and A is the UV absorbance. The extinction coefficient can be determined using the absorption spectra for each polymer.[123, 149]

Characterization

^{1}H and ^{19}F NMR analysis was performed on a Varian Inova spectrometer operating at 400 MHz (376 MHz for ^{19}F NMR). Spectra were obtained from 1 mL of a 15% (w/v) solution in CD_2Cl_2. The PPO-PAEK copolymers had limited solubility in $CDCl_3$ so CD_2Cl_2 was used instead. Glass transition temperatures (Tg's) were determined by differential scanning calorimetry (DSC) with a TA Instruments DSC Q-200 under nitrogen gas with a heating rate of 10^{o}C/min. DSC spectra were conducted in the temperature range of 150-350^{o}C. The samples were first held isothermally at 150^{o}C for 5 min to remove any residual solvents. Glass transition

temperatures were determined from the second scan. Fourier Transform Infrared Spectroscopy with attenuated total reflectance (FTIR-ATR) was performed to observe carbonyl groups in the PPO-PAEK copolymers, the TMBPA-BP homopolymer, and their corresponding crosslinked membranes. Observance of the carbonyl groups were used for conformation of crosslinking in the polymer membrane samples, via disappearance of the benzophenones peaks from the uncrosslinked membranes and appearance of hydroxyl and oxidation peaks in the crosslinked membranes. The FTIR-ATR spectra were recorded on an FTIR spectrometer (Agilent Technologies Cary 630 FTIR) equipped with an ATR attachment with a diamond crystal. The spectral resolution was 4 cm^{-1}, and 32 background scans were performed. A small amount of polymer film was placed on the diamond crystal, and the FTIR spectrum was measured with 32 scans. Spectrums were normalized via the peak at 1200 cm^{-1}. Number average molecular weight of the difunctional PPO oligomer was obtained via a multi-detector size-exclusion chromatography system with an isocratic pump (Agilent 1260 infinity, Agilent Technologies) with an online degasser (Agilent 1260, Agilent Technologies), using chloroform as the mobile phase (30ºC) with 3 PLgel 10 μm mixed-B 300 x 7.5 mm columns in series with a Wyatt Viscostar II Viscometer, a Wyatt Heleos II multi-angle light scattering detector, and a Wyatt T-Rex refractive index detector.

Gel fractions

Gel fractions of the crosslinked samples were measured by extraction using a Soxhlet extractor (Wilmad-LabGlass, Vineland, NJ, USA). DMAc was used for both

the PPO copolymers and the TMBPA-BP homopolymer, with approximately 20 mg of material for each sample. The initial mass of the film was weighed before the sample was extracted. Crosslinked polymers were extracted by refluxing with DMAc. After 24 h, the crosslinked samples were heated for 24 h under vacuum, and then the final film mass was recorded. Gel fractions were calculated by Equation 4-2:

$$\text{Gel Fraction} = W_{final}/W_{initial} \times 100\% \quad (4\text{-}2)$$

Pure gas permeability measurements

Pure gas permeabilities of H_2, N_2, CH_4, O_2 and CO_2 were measured using a constant volume, variable pressure apparatus.[10, 138] The film sample was housed in a stainless steel Millipore filter holder (Millipore, Billerica, MA, USA).[138] Upstream pressure was measured with a Honeywell Super TJE 1500 psi transducer (Honeywell Sensotec, Columbus, Ohio, USA), and downstream pressure was measured using a MKS Baratron 626 transducer (MKS, Andover, MA, USA). Pressure readings were recorded using National Instruments in either LABVIEW or Python software. All of the permeation experiments were conducted at 35^{o}C with feed pressures ranging from 3 to 17 atm.

4.4 Results and Discussion

Synthesis of the tetramethyl bisphenol A-benzophenone (TMBPA-BP) homopolymer and PPO block copolymers

Figures 4.1 and 4.2 display the reaction schemes employed for the PPO block copolymers and tetramethylbisphenol A poly(arylene ether ketone) homopolymer.

Difunctional PPO oligomers were reacted with difluorobenzophenone or bis(4-fluorobenzoyl)benzene via step growth polycondensation to form fibrous polymeric materials. The difunctional PPO oligomer obtained from Sabic was believed to be synthesized by introducing 2,2-bis(4-hydroxy-3,5-dimethylphenyl)propane (tetramethylbisphenol A) into the PPO oligomer. This was supported by the ^{1}H NMR spectrum of the final block copolymers that showed the bridging methyl groups in the upfield region of the spectrum (Figure 4.3, 1.7 ppm). A molecular weight of ~1650 g/mol was calculated for the PPO oligomer via ^{1}H NMR spectroscopy and confirmed with SEC. A 1:1 mole ratio was used between the oligomers and the difunctional ketone monomers in order to achieve high molecular weights. The progress of the reactions was monitored via ^{19}F NMR spectroscopy by noting the disappearance of the fluorine substituents of the benzophenone moieties.

Two reactions were conducted with the difunctional PPO oligomer, one with the monoketone difluorobenzophenone monomer and a second with the diketone monomer, bis(4-fluorobenzoyl)benzene. This created two PPO copolymers with a varied amount of ketone relative to benzylic methyl groups in the copolymers. The PPO copolymer with the monoketone monomer is referred to as PPO-PAEK and the diketone copolymer is referred to as PPO-PAEKK. The addition of the diketone monomer created approximately twice the ratio between the benzylic methyl to ketone content in the PPO copolymer (Table 4.1). Additionally the PPO-PAEK copolymer had approximately 10 wt% of the copolymer corresponding to the ketone

monomer, 15 wt% corresponding to the tetramethylbisphenol A moieties, and 75 wt% of the PPO, while the PPO-PAEKK had 15 wt%, 14 wt%, and 71 wt% respectively. To make a series for comparing properties with a varying level of ketone to benzylic methyl compositions, tetramethylbisphenol A was also polymerized with difluorobenzophenone to produce the poly(arylene ether ketone) homopolymer (Figure 4.2). This homopolymer was prepared using a previously reported procedure and had the highest value of ketone inclusion with ~ 39 wt% of the composition corresponding to the ketone-containing monomer and a 4:1 ratio of benzylic methyl relative to ketone groups (Table 4.1).[174] The compositions of the polymers were confirmed with ^{1}H NMR spectroscopy as depicted in Figure 4.3. Clear and transparent membranes were obtained upon casting of the polymers from their corresponding solutions.

Table 4.1 Composition of TMBPA-BP and Ketone-Containing PPO Copolymers

Sample	PPO wt%	TMBPA wt%	Ketone Monomer wt%	Benzylic Methyl to Ketone Ratio
TMBPA-BP	-	61	39	4:1
PPO-PAEKK	71	14	15	14:1
PPO-PAEK	75	15	10	28:1

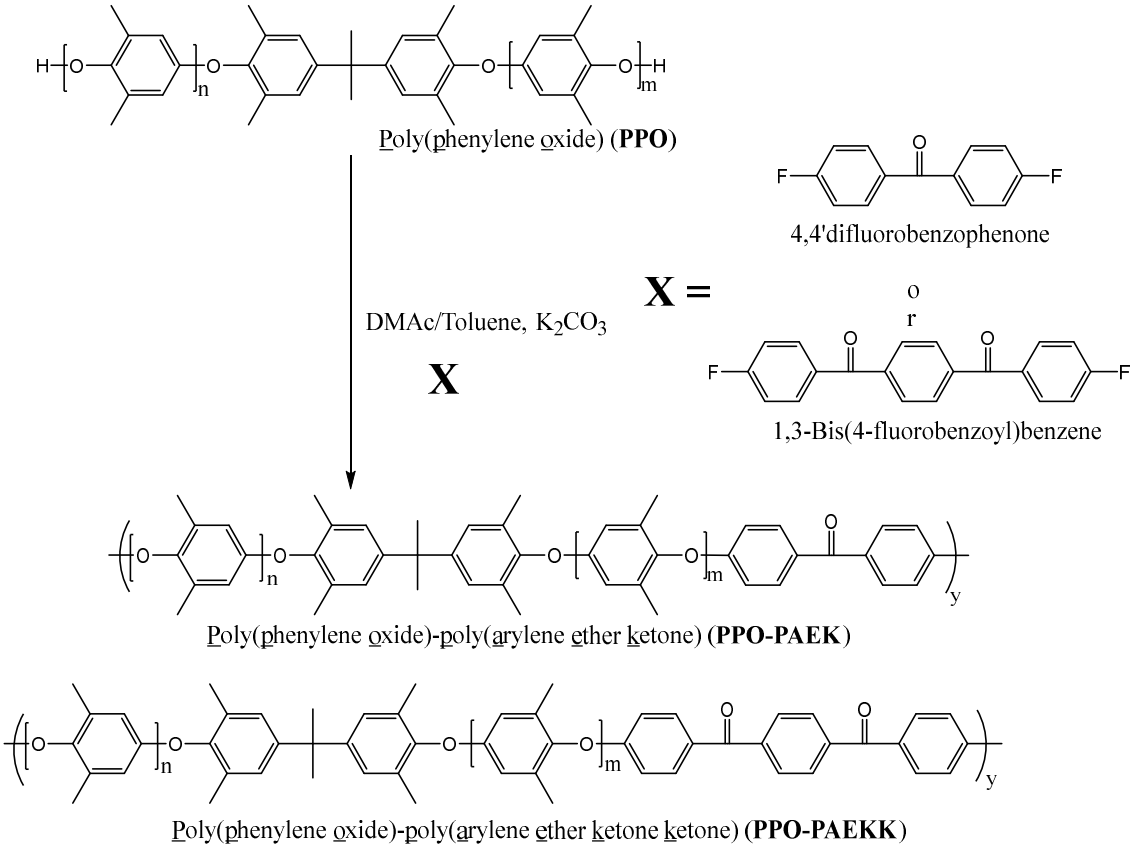

Figure 4.1 Synthesis of poly(phenylene oxide)-poly(arylene ether ketone) copolymers

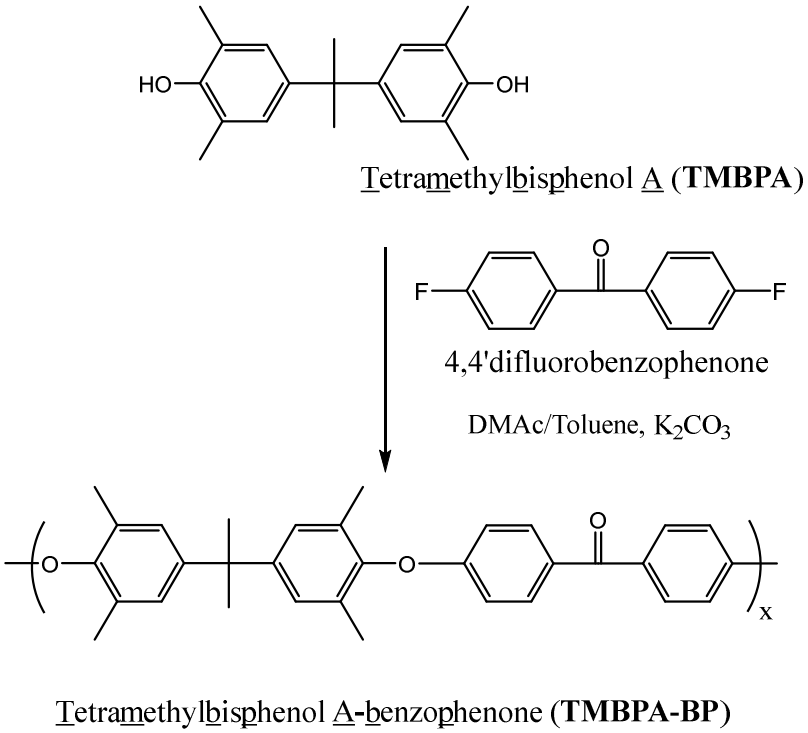

Figure 4.2 Synthesis of tetramethylbisphenol A poly(arylene ether ketone) homopolymer TMBPA-BP

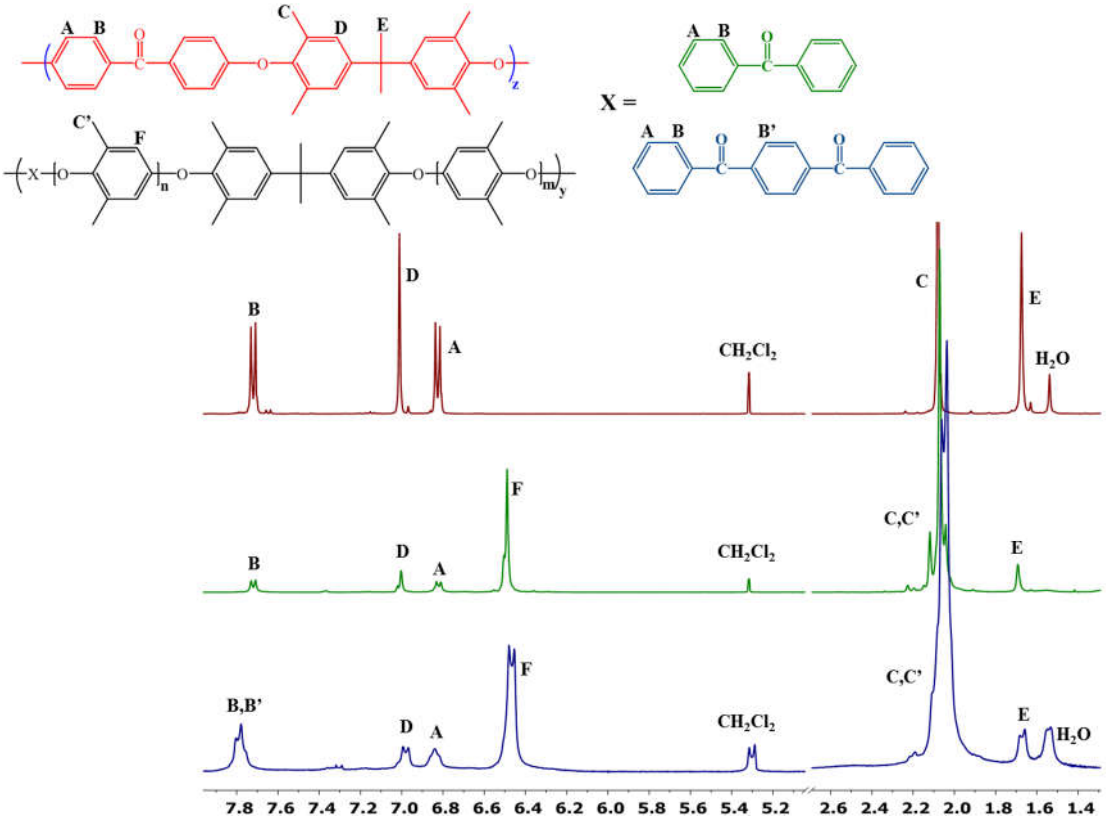

Figure 4.3 ^{1}H NMR spectra of the copolymers and homopolymer: (top) TMBPA-BP, (middle) PPO-PAEK, and (bottom) PPO-PAEKK.

Crosslinking and characterization

The PPO copolymers and TMBPA-BP homopolymer membranes were crosslinked using 365 nm UV light to produce membranes with high gel fractions (Table 4.2). The UV crosslinking most likely occurred through excitation of the carbonyl group from the singlet to triplet state and then intermolecular hydrogen abstraction of a benzylic hydrogen, followed by coupling of the benzylic radical with the benzophenone carbon. This mechanism has been studied and proposed by many different groups utilizing benzophenone as a crosslinking agent. Figure 4.4 presents the proposed mechanism for the UV crosslinking.[112, 123, 125, 175-177] In this paper, the

crosslinked samples are designated as PPO-PAEK XL, PPO-PAEKK XL, and TMBPA-BP XL, with XL being the acronym indicating crosslinking.

After UV irradiation, a hydroxyl peak (~ 3500 – 3100 cm^{-1}) developed in the FTIR spectra of both PPO films (Figure 4.5). Although very broad, this peak was clearly absent in the non-crosslinked films. This absorption was consistent with the proposed UV light-activated mechanism, with formation of alcohol groups upon irradiation of the membranes.[125] In addition to the hydroxyl formation, treatment of the membranes resulted in the formation of a new carbonyl peak (~1750 cm^{-1} in both crosslinked spectra). Similar observations were made in previously reported work using UV irradiation and benzophenone to induce crosslinking.[179] This peak's origin most likely resulted from side reactions in an oxidation process, forming carboxylic acids. In addition, although there is only a small fraction of benzophenone in the PPO copolymers, a UV absorption attributed to the benzophenone is visible in both spectra of the non-irradiated copolymers.[123, 175] This peak is located at 1650 cm^{-1} in the FTIR spectra, and after crosslinking, this benzophenone peak is reduced, indicating loss of the benzophenone absorption.[124, 179] Combined, these three factors make a strong case for the suggested crosslinking mechanism of the benzophenone and benzylic methyl-containing polymers. As the composition of the TMBPA-BP copolymer was greatly different from the PPO copolymers, a direct IR comparison was not made between the homopolymer and copolymers. Nevertheless, the appearance of the hydroxyl and oxidized carbonyl peak, along with disappearance of the benzophenone was still evident.

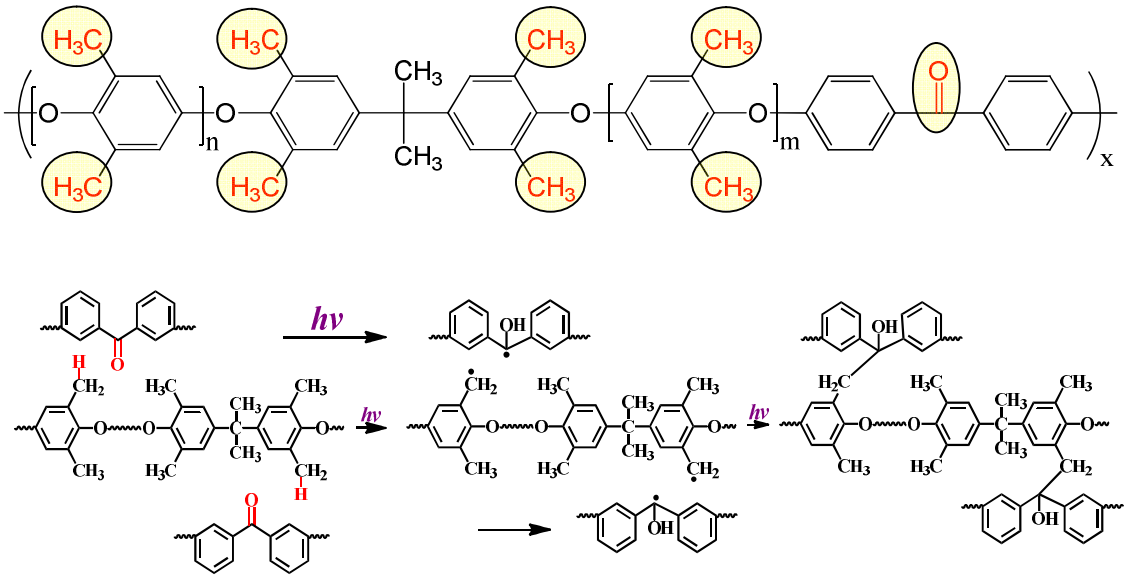

Figure 4.4 The proposed UV crosslinking mechanism for the PPO-PAEK copolymer[112, 123, 125, 175-177]

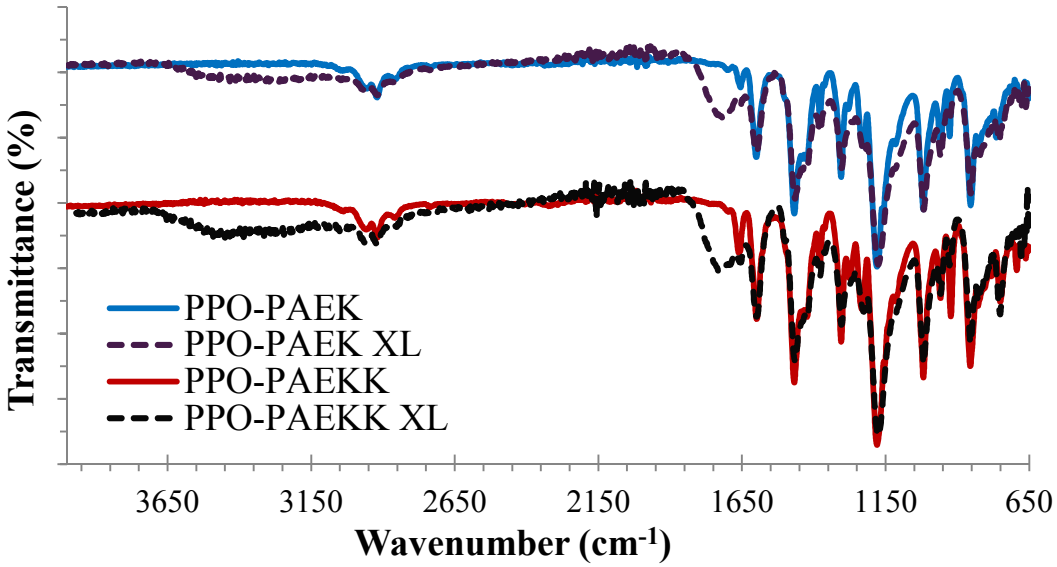

Figure 4.5 IR spectra of crosslinked and non-crosslinked ketone-containing PPO copolymers normalized with peak at ~1200 cm^{-1}. PPO-PAEK is the top spectra and PPO-PAEKK is the bottom.

Table 4.2 compares the gel fractions and glass transition temperatures (Tg's) of the linear and crosslinked films with those of the pure PPO films. The glass transition

temperature of PPO was obtained from the literature.[67] All of the crosslinked polymers had high gel fractions, which confirms that UV irradiation is producing crosslinked membranes for the benzophenone-containing polymers presented in this manuscript. Additionally, as presented in Table 2, the Tg increases after UV irradiation with TMBPA-BP XL having the largest increase in Tg. One would expect that highest crosslinking would occur in the polymers with the highest concentration of benzophenone. This is because the proposed crosslinking mechanism requires both methyl and ketone moieties, and therefore if a smaller fraction of benzophenone ketones are used, this may have a direct effect on the amount of crosslinking (see Table 1 for benzylic methyl to ketone ratio). Thus, the higher fraction of ketone functional groups in the TMBPA-BP and PPO-PAEKK polymers provides more crosslinking sites closer together, as the ketone moiety is the limiting factor.

In comparing and quantifying the amount of crosslinking occurring in the membranes we have two pieces of evidence, which is gel fraction and change in glass transition temperature. As bulk films are used, IR analysis can really only provide information about the surface of the polymer membranes. Both of these data are important as although the PPO-PAEK and TMBPA-BP membranes can have the same amount of chains that are crosslinked (gel fraction), the TMBPA-BP membrane contains many more crosslinking sites and therefore has the potential for higher crosslink density (Figure 4.6). This is supported by the results of thermal analysis, which showed a clear difference in the change of glass transition temperatures. The thermal analysis showed that with higher concentration benzophenone a higher crosslink density is

seen. However, this trend was not so clear in the gel fraction results, with the lowest gel fraction occurring for the PPO-PAEKK membrane.

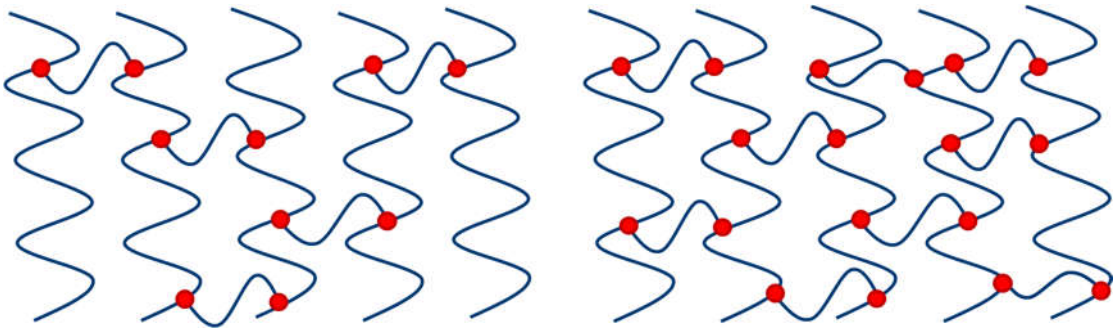

Figure 4.6 A scheme representing difference between crosslinking percentage and crosslink density. In both figures all of the chains are crosslinked (100 percent crosslinked). However, the chains in the right figure contain more crosslink sites. Thus, the figure on the right has a higher "crosslink density".

Table 4.2 Comparison of crosslinked and non-crosslinked PPO-PAEK and TMBPA-BP

Sample	Gel Fraction (%)	T_g (°C)
PPO Oligomer	-	136
PPO	-	207
PPO-PAEK	-	209
PPO-PAEK XL	95	216
PPO-PAEKK	-	207
PPO-PAEKK XL	84	227
TMBPA-BP	-	217
TMBPA-BP XL	95	238

While there is no question that the polymer films underwent crosslinking, anytime bulk films are used with a UV source, concerns must be made towards crosslinking homogeneity.[178-179] With high adsorption of the UV light, full penetration of the UV light into the membrane might be prevented, resulting in asymmetric films. Some evidence supports this hypothesis, as the PPO-PAEKK film had the lowest gel fraction but had a significantly higher change in glass transition temperature than the

PPO-PAEK membrane. To better gauge what was happening with these membranes, UV-vis analysis was conducted to see how strongly the light at 365 nm was being absorbed by each membrane. Furthermore by using the Beer-Lambert law, the intensity and adsorption of the incumbent light was calculated as a function of film thickness. The UV-vis spectra for each film and the absorbance normalized for the film thickness is shown in Figure 4.7. The UV intensity profile at 365 nm was calculated for both sides of the film receiving the same amount of irritation.

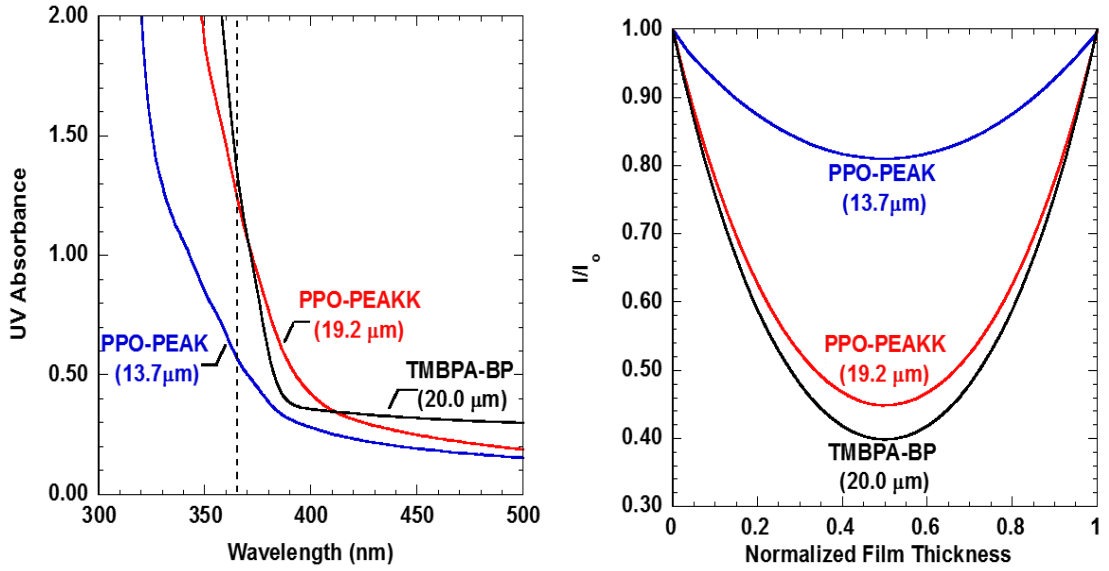

Figure 4.7 (A) UV-vis spectra for the ketone containing films, and (B) calculated UV intensity profile at 365 nm for the films irradiated on both sides.

From the UV-vis data it was discovered that there was a large difference in the absorption behavior and uniformity between the PPO-PAEK and the higher ketone containing films PPO-PAEKK and TMBPA-BP. While PPO-PAEK shows only a small difference between the UV intensity at the center and the edges of the film (0.5 is the center, 0 and 1 are the edges), the PPO-PAEKK and TMBPA-BP films had a much larger difference, with less than fifty percent intensity reaching the center.

Although the PPO-PAEK is a slightly thinner film compared to the other two polymer films, it doesn't fully explain the vast difference between the absorption behaviors. This is because the higher ketone containing films absorbed a higher amount of the UV light at 365 nm. In fact, the absorption of the PPO-PAEKK and TMBPA-BP films was more the double than that of the PPO-PAEK film. Thus, the higher ketone content in the PPO-PAEKK and TMBPA-BP films allows for more adsorption of the UV light though excitation of the ketone groups. These factors would cause a greater non-uniformity in crosslinking of the membranes as the high absorbance is inhibiting full penetration of the UV light into the middle of the membrane. Based on the UV-vis data and the gel fraction and DSC results, it can be assumed that the crosslinking in the membranes are asymmetrical, with higher non-uniformity being seen in the PPO-PAEKK and TMBPA-BP films.

In order to ensure that full crosslinking uniformity is occurring, thin films would have to be used. However when going to thin films, studies of the TMBPA-BP homopolymer showed that physical aging was highly prevalent, and required films of less than 150 nm thickness to get 90% intensity in the center of the films.[149] Nevertheless to truly gauge the material properties of the crosslinked systems, thin films studies should be conducted in the future, but are beyond the scope of this paper. This same reservation of crosslink uniformity should also be applied to the gas properties of the crosslinked membranes, as high asymmetry would provide a surface layer effect for the membranes.

Gas transport properties

Pure gas transport properties of the benzophenone-containing membranes are displayed in Table 4.3, with the transport properties of PPO-PAEK, PPO-PAEKK, TMBPA-BP, and the crosslinked polymers compared with literature values for PPO, polysulfone (PSF), and Matrimid.[26, 67] Furthermore the polymeric membranes are plotted on the upper bound for CO_2/CH_4 and O_2/N_2 gas pairs in Figure 4.8. Based on the pure gas results it was perceived that addition of the ketone into the PPO polymer resulted in a decrease in permeability for all the gases and an increase in the selectivity for CO_2/CH_4 and O_2/N_2 gas pairs in the uncrosslinked membranes. This formed a trend with the lowest permeability and highest selectivity recorded for the TMBPA-BP polymer film and the highest permeability and lowest selectivity occurring in the PPO-PAEK polymer film. After crosslinking, all of the polymers showed a significant increase in selectivity, with a 35-50% increase in CO_2/CH_4 and a 12-20% increase in O_2/N_2 selectivity. With only around a 50% decrease in the gas permeabilities for CO_2 and O_2. While the two non-crosslinked PPO copolymers exhibited very similar selectivities for both gas pairs, upon crosslinking the CO_2/CH_4 and O_2/N_2 selectivities of the TMBPA-BP and PPO-PAEKK-XL increased by a larger percentage than those of the PPO-PAEK-XL. However, the drop in permeability was nearly the same for all of the crosslinked polymers with every crosslinked membrane failing in the range a decrease of 54-59%. The presence of additional ketone functional groups should allow for higher crosslink densities to be achieved, and therefore inhibition of chain mobility that would lead to a decrease in permeability

and a corresponding increase in selectivity due to size-sieving. However, one would expect that with a higher increase in selectivity, a larger decrease in permeability should occur. This could also be an effect of crosslinking asymmetry in the membranes. From the UV-vis analysis it was shown that PPO-PAEKK and TMBPA-BP have much higher asymmetry than the PPO-PAEK membrane, likely resulting in membranes that are highly crosslinked at the surface and lightly crosslinked or uncrosslinked in the center. This would create a surface effect for the membranes, and help to explain the results seen in the gas properties. This effect has been seen in highly permeable membranes which undergo surface modification to create a layer of high impermeability. In these membranes a large increase in selectivity is observed without a huge penalty in permeability, similar to what was seen in the systems presented in this paper.[178-179]

In comparing the ketone-based polymers to commercial polymers such as PSF and Matrimid, all of the membranes, as well as the crosslinked derivatives, showed superior performance to the PSF membrane. In particular, the crosslinked derivatives exhibited selectivities similar to those of PSF while having permeabilities that were 2-4 times higher. In comparison to Matrimid, the PPO copolymers and TMBPA-BP exhibited gas transport properties with parallel performance relative to the commercial membrane on the upper bound plot. The PPO copolymers and TMBPA-BP homopolymer had higher permeabilities, but lower selectivities than the commercial Matrimid membrane. Furthermore, both incorporation of arylene ether ketone groups into PPO as well as crosslinking result in a shift up and to the left in the

upper bound plots in a manner that is parallel to the present upper bound lines. Addition of the ketone groups in the non-crosslinked polymers decreased the free volume in the membranes. Since benzophenone lacks the bulky methyl groups that are on the PPO polymer which could result in improved packing efficiency of the polymer chains, the observed decrease in permeability and corresponding increase in selectivity would be expected for these systems.[180]

PPO based systems have traditionally been explored as gas separation membranes for CO_2/CH_4 gas pairs.[4, 57, 153] However, the performance of the PPO based materials were also good for O_2/N_2 separation, with the values very near the 1991 upper bound. It suggests that these could also be suitable membranes for separations of O_2/N_2. Like the unmodified PPO, it is anticipated that these polymers could be fabricated into hollow fiber or spiral wound modules for gas separations. Crosslinking the membrane or hollow fiber may provide additional benefits of increased durability, operation time, mechanical properties, and resistance to CO_2-induced plasticization.[168-169] Furthermore, crosslinking would most likely result in reduced swelling and water uptake, which might be advantageous in vapor/gas separation applications that currently use unmodified PPO.[4]

Table 4.3 Gas transport properties of PPO, PPO-poly(arylene ether ketone) block copolymers, and standards in pure gases at 35°C and 10 atm.

Polymer	P_{CO_2}	P_{CH_4}	P_{N_2}	P_{O_2}	P_{H_2}	P_{CO_2}/P_{CH_4}	P_{O_2}/P_{N_2}
PPO	58.0	4.0	3.6	16.0	-	14.3	4.4
PPO-PAEK	43.2	2.7	2.4	11.3	92.0	16.2	4.7
PPO-PAEK XL	19.6	0.89	0.95	5.0	52.4	22.0	5.3
PPO-PAEKK	36.1	2.2	1.9	9.2	75.9	16.7	4.7
PPO-PAEKK XL	15.2	0.61	0.67	3.8	44.5	25.1	5.6
TMBPA-BP	18.4	0.93	0.89	4.8	45	19.8	5.4
TMBPA XL	8.4	0.29	0.34	2.1	28	29.0	6.2
Polysulfone	5.5	0.24	0.22	1.3	-	22.9	5.7
Matrimid	10.0	0.28	0.32	2.1	23.7	35.3	6.6

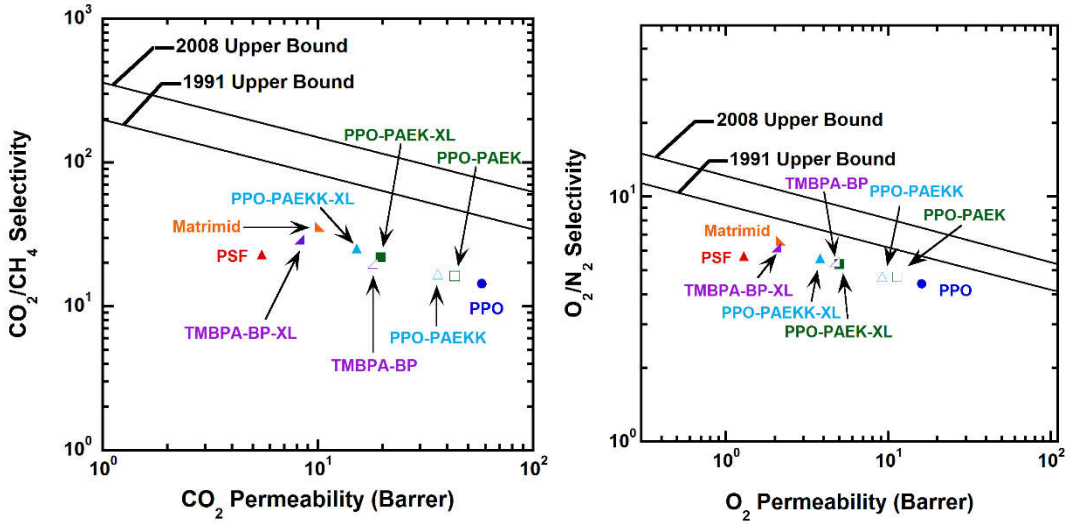

Figure 4.8 Upper bound plots for CO_2/CH_4 and O_2/N_2 gas pairs of PPO, PPO poly(arylene ether ketone) block copolymers, TMBPA-BP, and industrial PSF and Matrimid membranes. Values used for PPO-PAEK, PPO-PAEK XL, TMBPA-BP, and TMBPA-BP XL are for pure gases at 35°C and 10 atm, with other membrane values being obtained from literature with the same testing conditions.[26, 67, 181]

4.5 Conclusions

The polymerization of a ketone monomer with a difunctional PPO oligomer resulted in PPO based copolymers with increased selectivity and reduced permeability relative to unmodified PPO. Glass transition temperatures and transport properties were found to be directly related to the ketone content in the membranes, with the polymer containing the highest density of ketones (TMBPA-BP) also showing the largest increase in selectivity upon crosslinking. The crosslinking reaction was conducted in the solid state at room temperature, and thus, the cast membrane remained intact. Crosslinking also led to an increase in Tg for both the PPO copolymers and the TMBPA-BP homopolymer. High surface absorption in the membranes lead to asymmetry in the crosslinking, with higher asymmetry being observed in the higher ketone containing polymers PPO-PAEK and TMBPA-BP. Transport properties of PPO derivatives and TMBPA-BP were parallel and/or superior to the state of the art membranes when looking at both the CO_2/CH_4 and O_2/N_2 gas pair upper bond plots. With the crosslinking asymmetry possibly creating a surface effect for the membranes, allowing for a lower loss in the gas permeability than expected.

CHAPTER 5: POLY(PHENYLENE-OXIDE) BASED POLYMER BLENDS FOR GAS SEPARATION MEMBRANES

Andrew Shaver,[a] Joshua D. Moon,[b] Donald Savacool,[a] Wenrui Zhang,[a] Gurtej Narang,[a] Gregory Miller,[a] Britannia Vondrasek,[a] J.J. Lesko,[a] Benny D. Freeman,[b] J.S. Riffle,[a] James E. McGrath[a]

[a] Macromolecules Innovation Institute, Department of Chemistry, Virginia Tech, 325 Stanger Street, 133 Kelly Hall, Blacksburg, VA 24061, USA

[b] Department of Chemical Engineering, Texas Materials Institute, Center for Energy and Environmental Research, The University of Texas at Austin, 10100 Burnet Road, Bldg. 133, Austin, TX 78758, USA

From Polymer 2017, 114, 135-143. Used with permission of Elsevier, 2017.

5.1 Abstract

Poly(2,6-dimethyl-1,4-phenylene oxide) (PPO) is utilized for gas separation membranes. It has a relatively high free volume with high gas permeabilities but suffers from low selectivities. PPO polymers with M_n's from 2000-22,000 g/mole were synthesized and blended with a poly(arylene ether ketone) derived from bisphenol A and difluorobenzophenone (BPA-PAEK). DSC showed that the blends with all but the lowest molecular weight PPO had two T_g's, thus suggesting that two phases were present. The ketone carbon and benzylic methyl groups on the BPA-PAEK and the PPO polymers crosslinked upon exposure to UV light. The gel fractions after UV exposure were high and the tensile properties were similar to the

PPO control polymer that is currently used as a gas separation membrane. The crosslinked blends had improved gas selectivities over their linear counterparts. The 90/10 wt/wt 22k PPO/BPA PAEK crosslinked blends gained the most O_2/N_2 selectivity and maintained a high permeability.

5.2 Introduction

Gas separations via membranes have grown over approximately the past 50 years due to reduced energy consumption, equipment size, and waste generation relative to cryogenic distillation and absorption processes.[4, 182-183] Currently, membranes are used to separate various gas pairs in applications including nitrogen enrichment, acid gas treatment, ammonia purge gas recovery, refinery gas purification, syngas ratio adjustment, and dehydration.[4, 32, 182] There are several challenges that need to be addressed within these areas such as low selectivities, plasticization caused by CO_2 and other condensable gas absorption, physical aging, and thermal and mechanical stability of the membranes.[32]

Gas transport performance for non-porous gas separation membranes is primarily characterized in terms of permeability and selectivity. Permeability is the pressure- and thickness-normalized gas flux through the membrane, and selectivity is the permeability ratio of two gases of interest.[133, 141] The best performance occurs when the permeability and selectivity of the membrane are high.[133, 141] However, it is known that there is a tradeoff between permeability and selectivity which was described in terms of an upper bound by Robeson in 1991 and later theoretically explained by

Freeman.[22-23, 26]

Glassy polymers such as poly(arylene ether)s including polysulfones and poly(2,6-dimethyl-1,4-phenylene oxide), polycarbonates, polyimides, cellulose acetates, and aramids are all used as membrane materials and show great performance and processability for various applications.[32] This paper will focus on poly(2,6-dimethyl-1,4-phenylene oxide) (PPO) as a membrane material. PPO was first commercialized over 50 years ago by General Electric and it is now marketed by Sabic.[51] It gained interest as a material for gas separation membranes due to its aromatic ether structure. Its kinked ether linkages and benzylic methyl groups inhibit chain packing and lead to a high fractional free volume and consequently high permeabilities.[32, 157] However, the high free volume leads to reduced selectivities when compared to other commercial materials, and several research efforts have been undertaken to solve this problem.[57, 67]

Crosslinking is of great interest for dense-film gas separation membranes due to the potential to increase selectivity, decrease gas plasticization, and decrease the effect of physical aging.[32, 112] Crosslinking controllably reduces the mobility of polymer chains, which can improve the size sieving capability of glassy polymers and increase selectivity. Gas plasticization occurs when a sufficiently high concentration sorbs into a film and causes swelling that can decrease selectivity. Crosslinking inhibits this swelling and can reduce the overall effect of plasticization. Physical aging involves the gradual densification of a non-equilibrium glassy polymer over time towards its equilibrium state and decreases permeability and increases selectivity. By crosslinking

the film, the aging rate may be reduced. Both crosslinking and aging increase selectivity. However, literature has reported that crosslinking has a more pronounced effect for UV-irradiated polyarylates.[112, 184]

The focus of this study has been to UV crosslink PPO to enhance its transport properties. A poly(arylene ether ketone) based on bisphenol A (BPA-PAEK) was blended with PPO to produce a UV crosslinkable material with improved selectivity. Structures are shown in Figure 5.1. The key crosslinking groups within the polymers are the benzophenone in the BPA-PAEK and the benzylic methyl groups on the PPO. UV light was used to excite a benzophenone moiety that could subsequently abstract a hydrogen radical from a benzylic methyl group. This creates two free radicals that can then combine to form a covalent crosslinked bond. Liu et al. have extensively described this crosslinking reaction and explored the effect of thickness, atmosphere, and aging.[184] Other systems have been studied utilizing this crosslinking reaction.[116, 184-185] However, in the previous work, the two key components were within the same polymer by polymerizing tetramethylbisphenol A or tetramethylbisphenol F with 4'4-difluorobenzophenone.

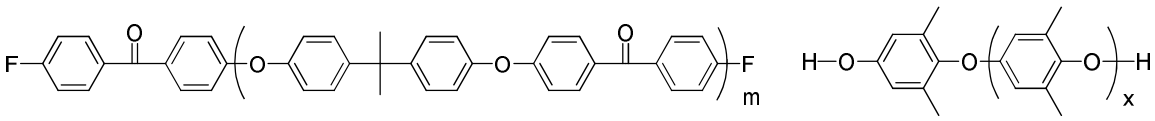

Figure 5.1 Bisphenol A poly(arylene ether ketone) and poly(2,6-dimethyl-1,4-phenylene oxide)

In this study, blends were explored as a function of the molecular weight of the PPO. The 22,000 Mn PPO was used to study the effect of PPO/BPA-PAEK composition on the properties of the blended films. NMR, DSC, gel fractions, tensile and transport properties were used to characterize the films.

5.3 Experimental

Materials

N,N-Dimethylacetamide (DMAc), toluene, pyridine, and 2,6-dimethylphenol were purchased from Sigma Aldrich. DMAc was vacuum distilled from calcium hydride. Toluene, pyridine, and 2,6-dimethylphenol were used as received. 4,4'-Difluorobenzophenone and bisphenol A were kindly donated by Solvay and recrystallized from 2-propanol and toluene, respectively. Potassium carbonate was purchased from Fisher Scientific and dried at 150 °C under vacuum. Copper(I) chloride was purchased from Alfa Aesar and used as received. Hydrochloric acid and methanol were purchased from Spectrum Chemicals and used as received. Chloroform, purchased from Spectrum Chemicals, was stored over activated 3Å molecular sieves. Ultra-high purity (UHP) oxygen gas (99.993%) used for synthesis was purchased from Praxair, and UHP gases (99.999%) used for gas transport measurements were purchased from Airgas.

Synthesis of BPA-PAEK

Synthesis of the BPA-PAEK polymer was adapted from previous literature.[139, 186-188] Bisphenol A (67.713 g, 296.6 mmol), 4,4'-difluorobenzophenone (65.643 g, 306.4 mmol), and DMAc (600 mL) were charged to a three-neck flask equipped with a N2 inlet, mechanical stirrer, and Dean-Stark trap. Toluene (300 mL) and K_2CO_3 (48.352 g, 349.8 mmol) were added to the flask, and the Dean Stark trap was filled with toluene. The apparatus was placed in a silicone oil bath that was heated to 155 °C to begin azeotropic removal of water. After 4 h, the toluene and water were

removed from the Dean-Stark trap. The oil bath was maintained at 150 °C for 12 h, then the reaction was allowed to cool to room temperature. The polymer solution was filtered to remove any excess K_2CO_3 or by-product salts. The polymer solution was precipitated into deionized water, then the polymer was stirred in deionized water at 80 °C to further assist in the removal of salts and solvents. The white polymer was filtered and dried at 110 °C under vacuum. Yield was 81%.

Synthesis of 6,000, 17,000 and 22,000 M_n poly(2,6-dimethyl-1,4-phenylene oxide)s

PPO synthesis was adapted from Hay et al., [164] and the protocol for synthesizing an ~6,000 Mn oligomer is provided. A 500-mL, 4-neck, round bottom flask equipped with an overhead stirrer, oxygen inlet tube, and condenser was charged with 250 mL of pyridine and 0.5 g (0.005 mol) of copper(I) chloride. Oxygen gas (0.1 SCFH) was passed through the vigorously stirred solution for 30 min, and the solution became dark green. Then, 10 g (0.082 mol) of 2,6-dimethylphenol was added. The reaction mixture became dark orange and the temperature was increased from 25 to 45 °C. Oxygen flow was terminated after 1 h and the reaction was stirred for 2 h. The solution became viscous and the color of the solution returned to dark green. The reaction mixture was cooled to room temperature and slowly added into 500 mL of methanol to precipitate the polymer, then the polymer was filtered and washed thoroughly with methanol containing a small amount of hydrochloric acid. The product was dissolved in chloroform, filtered and re-precipitated into methanol. After filtration, the faint yellow powder was dried at 110 °C for 24 h under vacuum. Yield: 7.1 g, 71%. The structure was confirmed by ^{1}H-NMR.

For the 17,000 M_n PPO, a 1-L, 4-neck, round bottom flask was used and 800 mL of pyridine, 2.0 g (0.02 mol) of copper(I) chloride. Oxygen gas (0.1 SCFH) was passed through the vigorously stirred solution for 30 min, and then 30 g (0.246 mol) of 2,6-dimethylphenol was added. Oxygen flow was terminated after 3 h and the reaction was stirred for 2 h. The product (23.4 g, yield 78%) was obtained and the structure was confirmed by ^{1}H-NMR. For the 22,000 M_n PPO, a 500-mL, 4-neck, round bottom flask was used and 250 mL of pyridine, 1.0 g (0.01 mol) of copper(I) chloride. Oxygen gas (0.1 SCFH) was passed through the vigorously stirred solution for 30 min, and then 10 g (0.082 mol) of 2,6-dimethylphenol was added. Oxygen flow was terminated after 4 h and the reaction was stirred for 2 h. The product (8.0 g, yield 80%) was obtained and the structure was confirmed by ^{1}H-NMR.

Size Exclusion Chromatography (SEC)

SEC of the PPO Series of Polymers

SEC was conducted to measure molecular weights and distributions of the PPO polymers. The eluent was $CHCl_3$. The column set consisted of two Shodex KF-801 columns connected in series with a guard column having the same stationary phase. The columns and detectors were maintained at 35 °C. An isocratic pump (Waters 515 HPLC Pump, Waters Technologies) and 717 Waters autosampler were used for mobile phase delivery and sample injection. Calibrations were performed using a set of nine Shodex polystyrene standards spanning the entire column molecular weight range. Molecular weights were calculated based on the polystyrene standards.

SEC of BPA-PAEK

SEC was conducted to measure the molecular weight and distribution of the BPA-PAEK. The mobile phase was DMAc distilled from CaH_2 containing dry LiCl (0.1 M). The column set consisted of 3 Agilent PLgel 10-μm Mixed B-LS columns 300 x 7.5 mm (polystyrene/divinylbenzene) connected in series with a guard column having the same stationary phase. The columns and detectors were maintained at 50 oC. An isocratic pump (Agilent 1260 infinity, Agilent Technologies) with an online degasser (Agilent 1260), autosampler and column oven were used for mobile phase delivery and sample injection. Multiple detectors connected in series were used for the analyses. A multi-angle laser light scattering detector (DAWN-HELEOS II, Wyatt Technology Corp.), operating at a wavelength of 658 nm, a viscometer detector (Viscostar, Wyatt Technology Corp.), and a refractive index detector operating at a wavelength of 658 nm (Optilab T-rEX, Wyatt Technology Corp.) provided online results. The system was corrected for interdetector delay and band broadening using a 21,000 g/mole polystyrene standard. Data acquisition and analysis were conducted using Astra 6 software from Wyatt Technology Corp. Validation of the system was performed by monitoring the molar mass of a known molecular weight polystyrene sample by light scattering. The accepted variance of the 21,000 g/mole polystyrene standard was defined as 2 standard deviations (11.5% for M_n and 9% for M_w) derived from a set of 34 runs. The specific refractive index value was calculated based on the assumption of 100% recovery. Molecular weights were calculated from the light scattering data.

Film-casting

The polymers (0.6 g) were weighed into a small glass vial with a magnetic stir bar at the desired wt/wt ratio. Chloroform (20 mL) was added to the vial. The solution was filtered through a 0.45-μm syringe filter into a clean glass vial. A 6" x 6" glass plate with the corners cut off (34 in^2 area) was placed in a base bath for 30 min to clean the surface. The glass plate was rinsed and dried, then placed on a level surface for casting. The solution was poured onto the plate and the solution was spread to the edges of the plate until it covered the whole glass plate. A glass dome with 2 outlets was used to cover the plate. One outlet was fitted with a syringe filter to inhibit dust from entering the glass container and the other was connected to the house air stream running at 2 SCFH. The plate was left undisturbed for a minimum of 30 min, then transferred to an oven at 110 °C for an additional 30 min. Once removed from the oven, the film was secured to the glass plate with clips and placed into a DI water bath for 1 min to assist with film removal. The free-standing films were then placed in a vacuum oven set at 110 °C for 2 h without vacuum and then for 10 h with vacuum. The resulting films were between 20 and 30 μm thick.

Proton Nuclear Magnetic Resonance (NMR) Spectroscopy

The compositions of the blends were confirmed via NMR. 1H-NMR analysis was performed on a Varian Inova spectrometer operating at 400 MHz. All spectra were obtained from 15% (w/v) 1-mL solutions in chloroform-d. The NMR signals of PPO were assigned based on the literature.[189] PPO ^1H NMR (400 MHz, Chloroform-d6): a[7.1-6.8 ppm (Brs, H_{ar})], b[6.5-6.2 ppm (Brs, H_{ar})], c[2.3-1.8 ppm (Brs, H)]. The peaks in 7.1-6.8 ppm region are the end group signal from 3 aromatic

protons, the peaks in 6.5-6.2 ppm region are the aromatic protons from repeat units, and the peaks in 2.3-1.8 ppm region are the proton methyl group. The molecular weight can be calculated by equation 5-1 below:

$$Mn= 3b/2a\times120+1 \quad (5\text{-}1)$$

Thermogravimetric Analysis (TGA)

Thermal stabilities of the polymers were investigated using a TA Instruments TGA Q5000 under a N_2 atmosphere with a purge rate of 25 mL/min. The heating rate was 10 °C/min from room temperature to 700 °C.

Differential Scanning Calorimetry (DSC)

The thermal properties were investigated with a TA Instruments DSC Q2000. The polymers were heated under N_2 at 60 mL/min to ensure an inert atmosphere. The heating rate was 10 ^{o}C/min to 350 °C, then the sample was cooled to 0 °C at 10 °C/min. It was heated once more to 350 °C at 10 °C/min and the reported DSC thermograms are from the second scans. Reported T_g's were measured at the midpoint.

UV Spectroscopy

UV spectra of the bulk polymers and the blends were collected using a Shimadzu Corp. UV – 1601 UV analyzer. Solutions (0.05 mg/mL) of the samples in chloroform were analyzed in quartz cuvettes placed in the sample cell with chloroform in a similar cuvette in the reference cell. A 50 W Tungsten bulb (from 1100 to 340.8 nm) and a deuterium bulb (340.8 to 190 nm) were used as the light sources. Scans were conducted in 'Spectrum Mode' sweeping wavelengths from 700 to 190 nm.

UV Crosslinking

The polymer membranes were placed between an upper quartz and a lower glass plate. The setup was passed under a Heraeus UV Fusion "H+" bulb (200 to 450 nm wavelength range) via a conveyor belt set at 6 ft/min. This procedure was repeated until the film was exposed to the desired amount of radiation. A UV Power Puck was used to measure the amount of energy that the sample was exposed to, and this was multiplied by the number of passes.

Gel Fraction Measurements

Crosslinked films were dried at 120 °C under vacuum overnight. Then 0.1-0.2 g of the crosslinked film was placed in a 20-mL scintillation vial filled with chloroform and stirred overnight. The remaining solid was filtered through a Buchner funnel having a pre-weighed filter paper. The filter paper with the gelled polymer on it were dried at 120 °C under vacuum overnight, then weighed once more to obtain the final weight. Gel fractions were calculated by Equation 5-2.

$$Gel\ Fraction\ (\%) = \frac{W_{final}}{W_{initial}} \text{ x } 100 \tag{5-2}$$

Pure Gas Permeability Measurements

The pure gas permeabilities for a series of light gases (H_2, CH_4, N_2, O_2, CO_2) were measured at 35 °C in a constant-volume, variable-pressure apparatus as described elsewhere. The membrane sample, after being epoxied to a brass support disk, was loaded into a stainless steel Millipore filter holder (Millipore, Billerica, MA, USA) inside a temperature-regulated water bath. The downstream pressure was

measured with a MKS Baratron 626B transducer (MKS, Andover, MA, USA) with a max pressure of 10 Torr, and the pressure in the upstream was measured using a Honeywell Super TJE transducer (Honeywell Sensotec, Columbus, Ohio, USA) with a max pressure of 1500 psig. The feed pressure of each gas was varied between 3 and 17 atm, and both the upstream and downstream pressures were recorded in a custom Python application using National Instruments. Each sample was degassed overnight prior to measuring transport of the gas, and the stainless steel upstream line connected to the feed gas cylinder was flushed and degassed for a minimum of 45 min prior to each test to prevent contamination from other gases.

Tensile Properties

Tensile samples were cut from solvent cast films using a Cricut Explore One™ computer controlled cutting machine. The resulting samples were consistent with sample Type V described in ASTM D638-14. Nine samples produced by the cutter were inspected for any visible flaws, defects, or inclusions that arose during the casting process. The six highest quality samples were selected for testing. The sample thickness was measured at both ends of the narrow section using a Mitutoyo digimatic micrometer model MDC-1”SXF. Uniaxial load tests were performed using an Instron ElectroPuls E1000 testing machine equipped with a 250-N Dynacell load cell. The crosshead displacement rate was 5 mm/min and the initial grip separation was 25 mm. Nominal strain was calculated by dividing the change in grip separation by the initial grip separation. Tensile strength was calculated by dividing the load by the average cross-sectional area of the narrow section, which was based on the average of the two

sample thickness measurements and a sample width of 3.18 mm.

5.4 Results and Discussion

NMR and SEC were used to characterize the PPO and BPA-PAEK molecular weights and the results are shown in Table 5.1 and Figure 5.2. The PPO nomenclature is based on the M_n's from SEC. PPO oligomers with a series of molecular weights were produced to investigate structure-property behavior as a function of the molecular weights of the PPO component.

Table 5.1 Molecular weights of the polymers

	M_n (kDa) NMR	M_n (kDa) SEC	M_w (kDa) SEC	PDI SEC
BPA-PAEK	-	52	78	1.5
2k PPO	1.4	2	3.2	1.7
6k PPO	4.1	6	11.8	2.0
17k PPO	14	17	50.2	3.0
19k PPO	19	19	55.8	2.9
22k PPO	19	22	109	5.0

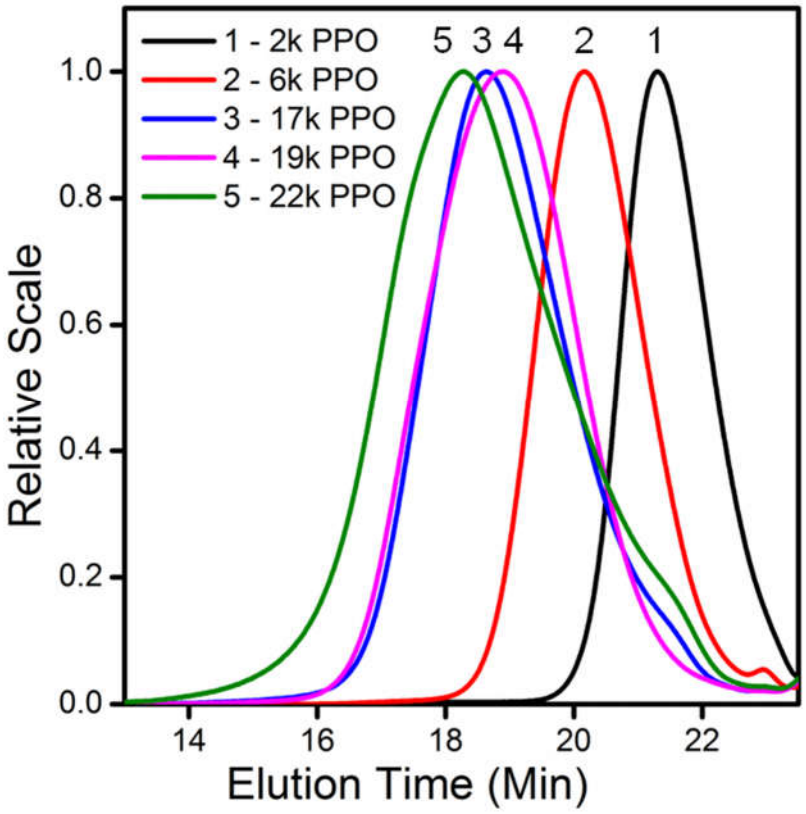

Figure 5.2 SEC refractive index curves of the PPO oligomers

DSC thermograms of the films are shown in Figure 5.3. Figure 5.3A compares two films of blends with different PPO molecular weights of 2,000 and 22,000 g/mole at a wt/wt composition of 33/67 PPO/BPA-PAEK relative to their controls. Thermogram 2 shows the 2,000 g/mole PPO/BPA-PAEK blend with a Tg of 149 ºC. This Tg is located between the two control Tg's, curves 1 and 3, which suggests that the 2,000 g/mole PPO is miscible with BPA-PAEK at those compositions. Curve 4 shows the thermogram of a high molecular weight 22,000 g/mole PPO/BPA-PAEK blend that produced two Tg's, one at 152 and another at 213 ºC. These two Tg's correspond with the control Tg's in curves 3 and 5 which indicates that the 22,000 Mn PPO produced an immiscible blend with BPA-PAEK at those compositions. The Tg's of the blend are slightly reduced in comparison to the respective control polymers. A

definite reason for this behavior is unclear, but it does occur consistently. This can be observed in Figure 3B with the lower Tg's corresponding to the BPA-PAEK in blends with the 6,000, 17,000, 19,000 and 22,000 PPO.

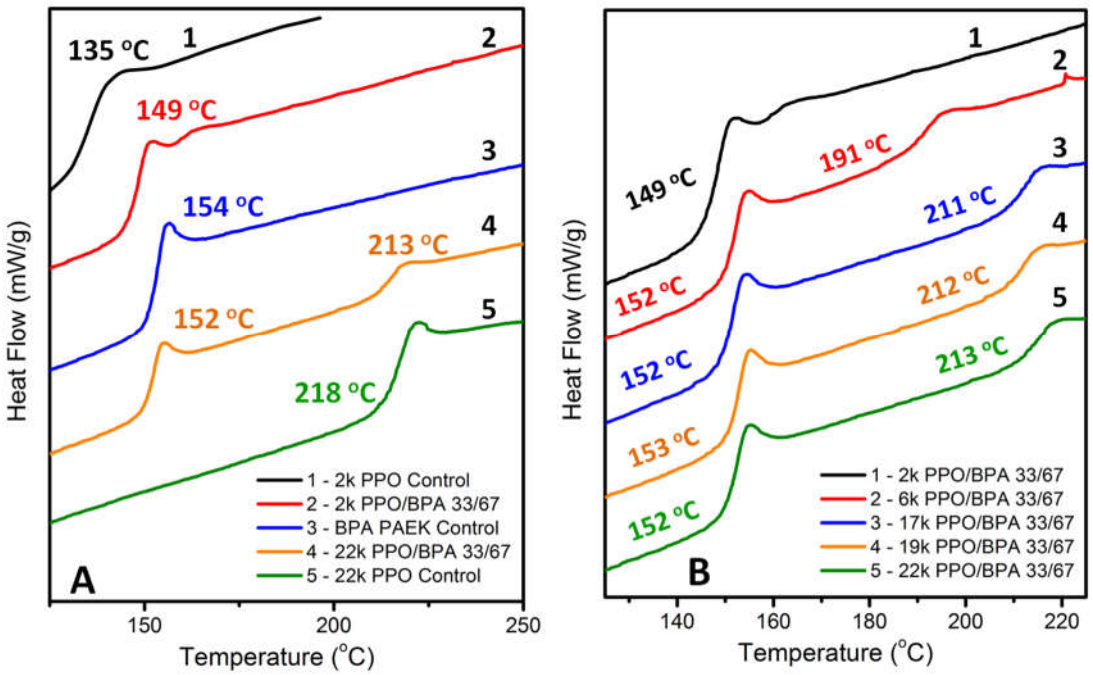

Figure 5.3 A) DSC thermograms of the 2,000 g/mole PPO/BPA-PAEK 33/67 wt/wt and the 22,000 g/mole PPO/BPA-PAEK 33/67 wt/wt blends with their respective controls. B) comparison of each of the PPO molecular weights blended with BPA-PAEK at the 33/67 wt/wt composition of PPO/BPA-PAEK

Figure 5.3B compares blends with the five PPO polymers with different molecular weights with 67 wt% of BPA-PAEK. Thermogram 1 shows the single Tg for the 2,000 g/mole PPO/BPA-PAEK blend. Once the molecular weight of the PPO in the blends was increased to 6,000 Mn, two clear Tg's emerged, and this was also true as the molecular weight was increased further, thus indicating the presence of two phases. The upper Tg in the 6,000 Mn PPO/BPA-PAEK blend, which correlates to the PPO phase, is lower than the 17,000, 19,000, and 22,000 upper PPO Tg's in the blends. This is expected since Tg is a function of molecular weight.[190] In Figure 5.4,

the 6,000 Mn PPO non-crosslinked blend (curve 2) is compared to its BPA-PAEK control (curve 1), the 6,000 PPO control (curve 4), and the crosslinked blend (curve 3). The PPO Tg in the non-crosslinked blend correlates with the control 6,000 Mn PPO Tg. Once crosslinked, at least the upper Tg was slightly raised, and this was attributed to reduced mobility, particularly of the PPO chains.[123]

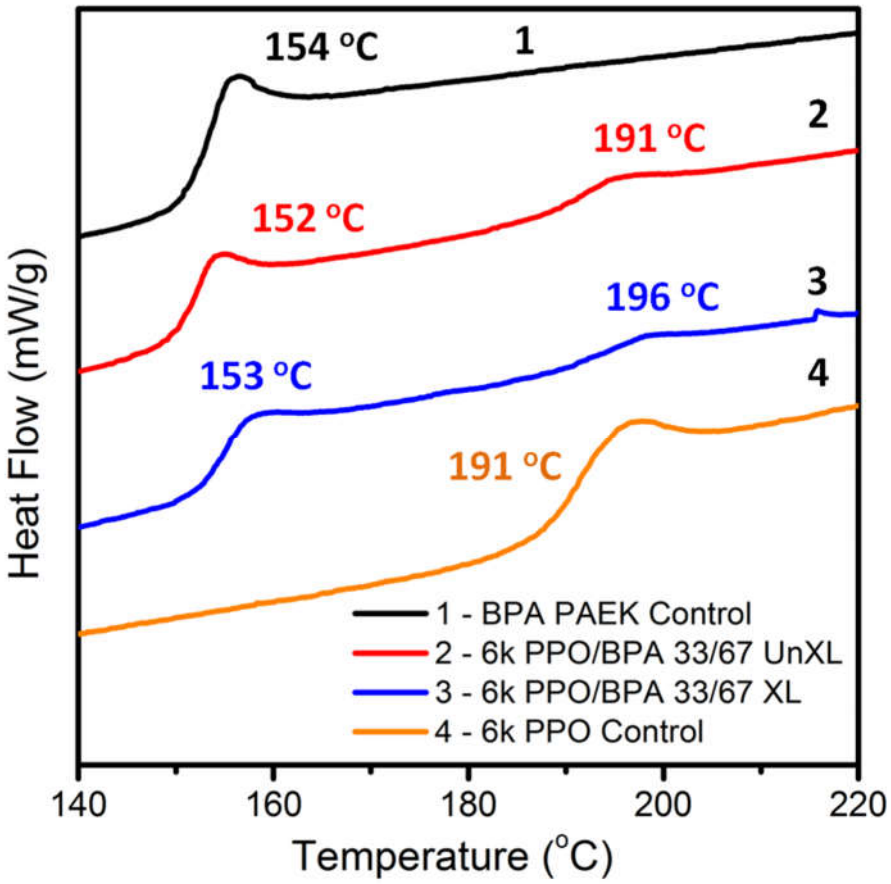

Figure 5.4 DSC thermograms of 6,000 g/mole PPO/BPA-PAEK 33/67 wt/wt non-crosslinked and crosslinked blends with the controls

The crosslinking reaction is activated via UV light and occurs between the activated ketone carbon and benzylic radical. Figure 5.5 shows the solution UV absorbance spectra of the six control polymers. At a given concentration, the PPO absorbs significantly less light than BPA-PAEK in the wavelength range of interest (200 to 450 nm). The absorbance of the BPA-PAEK results in ketone excitation from

the nonbonding to the antibonding state.[191] Therefore, in later discussions regarding the gel fractions as a function of PPO weight composition, it will be important to remember that blends containing a greater PPO content will not absorb as much light as blends with higher compositions of the BPA-PAEK. This is beneficial because the UV light will penetrate further into the film to crosslink more polymer chains.

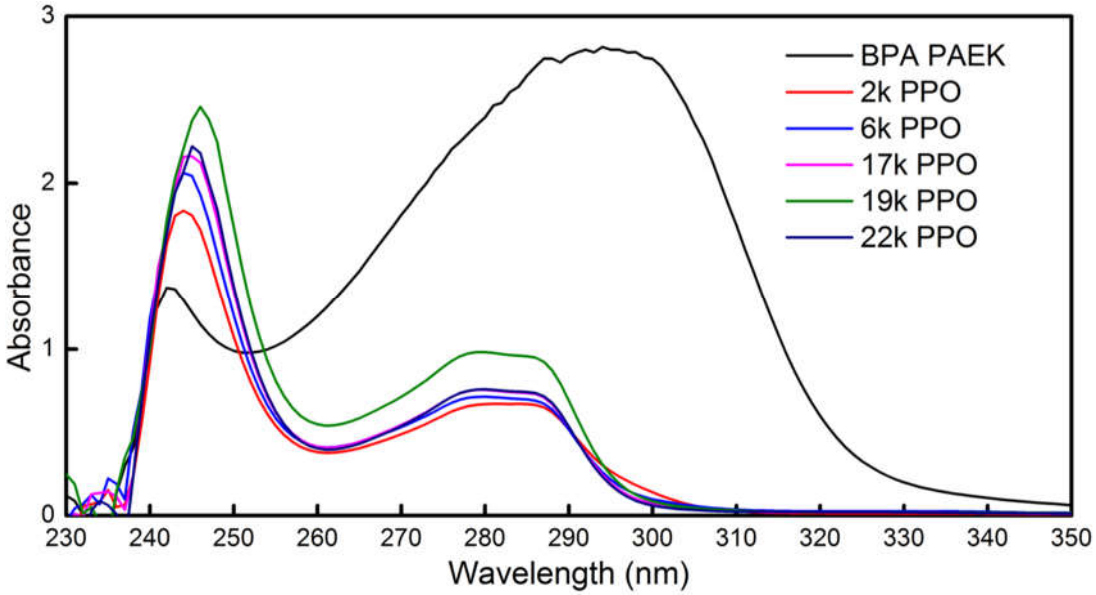

Figure 5.5 Solution UV absorption spectra of the PPO and BPA-PAEK

The extent of crosslinking was explored by measuring gel fractions. The set of gel fractions shown in Figure 5.6 compares the five PPO molecular weights blended with BPA-PAEK along with those for the 19,000 g/mole PPO homopolymer. The films were exposed to 11, 23, or 34 J/cm2 of energy in efforts to optimize the UV exposure. The higher exposure resulted in increased gel fractions in the blended films but not in the PPO homopolymer control. The control PPO film did not undergo significant crosslinking which showed the importance of the ketone group to the crosslinking reaction. The blend with the 2,000 PPO/BPA-PAEK 33/67 wt/wt composition only reached gel fractions a little above 20%, and this was much lower

than the gel fractions obtained with blends having higher molecular weight PPOs. This was attributed to the fact that higher molecular weight PPO contains more benzylic crosslinkable methyl groups per mole (i.e., higher functionality), and thus requires fewer crosslinks to reach gelation.

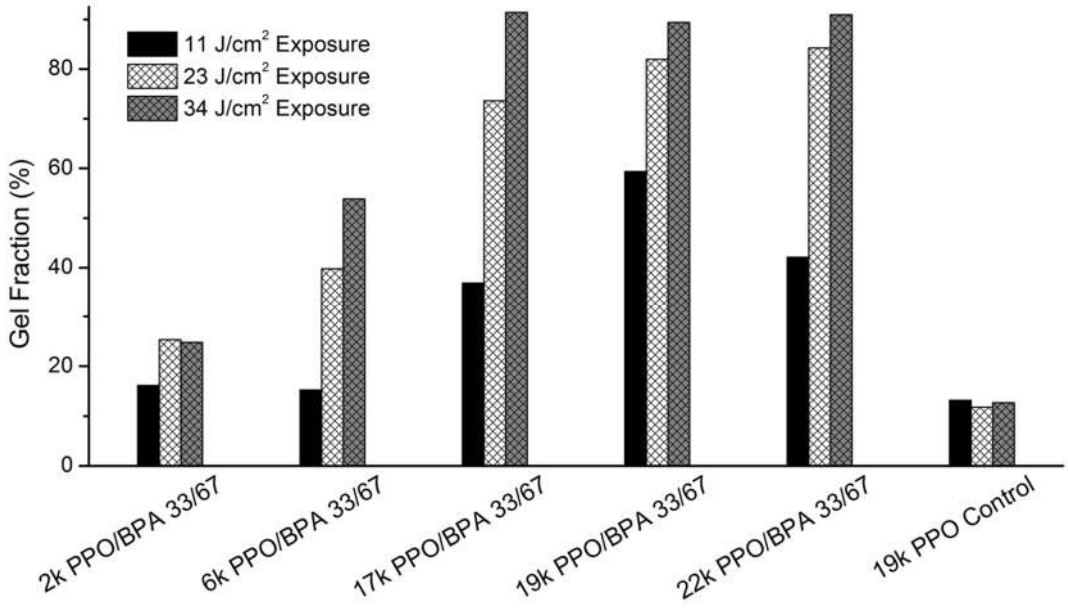

Figure 5.6 Gel fractions after UV crosslinking of PPO/BPA-PAEK blends over a range of PPO molecular weights

The 22,000 M_n PPO was used to explore gel fractions and gas separation properties in these blends as a function of PPO composition. Figure 5.7 compares the gel fractions of four blend compositions. Unexpectedly, there was not a significant change in gel fraction as a function of composition. This is likely a result of several competing factors. One is that the amount of crosslinks may have decreased with less BPA-PAEK content simply because fewer ketone groups that participate in the crosslinking reaction were present. Secondly, the UV light should penetrate more deeply into the film with increased PPO content since the PPO absorbs less light relative to the BPA-PAEK. These factors produce results that are counter to each other,

so this may lead to the insignificant change shown in Figure 5.7.

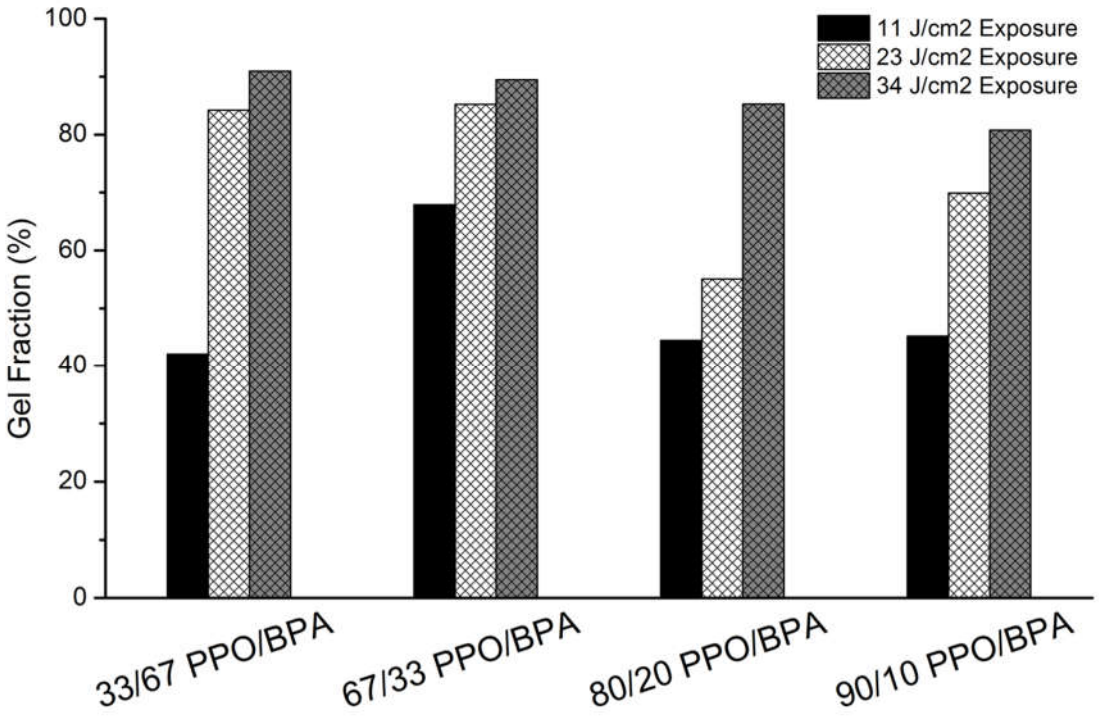

Figure 5.7 Gel fractions after UV crosslinking of blends of 22,000 M_n PPO with BPA-PAEK over a range of compositions

It is expected that the phase structure of the blends is also a contributing factor. The DSC thermograms in Figures 5.3-5.4 show two Tg's for all of the PPO molecular weights except for the very low 2000 M_n polymer, thus strongly suggesting that two phases are present. However, high gel fractions were obtained after crosslinking blends of the 22,000 M_n PPO/BPA-PAEK, and it is postulated that this can only occur when the benzylic methyl groups are in the same phase as the ketone groups. This suggests some level of miscibility within the system. It is believed that there are two phases within the blends and that each contain both PPO and BPA-PAEK. Referring back to Figure 5.4 where Tg's measured by DSC are reported for blends of the PBA-PAEK with the 6,000 M_n PPO, the Tg of the phase that contains the higher

volume fraction of PPO increases upon crosslinking. This suggests a decrease in molecular mobility after crosslinking. While it is reasoned that crosslinking may increase compatibility (or the level of miscibility), we are cognizant of the fact that these films were crosslinked in the solid state well below either Tg, and also that Tg would reflect both any change in miscibility but also changes in mobility. The morphology of the blends was not explored in this study but would provide information regarding the unique behavior of this system.

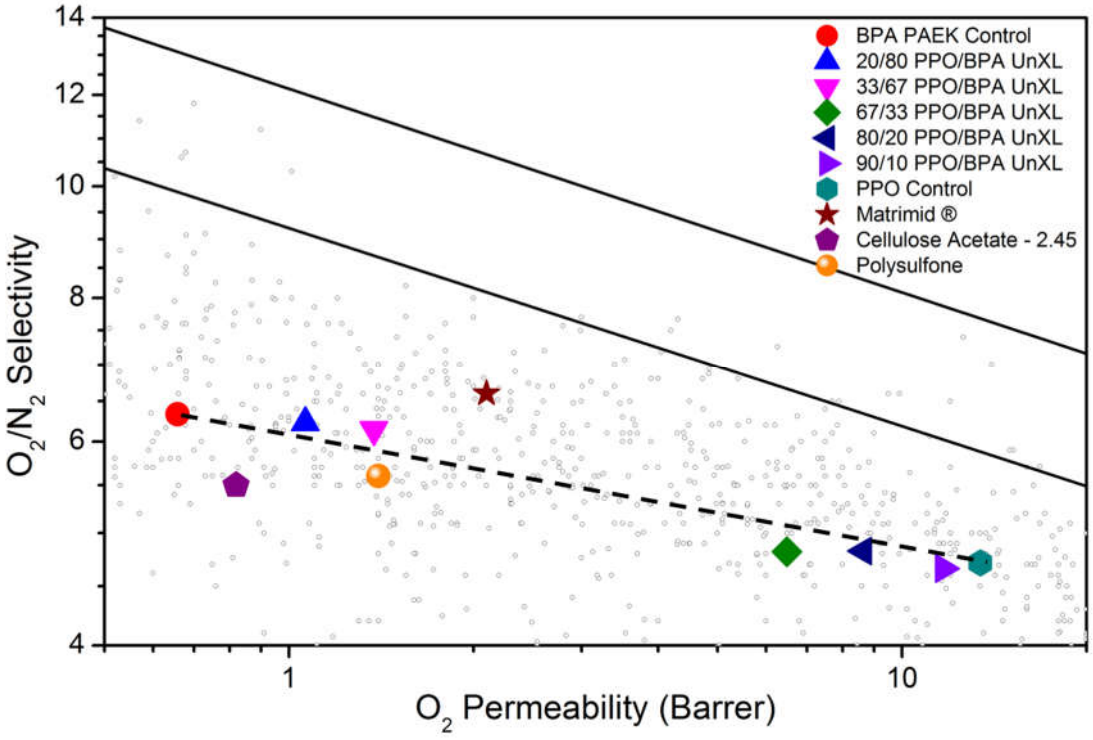

Figure 5.8 Comparison of oxygen and nitrogen transport in blends of the 22,000 M_n PPO/BPA-PAEK at different compositions and the controls. The dashed line represents linear behavior. [22, 26, 32]

The permeabilities and ideal selectivities for the 22,000 g/mole PPO/BPA-PAEK films with different compositions are shown in Table 5.2, and a graph showing their placement on the O_2/N_2 upper bound is given in Figure 5.8. The linear dashed line in Figure 5.8 represents the transport properties that would be expected for miscible

blends.[192-193] As would be expected in these multiphase blends, the membranes with high compositions of PPO have higher permeabilities and lower selectivities and this is attributed to the high free volume of PPO. A few commercial polymers are included in Figure 5.8, and the 33/67 22,000 M_n PPO/BPA-PAEK showed better selectivity than either polysulfone or cellulose acetate.

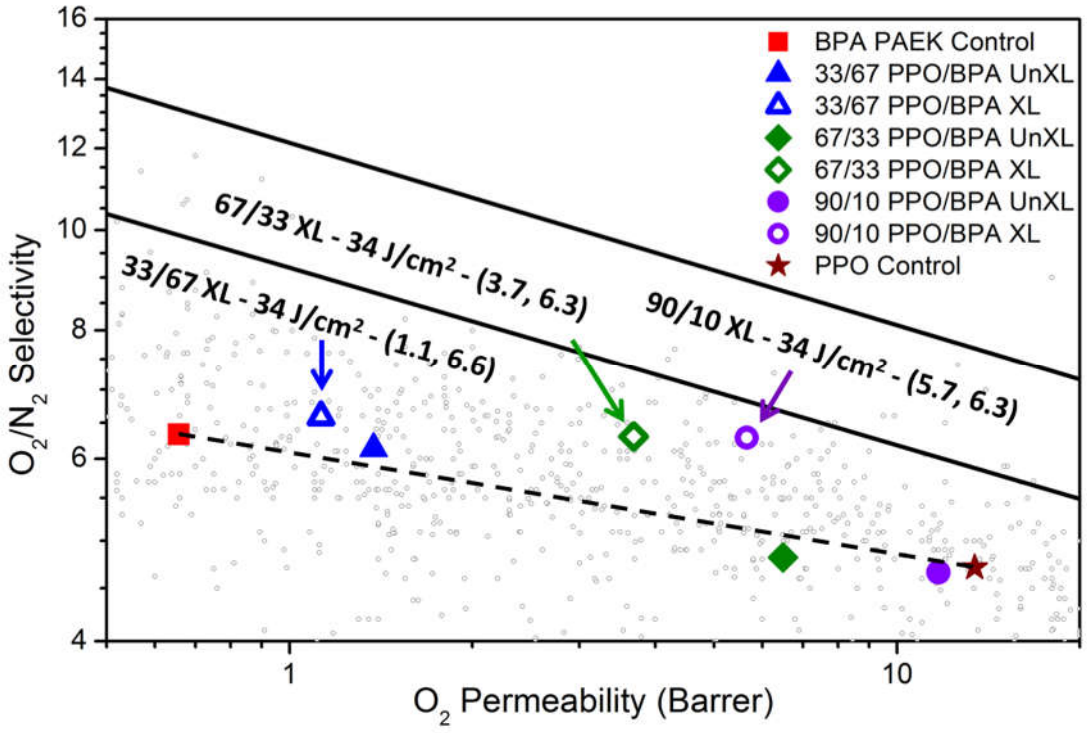

Figure 5.9 Comparison of 22,000 M_n PPO/BPA PAEK non-crosslinked and crosslinked blends at different compositions relative to the controls. The dashed line represents the linear behavior and the numbers on the graph are permeabilities and selectivities with the format (x,y). [23, 27]

The 33/67, 67/33, and 90/10 22,000 M_n PPO/BPA-PAEK films were crosslinked via exposure to UV radiation and the results are provided in Figure 5.9 along with the bulk and non-crosslinked controls. The 90/10 22,000 M_n PPO/BPA-PAEK crosslinked membrane exhibited good selectivity and permeability for O_2/N_2 separation in a film that was comprised largely of a readily available commercial polymer. As discussed

previously, the UV light was able to penetrate further into this film to crosslink more polymer and therefore increase the selectivity substantially. Secondly, the UV exposure created a gradient of crosslinked material through the thickness of the film. Therefore, the highly crosslinked surface likely contributed to the high selectivity while the lightly crosslinked center of the film likely contributed to the high permeability.[184-185]

Pure 22,000 g/mole PPO has suitable mechanical properties for application in gas separation membranes. Therefore, the tensile properties of the non-crosslinked blends at all blend ratios were compared to those of pure PPO films. Steel with control nonparametric multiple comparisons analysis[194] (conducted using a 95% confidence interval and 100% PPO as the control data set) shows no statistical differences between the modulus data sets or the tensile strength at yield data sets for any of the samples. Using the same type of analysis for the elongation and strength at break data sets, the only blends that showed a statistical difference were those comprised of 20 and 33% PPO (Figure 5.10). Thus, even though these are two-phase blends, the mechanical properties remain consistent with those of pure PPO over a wide range of PPO-rich blend ratios. For BPA-PAEK-rich blends (33% PPO or less) the properties of BPA-PAEK dominate the mechanical responses, which result in higher strength and elongation at break.

Table 5.2 Transport properties of BPA-PAEK blends with PPO at 35 °C and 3 atm

* Values are from Sanders et al.[32]

	O_2 (Barrer)	N_2 (Barrer)	O_2/N_2 Selectivity	H_2 (Barrer)	CH_4 (Barrer)	CO_2 (Barrer)
BPA-PAEK Control	0.66	0.10	6.3	8.2	0.12	2.7
20/80 22k PPO/BPA-PAEK NonXL	1.1	0.17	6.2	13	0.19	4.5
33/67 22k PPO/BPA-PAEK NonXL	1.4	0.22	6.1	16	0.24	5.8
33/67 22k PPO/BPA-PAEK XL	1.1	0.17	6.6	16	0.15	4.5
67/33 22k PPO/BPA-PAEK NonXL	6.5	1.3	4.8	54	1.5	28
67/33 22k PPO/BPA-PAEK XL	3.7	0.58	6.3	45	0.47	14
80/20 22k PPO/BPA-PAEK NonXL	8.6	1.8	4.8	70	2.1	36
90/10 22k PPO/BPA-PAEK NonXL	11.7	2.5	4.7	90	2.9	50
90/10 22k PPO/BPA-PAEK XL	5.7	0.90	6.3	68	0.71	22
22k PPO Control	13.4	2.8	4.7	105	3.3	57
Matrimid® *	2.1	0.32	6.6	18	0.28	10
Cellulose Acetate - 2.45 *	0.82	0.15	5.5	12	0.15	4.8
Polysulfone *	1.4	0.25	5.6	14	0.25	5.6

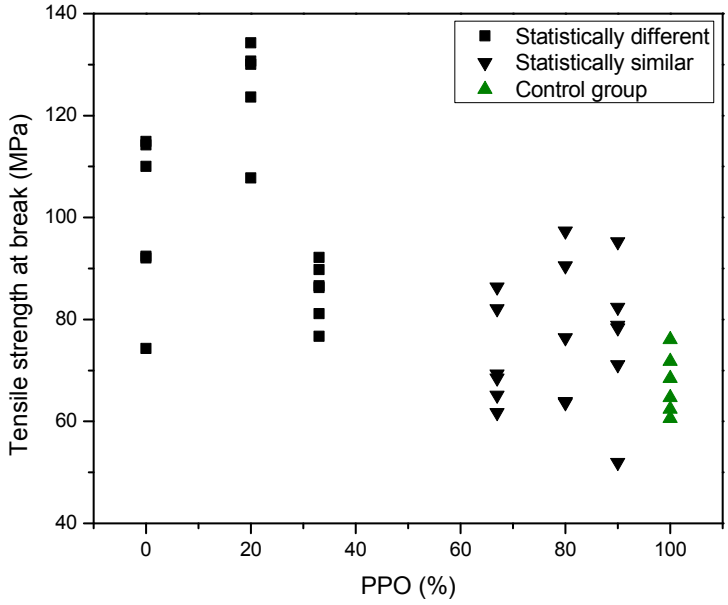

Figure 5.10 Tensile strength at break data. Only the 0, 20, and 33% PPO data sets are statistically different from the 100% PPO control data set.

Blends containing 33 wt% PPO and 67 wt% of BPA-PAEK of varying molecular weights were also tested in tension. Despite the higher fraction of BPA-PAEK, the molecular weight of the PPO had a significant impact on the mechanics of the films. Films containing the 2,000 and 6,000 g/mole PPO exhibited a brittle failure mechanism with little to no yielding (Figure 5.11-A) while films containing higher molecular weight PPO displayed yielding and drawing behavior (Figure 5.11-B). This result confirms that the mechanics of the blends are highly dependent on the molecular weight of the PPO, even when the BPA-PAEK is the dominant phase.

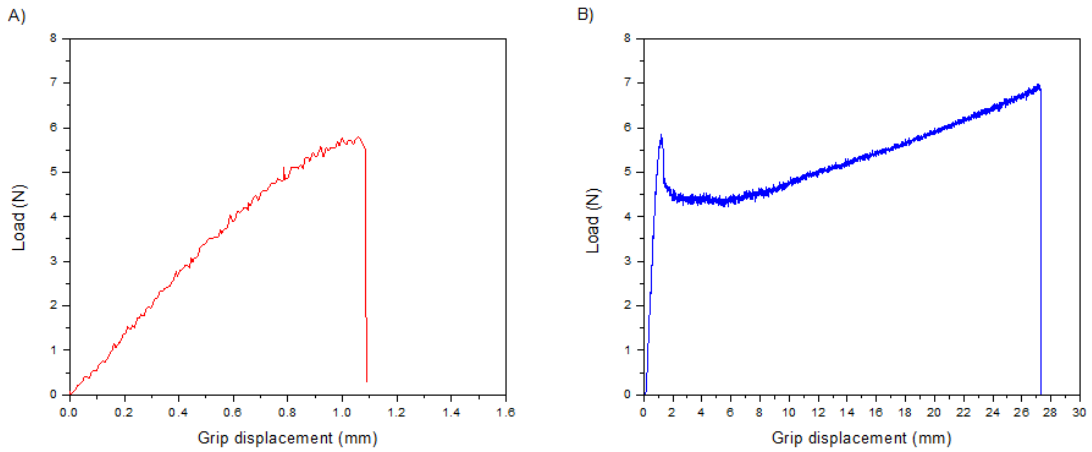

Figure 5.11 Representative load-displacement curves for A) 67% BPA-PAEK blended with 33% 6,000 g/mole PPO (shows brittle failure mode), B) 67% BPA-PAEK blended with 33% 22,000 g/mole PPO (shows yielding, drawing, and strain hardening behavior)

5.5 Conclusions

PPO and BPA-PAEK were blended to form membranes that were phase separated except for the samples with the very low M_n PPO. The DSC results showed that the 6000, 17,000, 19,000, and 22,000 blended films had two Tg's that closely correlated with the corresponding homopolymer Tg's, suggesting that they had a two-phase nature. Despite the immiscibility of these films, the gel fractions showed significant insolubility after UV exposure. Gel fractions as a function of the 22,000 M_n PPO composition were explored and did not show any significant change. This is likely a result of several competing factors. One trend is that as the PPO composition is increased, there is a lower ketone content which participates in the crosslinking reaction. Counter to that is that with increased PPO content, UV light can penetrate further into the film and crosslink more chains. This is because PPO absorbs significantly less UV light than the BPA-PAEK as shown via solution UV absorbance

spectra.

The 33/67 wt/wt PPO/BPA-PAEK demonstrated the best permselectivity performance with respect to the linear behavior due to its increased permeability with little decrease in selectivity. However, with respect to the upper bound, the 90/10 PPO/BPA-PAEK had the best performance due to PPO's high permeability. Between the three crosslinked blended films, the 90/10 PPO/BPA-PAEK gained the most selectivity and maintained a larger amount of its permeability. This can be attributed to a greater degree of UV light penetration into the film to crosslink more polymer chains due to PPO's lower absorbance. Another reason is that the UV exposure created a gradient of crosslinked material that created a selective surface and a permeable center.

Overall, we were able to blend a small amount of BPA-PAEK with the commercially used PPO to create mechanically robust crosslinkable polymer films. In comparison to commercial gas separation polymers, the 33/67 wt/wt 22,000 PPO/BPA-PAEK blend outperformed polysulfone and cellulose acetate without any crosslinking.

CHAPTER 6: CONCLUSIONS AND SUGGESTED FUTURE RESEARCH

6.1 Conclusions

Several polymeric membrane materials have been explored in this dissertation for gas separation. Relationships among backbone composition, morphology of the membranes, gas transport and mechanical properties were the focus of this dissertation.

Traditional TR polymers suffer a critical problem in that the membrane's mechanical properties dramatically decrease after undergoing the TR process, and this severely limits their potential utilities. Reactive functional poly(arylene ether sulfones) can be used as good toughening agents to improve the mechanical property of TR polymers. Thermally rearranged (TR) block copolymers were prepared from a series of PAES oligomers based on HAB-6FDA polyhydroxyimide precursors. The 30%PAES-HAB-6FDA block copolymers exhibited the best mechanical properties with doubled tensile strength and elongation at break compared with the homo TR polymer 0%PAES-HAB-6FDA.

Difunctional poly(2,6-dimethylphenylene oxide) oligomers can be chain extended with different difluoro-monomers to form high molecular weight copolymers. The use of benzylic methyl substituents in combination with benzophenone groups creates UV-crosslinkable membranes that can achieve high gel fractions. Crosslink density is dependent on ketone concentration for these polymers,

with higher increases in glass transition temperatures occurring for polymers with higher ketone incorporation. After crosslinking, membranes show higher selectivity but lower permeability for O_2/N_2 and CO_2/CH_4 gas pairs. Control of the concentration of ketones through either backbone structure or oligomer molecular weight allows for poly(arylene ether)s with tunable gas transport properties.

Monofunctional poly(2,6-dimethyl-1,4-phenylene oxide)s were blended with a poly(arylene ether ketone) derived from bisphenol A and difluorobenzophenone. DSC showed that the blends with all but the lowest molecular weight PPO had two T_g's, thus suggesting that two phases were present. Under similar UV-crosslinking mechanism as above PPO copolymers, the gel fractions of these blends after UV exposure were high and the tensile properties were similar to the PPO control polymer that is currently used as a gas separation membrane. The crosslinked blends had improved gas selectivities over their linear counterparts. The 90/10 wt/wt 22k PPO/BPA PAEK crosslinked blends gained the most O_2/N_2 selectivity and maintained a high permeability.

6.2 Suggested future research

For toughening TR membrane research, a systematic study of morphology of toughened TR copolymers could be done in the future. Morphological investigations of these copolymer systems will provide more information about how PAES segments interact with polyhydroxylimide (precursor) or polybenzoxazole (TR polymer)

segments. To be more important, the toughening mechanism of PAES would be revealed by understanding morphological the behavior.

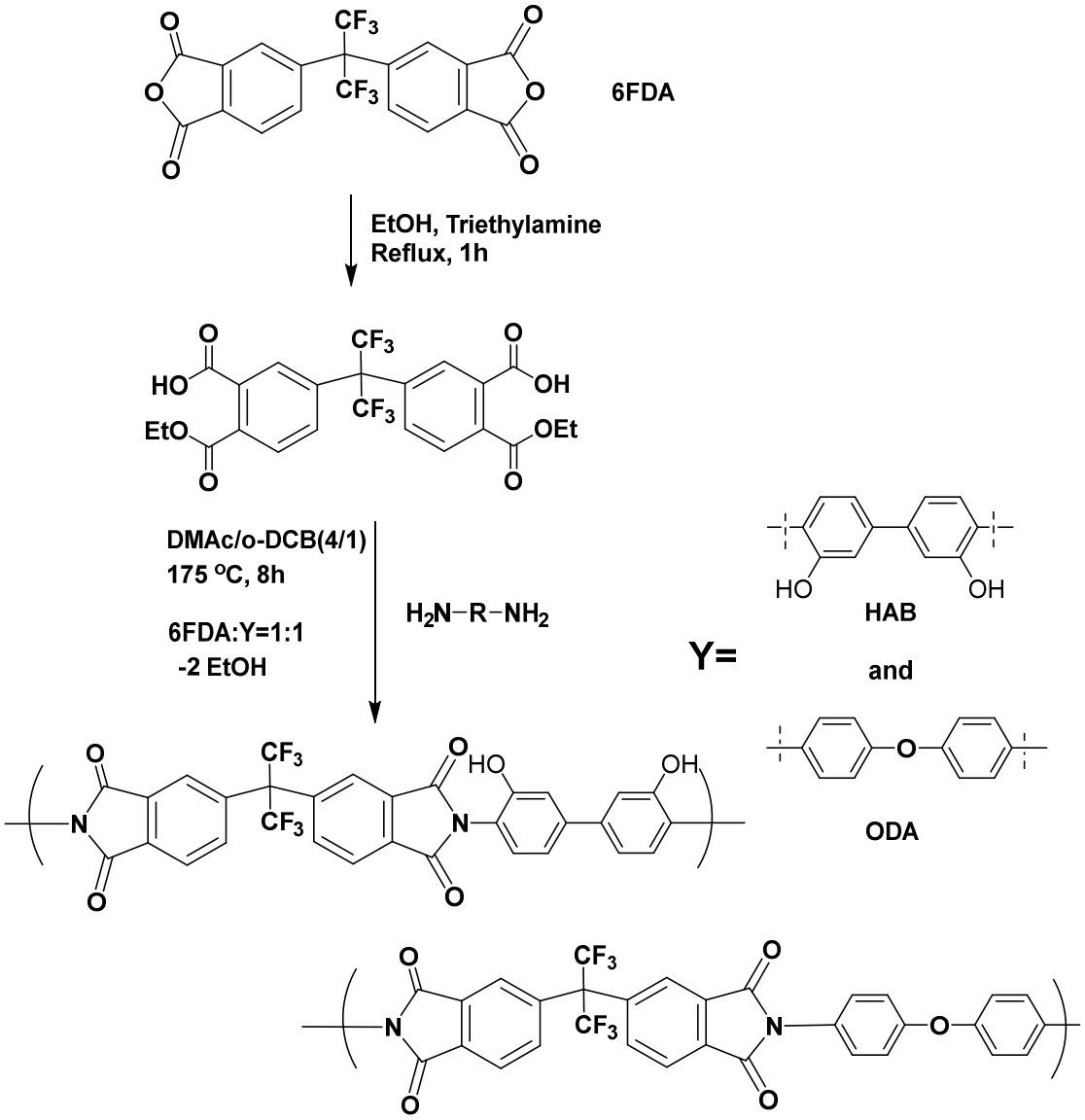

Figure 6.1 Synthesis of random TR copolymers via an ester-acid route

Additionally, some other toughening strategies could be adopted to improve mechanical property. Taking an example, we can synthesize TR precursor random copolymers based on both TR-able and non-TR-able monomers through ester-acid method in a one-pot reaction (Figure 6.1). In this strategy, 6FDA and HAB would be

used to produce polyhydroxylimides as TR precursor while 6FDA and mechanical tough monomer 4,4'-Oxydianiline (ODA) would provide more ductile backbone structure to toughen the TR polymer system.

For PPO based copolymer systems, further testing of different molecular weights of PPO difunctional oligomers and variations in membrane thickness would elicit a better understanding of crosslink density on membrane and transport properties for these systems. This control over structure, crosslinking, and membrane thickness, would allow for a system of PPO based membranes with a wide range of gas transport properties.

In the future, such PPO based polymer blending systems might be able to crosslink substantially with even less of the ketone-containing polymer. Additionally, PPO could be blended with other materials, such as a phosphine oxide based PAEK (Figure 6.1), to focus on other gas pairs and applications.

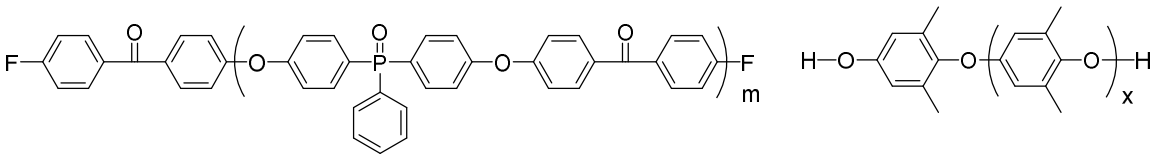

Figure 6.2 Phosphine oxide based PAEK and PPO

REFERENCE:

1. Nollet, J. A., Investigations on the causes for the ebullition of liquids. *J. Membr. Sci.* **1995,** *100* (1), 1-3.

2. Mitchell, J. K., On the penetrativeness of fluids. *Journal of Membrane Science* **1995,** *100* (1), 11-16.

3. Laidler, K. J.; Meiser, J. M., *Physical Chemistry*. 1982.

4. Baker, R. W., Future Directions of Membrane Gas Separation Technology. *Ind. Eng. Chem. Res.* **2002,** *41* (6), 1393-1411.

5. Spillman, R. W., Economics of Gas Separation by Membranes. *Chem. Eng. Prog.* **1989,** *85*, 41.

6. Sanders, E.; Clark, D. O.; Jensvold, J. A.; Beck, H. N.; Lipscomb, G. G.; Coan, F. L. Process for Preparing Powadir Membranes from Tetrahalobisphenol A Polycarbonates. 1988.

7. Matteucci, S.; Yampolskii, Y.; Freeman, B. D.; Pinnau, I., Transport of Gases and Vapors in Glassy and Rubbery Polymers. In *Materials Science of Membranes for Gas and Vapor Separation*, John Wiley & Sons, Ltd: 2006; pp 1-47.

8. Sanders, D. F.; Smith, Z. P.; Guo, R.; Robeson, L. M.; McGrath, J. E.; Paul, D. R.; Freeman, B. D., Energy-efficient polymeric gas separation membranes for a sustainable future: A review. *Polymer* **2013,** *54* (18), 4729-4761.

9. Ghosal, K.; Freeman, B. D., Gas separation using polymer membranes: an overview. *Polymers for Advanced Technologies* **1994,** *5* (11), 673-697.

10. Lin HQ; BD, F., Permeation and diffusion. In *Springer-Handbook of Materials Measurement Methods*, Czichos, H.; Smith, L. E.; Saito, T., Eds. Springer: Berlin, 2011; pp 426-444.

11. Fujita, H., Notes on Free Volume Theories. *Polym J* **1991,** *23* (12), 1499-1506.

12. Cohen, M. H.; Turnbull, D., Molecular Transport in Liquids and Glasses. *The Journal of Chemical Physics* **1959,** *31* (5), 1164-1169.

13. Turnbull, D.; Cohen, M. H., Free-volume model of the amorphous:glass transition. *J. Chem. Phys.* **1961,** *34*, 120-5.

14. Turnbull, D.; Cohen, M. H., Free‐Volume Model of the Amorphous Phase: Glass Transition. *The Journal of Chemical Physics* **1961,** *34* (1), 120-125.

15. Bondi, A., van der Waals volumes and radii. *J. Phys. Chem.* **1964,** *68* (3), 441-51.

16. Bondi, A., van der Waals Volumes and Radii. *The Journal of Physical Chemistry* **1964,** *68* (3), 441-451.

17. Yoshimizu, H.; Ohta, S.; Asano, T.; Suzuki, T.; Tsujita, Y., Temperature dependence of the mean size of polyphenyleneoxide microvoids, as studied by Xe sorption and 129Xe NMR chemical shift analyses. *Polym J* **2012,** *44* (8), 821-826.

18. Maeda, Y.; Paul, D. R., Effect of antiplasticization on selectivity and productivity of gas separation membranes. *J. Membr. Sci.* **1987,** *30* (1), 1-9.

19. Barbari, T. A.; Koros, W. J.; Paul, D. R., Polymeric membranes based on bisphenol A for gas separations. *J. Membr. Sci.* **1989,** *42* (1-2), 69-86.

20. Stern, S. A.; Mi, Y.; Yamamoto, H.; St. Clair, A. K., Structure/permeability relationships of polyimide membranes: applications to the separation of gas mixtures.

J. Polym. Sci., Part B: Polym. Phys. **1989,** *27* (9), 1887-909.

21. Kim, T. H.; Koros, W. J.; Husk, G. R.; O'Brien, K. C., Relationship between gas separation properties and chemical structure in a series of aromatic polyimides. *Journal of Membrane Science* **1988,** *37* (1), 45-62.

22. Robeson, L. M., Correlation of separation factor versus permeability for polymeric membranes. *J. Membr. Sci.* **1991,** *62* (2), 165-85.

23. Freeman, B. D., Basis of Permeability/Selectivity Tradeoff Relations in Polymeric Gas Separation Membranes. *Macromolecules* **1999,** *32* (2), 375-380.

24. Robeson, L. M.; Freeman, B. D.; Paul, D. R.; Rowe, B. W., An empirical correlation of gas permeability and permselectivity in polymers and its theoretical basis. *J. Membr. Sci.* **2009,** *341* (1-2), 178-185.

25. Krevelen, D. V., *Properties of polymers*. Elsevier: Amsterdam, 1972.

26. Robeson, L. M., The upper bound revisited. *J. Membr. Sci.* **2008,** *320* (1+2), 390-400.

27. Meares, P., The diffusion of gases through polyvinyl acetate. *J. Am. Chem. Soc.* **1954,** *76*, 3415-22.

28. Rowe, B. W.; Robeson, L. M.; Freeman, B. D.; Paul, D. R., Influence of temperature on the upper bound: Theoretical considerations and comparison with experimental results. *J. Membr. Sci.* **2010,** *360* (1-2), 58-69.

29. Leverette, L., The Global Market for Membrane Microfiltration. bccResearch: 2016.

30. Guo, R.; McGrath, J. E., Aromatic Polyethers, Polyetherketones, Polysulfides,

and Polysulfones. In *Polymer Science: A Comprehensive Reference*, Möller, M., Ed. Elsevier: Amsterdam, 2012; pp 377-430.

31. Liaw, D.-J.; Wang, K.-L.; Huang, Y.-C.; Lee, K.-R.; Lai, J.-Y.; Ha, C.-S., Advanced polyimide materials: Syntheses, physical properties and applications. *Prog. Polym. Sci.* **2012,** *37* (7), 907-974.

32. Sanders, D. F.; Smith, Z. P.; Guo, R.; Robeson, L. M.; McGrath, J. E.; Paul, D. R.; Freeman, B. D., Energy-efficient polymeric gas separation membranes for a sustainable future: A review. *Polymer* **2013,** *54* (18), 4729-4761.

33. H Ohya; V V Kudryavsev; Semenova, S. I., *Polyimide Membranes: Applications, Fabrications and Properties*. Tokyo: Kodansha Ltd.: 1996.

34. Farr, I. V.; Kratzner, D.; Glass, T. E.; Dunson, D.; Ji, Q.; McGrath, J. E., The synthesis and characterization of polyimide homopolymers based on 5(6)-amino-1-(4-aminophenyl)-1,3,3-trimethylindane. *J. Polym. Sci., Part A: Polym. Chem.* **2000,** *38* (15), 2840-2854.

35. Liu, S. L.; Chng, M. L.; Chung, T. S.; Goto, K.; Tamai, S.; Pramoda, K. P.; Tong, Y. J., Gas-transport properties of indan-containing polyimides. *J. Polym. Sci., Part B: Polym. Phys.* **2004,** *42* (14), 2769-2779.

36. Ismail, A. F.; Aziz, F. In *Chemical cross-linking modifications of polymeric membranes for gas separation applications*, CRC Press: 2012; pp 363-383.

37. Liu, Y.; Chung, T.-S.; Wang, R.; Li, D. F.; Chng, M. L., Chemical Cross-Linking Modification of Polyimide/Poly(ether sulfone) Dual-Layer Hollow-Fiber Membranes for Gas Separation. *Ind. Eng. Chem. Res.* **2003,** *42* (6), 1190-1195.

38. Yoshioka, T.; Kojima, K.; Shindo, R.; Nagai, K., Gas-separation properties of amine-crosslinked polyimide membranes modified by amine vapor. *J. Appl. Polym. Sci.* **2017,** *134* (10), n/a.

39. Liu, Y.; Wang, R.; Chung, T. S., Chemical cross-linking modification of polyimide membranes for gas separation. *J. Membr. Sci.* **2001,** *189* (2), 231-239.

40. Kim, J. H.; Koros, W. J.; Paul, D. R., Effects of CO2 exposure and physical aging on the gas permeability of thin 6FDA-based polyimide membranes. *J. Membr. Sci.* **2006,** *282* (1+2), 32-43.

41. Kim, J. H.; Koros, W. J.; Paul, D. R., Effects of CO2 exposure and physical aging on the gas permeability of thin 6FDA-based polyimide membranes. *J. Membr. Sci.* **2006,** *282* (1+2), 21-31.

42. Ghanem, B. S.; McKeown, N. B.; Budd, P. M.; Al-Harbi, N. M.; Fritsch, D.; Heinrich, K.; Starannikova, L.; Tokarev, A.; Yampolskii, Y., Synthesis, Characterization, and Gas Permeation Properties of a Novel Group of Polymers with Intrinsic Microporosity: PIM-Polyimides. *Macromolecules (Washington, DC, U. S.)* **2009,** *42* (20), 7881-7888.

43. Lin, W. H.; Chung, T. S., Gas permeability, diffusivity, solubility, and aging characteristics of 6FDA-durene polyimide membranes. *J. Membr. Sci.* **2001,** *186* (2), 183-193.

44. Wang, L.; Cao, Y.; Zhou, M.; Zhou, S. J.; Yuan, Q., Novel copolyimide membranes for gas separation. *J. Membr. Sci.* **2007,** *305* (1+2), 338-346.

45. Ghanem, B. S.; McKeown, N. B.; Budd, P. M.; Selbie, J. D.; Fritsch, D.,

High-performance membranes from polyimides with intrinsic microporosity. *Adv. Mater. (Weinheim, Ger.)* **2008,** *20* (14), 2766-2771.

46. Kim, H.-S.; Kim, Y.-H.; Ahn, S.-K.; Kwon, S.-K., Synthesis and Characterization of Highly Soluble and Oxygen Permeable New Polyimides Bearing a Noncoplanar Twisted Biphenyl Unit Containing tert-Butylphenyl or Trimethylsilyl Phenyl Groups. *Macromolecules* **2003,** *36* (7), 2327-2332.

47. Calle, M.; Lozano, A. E.; de La Campa, J. G.; de Abajo, J., Novel Aromatic Polyimides Derived from 5'-t-Butyl-2'-pivaloylimino-3,4,3",4"-m-terphenyltetracarboxylic Dianhydride with Potential Application on Gas Separation Processes. *Macromolecules (Washington, DC, U. S.)* **2010,** *43* (5), 2268-2275.

48. Hay, A. S.; Blanchard, H. S.; Endres, G. F.; Eustance, J. W., Polymerization by oxidative coupling. *J. Am. Chem. Soc.* **1959,** *81*, 6335-6.

49. Hay, A. S. Substituted poly(phenylene ethers). US3262892, 1966.

50. Van Dort, H. M.; De Jonge, C. R. H. I. Poly(phenylene ethers). US3400100A, 1968.

51. Hay, A. S. Oxidation of alcohols and ethers. US3173933, 1965.

52. Story, B. J.; Koros, W. J., Sorption of CO2/CH4 mixtures in poly(phenylene oxide) and a carboxylated derivative. *Journal of Applied Polymer Science* **1991,** *42* (9), 2613-2626.

53. Story, B. J.; Koros, W. J., Comparison of three models for permeation of carbon dioxide/methane mixtures in poly(phenylene oxide). *J. Polym. Sci., Part B: Polym.*

Phys. **1989,** *27* (9), 1927-48.

54. Chern, R. T.; Sheu, F. R.; Jia, L.; Stannett, V. T.; Hopfenberg, H. B., Transport of gases in unmodified and arylbrominated 2,6-dimethyl- 1,4-poly (phenylene oxide). *Journal of Membrane Science* **1987,** *35* (1), 103-115.

55. Chern, R. T.; Jia, L.; Shimoda, S.; Hopfenberg, H. B., A note on the effects of mono- and dibromination on the transport properties of poly(2,6-dimethylphenylene oxide). *J. Membr. Sci.* **1990,** *48* (2-3), 333-41.

56. Hamad, F.; Khulbe, K. C.; Matsuura, T., Characterization of gas separation membranes prepared from brominated poly(phenylene oxide) by infrared spectroscopy. *Desalination* **2002,** *148* (1-3), 369-375.

57. Sridhar, S.; Smitha, B.; Ramakrishna, M.; Aminabhavi, T. M., Modified poly(phenylene oxide) membranes for the separation of carbon dioxide from methane. *J. Membr. Sci.* **2006,** *280* (1+2), 202-209.

58. Edgar, K. J.; Buchanan, C. M.; Debenham, J. S.; Rundquist, P. A.; Seiler, B. D.; Shelton, M. C.; Tindall, D., Advances in cellulose ester performance and application. *Prog. Polym. Sci.* **2001,** *26* (9), 1605-1688.

59. Haggin, J., Air Products' James F. Roth wins 1988 Perkin Medal. *Chem. Eng. News* **1988,** *66* (10), 24-5.

60. Schell, W. J.; Wensley, C. G.; Chen, M. S. K.; Venugopal, K. G.; Miller, B. D.; Stuart, J. A., Recent advances in cellulosic membranes for gas separation and pervaporation. *Gas Sep. Purif.* **1989,** *3* (4), 162-9.

61. LS, W., Evolution of natural gas treatment with membrane systems. In *Membrane*

gas separation, Yampolskii Y, F. B., Ed. John Wiley & Sons Ltd: Chichester, 2010.

62. Saka, S., Wood as natural raw materials for cellulose acetate production. *Macromol. Symp.* **2004,** *208* (Cellulose Acetates), 7-28.

63. McGrail, P. T., Polyaromatics. *Polym. Int.* **1996,** *41* (2), 103-121.

64. Aguilar-Vega, M.; Paul, D. R., Gas transport properties of polycarbonates and polysulfones with aromatic substitutions on the bisphenol connector group. *J. Polym. Sci., Part B: Polym. Phys.* **1993,** *31* (11), 1599-610.

65. Ghosal, K.; Chern, R. T.; Freeman, B. D.; Daly, W. H.; Negulescu, I. I., Effect of Basic Substituents on Gas Sorption and Permeation in Polysulfone. *Macromolecules* **1996,** *29* (12), 4360-4369.

66. Aitken, C. L.; Koros, W. J.; Paul, D. R., Effect of structural symmetry on gas transport properties of polysulfones. *Macromolecules* **1992,** *25* (13), 3424-34.

67. Ghosal, K.; Chern, R. T., Aryl nitration of poly(phenylene oxide) and polysulfone. Structural characterization and gas permeability. *J. Membr. Sci.* **1992,** *72* (1), 91-7.

68. Yoon, T. H.; Priddy, D. B., Jr.; Lyle, G. D.; McGrath, J. E., Mechanical and morphological investigations of reactive polysulfone toughened epoxy networks. *Macromol. Symp.* **1995,** *98* (35th IUPAC International Symposium on Macromolecules, 1995), 673-86.

69. Wilkinson, S. P.; Ward, T. C.; McGrath, J. E., Effect of thermoplastic modifier variables on toughening a bismaleimide matrix resin for high-performance composite materials. *Polymer* **1993,** *34* (4), 870-84.

70. Yoon, T.-H.; McGrath, J. E., Curing and toughening of a styrene-modified epoxy

resin. *J. Appl. Polym. Sci.* **2001,** *80* (9), 1504-1513.

71. Varley, R. J.; Hodgkin, J. H.; Hawthorne, D. G.; Simon, G. P., Toughening of a trifunctional epoxy system. IV. dynamic mechanical relaxational study of the thermoplastic-modified cure process. *J. Polym. Sci., Part B: Polym. Phys.* **1997,** *35* (1), 153-163.

72. Varley, R. J.; Hodgkin, J. H.; Simon, G. P., Toughening of a trifunctional epoxy system Part VI. Structure property relationships of the thermoplastic toughened system. *Polymer* **2001,** *42* (8), 3847-3858.

73. Park, H. B.; Jung, C. H.; Lee, Y. M.; Hill, A. J.; Pas, S. J.; Mudie, S. T.; Van Wagner, E.; Freeman, B. D.; Cookson, D. J., Polymers with Cavities Tuned for Fast Selective Transport of Small Molecules and Ions. *Science* **2007,** *318* (5848), 254-258.

74. Han, S. H.; Lee, J. E.; Lee, K.-J.; Park, H. B.; Lee, Y. M., Highly gas permeable and microporous polybenzimidazole membrane by thermal rearrangement. *Journal of Membrane Science* **2010,** *357* (1–2), 143-151.

75. Jiang, Y.; Willmore, F. T.; Sanders, D.; Smith, Z. P.; Ribeiro, C. P.; Doherty, C. M.; Thornton, A.; Hill, A. J.; Freeman, B. D.; Sanchez, I. C., Cavity size, sorption and transport characteristics of thermally rearranged (TR) polymers. *Polymer* **2011,** *52* (10), 2244-2254.

76. Yampolskii, Y., Polymeric Gas Separation Membranes. *Macromolecules* **2012,** *45* (8), 3298-3311.

77. Freeman, B.; Yampolskii, Y., *Membrane Gas Separation*. Wiley: 2010.

78. Bogert, M. T.; Renshaw, R. R., 4-Amino-o-Phthalic Acid and Some of its

Derivatives. *J. Am. Chem. Soc.* **1908,** *30*, 1135-44.

79. Edwards, W. M.; Robinson, I. M. Polyimides of pyromellitic acid. US2710853, 1955.

80. Sroog, C. E., Polyimides. *Prog. Polym. Sci.* **1991,** *16* (4), 561-694.

81. Edwards, W. M.; Endrey, A. L. Polyimides. GB903271, 1962.

82. Pravednikov, A. N.; Kardash, I. Y.; Glukhoyedov, N. P.; Ardashnikov, A. Y., Some features of the synthesis of heat-resistant heterocyclic polymers. *Polymer Science U.S.S.R.* **1973,** *15* (2), 399-410.

83. Kaas, R. L., Autocatalysis and equilibrium in polyimide synthesis. *J. Polym. Sci., Polym. Chem. Ed.* **1981,** *19* (9), 2255-67.

84. Bell, V. L.; Stump, B. L.; Gager, H., Polyimide structure-property relations. II. Polymers from isomeric diamines. *J. Polym. Sci., Polym. Chem. Ed.* **1976,** *14* (9), 2275-91.

85. Sroog, C. E.; Endrey, A. L.; Abramo, S. V.; Berr, C. E.; Edwards, W. M.; Olivier, K. L., Aromatic polypyromellitimides from aromatic polyamic acids. *J. Polym. Sci., Part A: Gen. Pap.* **1965,** *3* (4), 1373-90.

86. Volksen, W., Condensation polyimides: synthesis, solution behavior, and imidization characteristics. *Adv. Polym. Sci.* **1994,** *117* (High Performance Polymers), 111-64.

87. Bender, M. L.; Chow, Y.-L.; Chloupek, F., Intramolecular catalysts of hydrolytic reactions. II. The hydrolysis of phthalamic acid. *J. Am. Chem. Soc.* **1958,** *80*, 5380-4.

88. Frost, L. W.; Kesse, I., Spontaneous degradation of aromatic poly(pyromellitamic

acids). *J. Appl. Polym. Sci.* **1964,** *8* (3), 1039-51.

89. Kudryavtsev, V. V., *Polyamic Acids and Polyimides: Synthesis, Transformations, and Structure;* . CRC Press: 1993.

90. Harris, F., *Polyimides*. Blackie and Son: 1990.

91. Preston, J., Polyimides – a new class of thermally stable polymers. N. A. Adrova, M. I. Bessonov, L. A. Laius, and A. P. Rudakov, technomic publishing Co., Inc., Stanford, Calif., 1970. ix + 200 pp. $26.50. *Journal of Polymer Science Part B: Polymer Letters* **1971,** *9* (3), 230-231.

92. Sacher, E.; Sedor, D. G., Possibility of further imidization in polyimide film. *J. Polym. Sci., Polym. Phys. Ed.* **1974,** *12* (3), 629-32.

93. Endrey, A. L.; Angelo, R. J. Polyimide films. GB945673, 1964.

94. Endrey, A. L. Aromatic polyimide particles from polycyclic diamines. US3179631, 1965.

95. Koton, M. M.; Meleshko, T. K.; Kudryavtsev, V. V.; Nechayev, P. P.; Kamzolkina, Y. V.; Bogorad, N. N., Investigation of the kinetics of chemical imidization. *Polymer Science U.S.S.R.* **1982,** *24* (4), 791-800.

96. Ghosh, M., *Polyimides: Fundamentals and Applications*. CRC Press 1996.

97. Bessonov, M. I.; Koton, M. M.; Kudryavtsev, V. V.; Laius, L. A., *Polyimides - Thermally Stable Polymers*. Plenum, New York: 1987.

98. Bessonov, M. I.; Zubkov, V. A., *Polyamic Acids and Polyimides: Synthesis, Transformations, and Structure*. CRC Press 1993.

99. Takekoshi, T.; Kochanowski, J. E.; Manello, J. S.; Webber, M. J., Polyetherimides.

II. High-temperature solution polymerization. *J. Polym. Sci., Polym. Symp.* **1986,** *74* (In Honor Charles G. Overberger His 65th Birthday), 93-108.

100. Kim, Y. J.; Glass, T. E.; Lyle, G. D.; McGrath, J. E., Kinetic and mechanistic investigations of the formation of polyimides under homogeneous conditions. *Macromolecules* **1993,** *26* (6), 1344-58.

101. Serafini, T. T.; Delvigs, P.; Lightsey, G. R., Thermally stable polyimides from solutions of monomeric reactants. *J. Appl. Polym. Sci.* **1972,** *16* (4), 905-15.

102. Johnston, J. C.; Meador, M. A. B.; Alston, W. B., A mechanistic study of polyimide formation from diester-diacids. *J. Polym. Sci., Part A: Polym. Chem.* **1987,** *25* (8), 2175-83.

103. Moy, T. M.; DePorter, C. D.; McGrath, J. E., Synthesis of soluble polyimides and functionalized imide oligomers via solution imidization of aromatic diester-diacids and aromatic diamines. *Polymer* **1993,** *34* (4), 819-24.

104. Spring, F. S.; Woods, J. C., The reaction between N-substituted phthalimides and primary amines. *Nature (London, U. K.)* **1946,** *158*, 754-5.

105. Imai, Y., Novel method for preparing polyimides from N,N'-bis(ethoxycarbonyl)pyromellitimide and diamines. *J. Polym. Sci., Part B* **1970,** *8* (8), 555-8.

106. Smith, Z. P.; Sanders, D. F.; Ribeiro, C. P.; Guo, R.; Freeman, B. D.; Paul, D. R.; McGrath, J. E.; Swinnea, S., Gas sorption and characterization of thermally rearranged polyimides based on 3,3'-dihydroxy-4,4'-diamino-biphenyl (HAB) and 2,2'-bis-(3,4-dicarboxyphenyl) hexafluoropropane dianhydride (6FDA). *J. Membr. Sci.*

2012, *415-416*, 558-567.

107. Sanders, D. F.; Smith, Z. P.; Ribeiro, C. P., Jr.; Guo, R.; McGrath, J. E.; Paul, D. R.; Freeman, B. D., Gas permeability, diffusivity, and free volume of thermally rearranged polymers based on 3,3'-dihydroxy-4,4'-diamino-biphenyl (HAB) and 2,2'-bis-(3,4-dicarboxyphenyl) hexafluoropropane dianhydride (6FDA). *J. Membr. Sci.* **2012,** *409-410*, 232-241.

108. Calle, M.; Lozano, A. E.; Lee, Y. M., Formation of thermally rearranged (TR) polybenzoxazoles: Effect of synthesis routes and polymer form. *Eur. Polym. J.* **2012,** *48* (7), 1313-1322.

109. Yeong, Y. F.; Wang, H.; Pallathadka Pramoda, K.; Chung, T.-S., Thermal induced structural rearrangement of cardo-copolybenzoxazole membranes for enhanced gas transport properties. *J. Membr. Sci.* **2012,** *397-398*, 51-65.

110. Tullos, G. L.; Powers, J. M.; Jeskey, S. J.; Mathias, L. J., Thermal Conversion of Hydroxy-Containing Imides to Benzoxazoles: Polymer and Model Compound Study. *Macromolecules* **1999,** *32* (11), 3598-3612.

111. Sanders, D. F.; Guo, R.; Smith, Z. P.; Liu, Q.; Stevens, K. A.; McGrath, J. E.; Paul, D. R.; Freeman, B. D., Influence of polyimide precursor synthesis route and ortho-position functional group on thermally rearranged (TR) polymer properties: Conversion and free volume. *Polymer* **2014,** *55* (7), 1636-1647.

112. McCaig, M. S.; Paul, D. R., Effect of UV crosslinking and physical aging on the gas permeability of thin glassy polyarylate films. *Polymer* **1999,** *40* (26), 7209-7225.

113. Callahan, R. W.; Johnson, R. D. Composite membranes from UV-curable

polyacrylates. EP321241A2, 1989.

114.Ouyang, M.; Muisener, R. J.; Boulares, A.; Koberstein, J. T., UV-ozone induced growth of a SiOx surface layer on a cross-linked polysiloxane film: characterization and gas separation properties. *J. Membr. Sci.* **2000,** *177* (1-2), 177-187.

115.Ritchie, S. M. C., Polymer grafted membranes. *Membr. Sci. Technol. Ser.* **2003,** *8* (New Insights into Membrane Science and Technology: Polymeric and Biofunctional Membranes, 2003), 299-327.

116.Sundell, B. J.; Shaver, A. T.; Liu, Q.; Nebipasagil, A.; Pisipati, P.; Mecham, S. J.; Riffle, J. S.; Freeman, B. D.; McGrath, J. E., Synthesis, oxidation and crosslinking of tetramethyl bisphenol F (TMBPF)-based polymers for oxygen/nitrogen gas separations. *Polymer* **2014,** *55* (22), 5623-5634.

117.Kita, H.; Inada, T.; Tanaka, K.; Okamoto, K.-i., Effect of photocrosslinking on permeability and permselectivity of gases through benzophenone- containing polyimide. *Journal of Membrane Science* **1994,** *87* (1), 139-147.

118.Decker, C.; Nguyen Thi Viet, T.; Decker, D.; Weber-Koehl, E., UV-radiation curing of acrylate/epoxide systems. *Polymer* **2001,** *42* (13), 5531-5541.

119.Shao, L.; Samseth, J.; Hagg, M.-B., Crosslinking and stabilization of high fractional free volume polymers for gas separation. *Int. J. Greenhouse Gas Control* **2008,** *2* (4), 492-501.

120. Amamoto, Y.; Kamada, J.; Otsuka, H.; Takahara, A.; Matyjaszewski, K., Repeatable Photoinduced Self-Healing of Covalently Cross-Linked Polymers through Reshuffling of Trithiocarbonate Units. *Angew. Chem., Int. Ed.* **2011,** *50* (7),

1660-1663.

121. Hayes, R. A. Polyimide membranes for gas separation. US4717394A, 1988.

122. Kita, H.; Inada, T.; Tanaka, K.; Okamoto, K., Effect of photocrosslinking on permeability and permselectivity of gases through benzophenone-containing polyimide. *J. Membr. Sci.* **1994,** *87* (1-2), 139-47.

123. Wright, C. T.; Paul, D. R., Gas sorption and transport in UV-irradiated polyarylate copolymers based on tetramethylbisphenol-A and dihydroxybenzophenone. *J. Membr. Sci.* **1997,** *124* (2), 161-174.

124. Scaiano, J. C.; Netto-Ferreira, J. C.; Becknell, A. F.; Small, R. D., The mechanism of photocure of inherently photosensitive polyimides containing a benzophenone group. *Polym. Eng. Sci.* **1989,** *29* (14), 942-4.

125. Lin, A. A.; Sastri, V. R.; Tesoro, G.; Reiser, A.; Eachus, R., On the crosslinking mechanism of benzophenone-containing polyimides. *Macromolecules* **1988,** *21* (4), 1165-9.

126. Shaver, A. T.; Yin, K.; Borjigin, H.; Zhang, W.; Choudhury, S. R.; Baer, E.; Mecham, S. J.; Riffle, J. S.; McGrath, J. E., Fluorinated poly(arylene ether ketone)s for high temperature dielectrics. *Polymer* **2016,** *83*, 199-204.

127. Hsiao, S.-H.; Chiang, H.-W., Synthesis and properties of new fluorinated polyarylates derived from 1,1-bis(4-hydroxyphenyl)-1-phenyl-2,2,2-trifluoroethane and aromatic diacid chlorides. *European Polymer Journal* **2004,** *40* (8), 1691-1697.

128. Borjigin, H.; Stevens, K. A.; Liu, R.; Moon, J. D.; Shaver, A. T.; Swinnea, S.; Freeman, B. D.; Riffle, J. S.; McGrath, J. E., Synthesis and characterization of

polybenzimidazoles derived from tetraaminodiphenylsulfone for high temperature gas separation membranes. *Polymer* **2015,** *71*, 135-142.

129. Mcgrath, J. E.; Grubbs, H.; Rogers, M. E.; Moy, T. M.; Joseph, W. A., Molecular Design of Processable High Tg Thermoplastic Matrix Resins and Structural Adhesives. *Interfaces & material systems* **1993**, 213.

130. Mecham, S. J. Synthesis and Characterization of Phenylethynyl Terminated Poly(arylene ether sulfone)s as Thermosetting Structural Adhesives and Composite Matrices. Virginia Polytechnic Institute and State University, 1997.

131. Jung, C. H.; Lee, J. E.; Han, S. H.; Park, H. B.; Lee, Y. M., Highly permeable and selective poly(benzoxazole-co-imide) membranes for gas separation. *Journal of Membrane Science* **2010,** *350* (1–2), 301-309.

132. Hodgkin, J. H.; Liu, M. S.; Dao, B. N.; Mardel, J.; Hill, A. J., Reaction mechanism and products of the thermal conversion of hydroxy-containing polyimides. *Eur. Polym. J.* **2011,** *47* (3), 394-400.

133. Yampolskii, Y., Polymeric Gas Separation Membranes. *Macromolecules (Washington, DC, U. S.)* **2012,** *45* (8), 3298-3311.

134. Baker, R. W.; Lokhandwala, K., Natural Gas Processing with Membranes: An Overview. *Industrial & Engineering Chemistry Research* **2008,** *47* (7), 2109-2121.

135. Guo, R.; Sanders, D. F.; Smith, Z. P.; Freeman, B. D.; Paul, D. R.; McGrath, J. E., Synthesis and characterization of thermally rearranged (TR) polymers: effect of glass transition temperature of aromatic poly(hydroxyimide) precursors on TR process and gas permeation properties. *J. Mater. Chem. A* **2013,** *1* (19), 6063-6072.

136. Moy, T. M.; DePorter, C. D.; McGrath, J. E., Synthesis of soluble polyimides and functionalized imide oligomers via solution imidization of aromatic diester-diacids and aromatic diamines. *Polymer* **1993,** *34* (4), 819-824.

137. Borjigin, H.; Liu, Q.; Zhang, W.; Gaines, K.; Riffle, J. S.; Paul, D. R.; Freeman, B. D.; McGrath, J. E., Synthesis and characterization of thermally rearranged (TR) polybenzoxazoles: Influence of isomeric structure on gas transport properties. *Polymer* **2015,** *75*, 199-210.

138. H. Lin; B.D. Freeman, Handbook of Materials Measurement Methods. In *Handbook of Materials Measurement Methods*, Springer: 2006; pp 371-387.

139. Srinivasan, S. A.; McGrath, J. E., Amorphous bisphenol-A based poly(arylene ether) modified cyanate ester networks. *High Perform. Polym.* **1993,** *5* (4), 259-74.

140. Hedrick, J. L.; Yilgor, I.; Jurek, M.; Hedrick, J. C.; Wilkes, G. L.; McGrath, J. E., Chemical modification of matrix resin networks with engineering thermoplastics. 1. Synthesis, morphology, physical behavior and toughening mechanisms of poly(arylene ether sulfone)-modified epoxy networks. *Polymer* **1991,** *32* (11), 2020-32.

141. Freeman, B. D.; Pinnau, I., Polymeric Materials for Gas Separations. In *Polymer Membranes for Gas and Vapor Separation*, American Chemical Society: 1999; Vol. 733, pp 1-27.

142. Guo, R.; McGrath, J. E., 5.17 - Aromatic Polyethers, Polyetherketones, Polysulfides, and Polysulfones A2 - Matyjaszewski, Krzysztof. In *Polymer Science: A*

Comprehensive Reference, Möller, M., Ed. Elsevier: Amsterdam, 2012; pp 377-430.

143. Jurek, M. J.; McGrath, J. E., Synthesis and characterization of amine-terminated poly(arylene ether sulfone) oligomers. *Polymer* **1989,** *30* (8), 1552-7.

144. Guo, R.; Sanders, D. F.; Smith, Z. P.; Freeman, B. D.; Paul, D. R.; McGrath, J. E., Synthesis and characterization of Thermally Rearranged (TR) polymers: influence of ortho-positioned functional groups of polyimide precursors on TR process and gas transport properties. *J. Mater. Chem. A* **2013,** *1* (2), 262-272.

145. Smith, Z. P.; Sanders, D. F.; Ribeiro, C. P.; Guo, R.; Freeman, B. D.; Paul, D. R.; McGrath, J. E.; Swinnea, S., Gas sorption and characterization of thermally rearranged polyimides based on 3,3′-dihydroxy-4,4′-diamino-biphenyl (HAB) and 2,2′-bis-(3,4-dicarboxyphenyl) hexafluoropropane dianhydride (6FDA). *Journal of Membrane Science* **2012,** *415–416*, 558-567.

146. Zhuang, Y.; Seong, J. G.; Lee, W. H.; Do, Y. S.; Lee, M. J.; Wang, G.; Guiver, M. D.; Lee, Y. M., Mechanically Tough, Thermally Rearranged (TR) Random/Block Poly(benzoxazole-co-imide) Gas Separation Membranes. *Macromolecules (Washington, DC, U. S.)* **2015,** *48* (15), 5286-5299.

147. Fried, J. R., *Polymer Science and Technology*. Prentice Hall: 2013.

148. Sur, G. S.; Sun, H. L.; Lyu, S. G.; Mark, J. E., Synthesis, structure, mechanical properties, and thermal stability of some polysulfone/organo-clay nanocomposites. *Polymer* **2001,** *42* (24), 9783-9789.

149. Liu, Q.; Paul, D. R.; Freeman, B. D., Gas permeation and mechanical

properties of thermally rearranged (TR) copolyimides. *Polymer* **2016,** *82*, 378-391.

150. Li, S.; Jo, H. J.; Han, S. H.; Park, C. H.; Kim, S.; Budd, P. M.; Lee, Y. M., Mechanically robust thermally rearranged (TR) polymer membranes with spirobisindane for gas separation. *J. Membr. Sci.* **2013,** *434*, 137-147.

151. Scholes, C. A.; Ribeiro, C. P.; Kentish, S. E.; Freeman, B. D., Thermal rearranged poly(benzoxazole)/polyimide blended membranes for CO2 separation. *Sep. Purif. Technol.* **2014,** *124*, 134-140.

152. Jo, H. J.; Soo, C. Y.; Dong, G.; Do, Y. S.; Wang, H. H.; Lee, M. J.; Quay, J. R.; Murphy, M. K.; Lee, Y. M., Thermally Rearranged Poly(benzoxazole-co-imide) Membranes with Superior Mechanical Strength for Gas Separation Obtained by Tuning Chain Rigidity. *Macromolecules (Washington, DC, U. S.)* **2015,** *48* (7), 2194-2202.

153. Toi, K.; Morel, G.; Paul, D. R., Gas sorption and transport in poly(phenylene oxide) and comparisons with other glassy polymers. *J. Appl. Polym. Sci.* **1982,** *27* (8), 2997-3005.

154. Alentiev, A.; Drioli, E.; Gokzhaev, M.; Golemme, G.; Ilinich, O.; Lapkin, A.; Volkov, V.; Yampolskii, Y., Gas permeation properties of phenylene oxide polymers. *J. Membr. Sci.* **1998,** *138* (1), 99-107.

155. Chern, R. T.; Sheu, F. R.; Jia, L.; Stannett, V. T.; Hopfenberg, H. B., Transport of gases in unmodified and aryl-brominated 2,6-dimethyl-1,4-poly(phenylene oxide). *J. Membr. Sci.* **1987,** *35* (1), 103-15.

156. Hay, A. S., Poly(phenylene oxide)s and poly(arylene ether)s derived from

2,6-diarylphenols. *Prog. Polym. Sci.* **1999,** *24* (1), 45-80.

157. Aguilar-Vega, M.; Paul, D. R., Gas transport properties of polyphenylene ethers. *J. Polym. Sci., Part B: Polym. Phys.* **1993,** *31* (11), 1577-89.

158. Story, B. J.; Koros, W. J., Sorption and transport of carbon dioxide and methane in chemically modified poly(phenylene oxide). *J. Membr. Sci.* **1992,** *67* (2-3), 191-210.

159. Story, B. J.; Koros, W. J., Sorption of carbon dioxide/methane mixtures in poly(phenylene oxide) and a carboxylated derivative. *J. Appl. Polym. Sci.* **1991,** *42* (9), 2613-26.

160. Hay, A. S., Polymerization by oxidative coupling: discovery and commercialization of PPO and Noryl resins. *J. Polym. Sci., Part A: Polym. Chem.* **1998,** *36* (4), 505-517.

161. Clark, R. F.; Krantz, K. W. Poly(phenylene oxide)-organopolysiloxane block copolymers as surface tension depressants. US3696137A, 1972.

162. Krijgsman, J.; Feijen, J.; Gaymans, R. J., Segmented copolymers of uniform tetraamide units and poly(phenylene oxide): 1. Synthesis and thermal-mechanical properties. *Polymer* **2004,** *45* (14), 4677-4684.

163. Kuo, S.-W.; Huang, C.-F.; Tung, P.-H.; Huang, W.-J.; Huang, J.-M.; Chang, F.-C., Synthesis, thermal properties, and specific interactions of high Tg increase in poly(2,6-dimethyl-1,4-phenylene oxide)-block-polystyrene copolymers. *Polymer* **2005,** *46* (22), 9348-9361.

164. Hay, A. S., Polymerization by oxidative coupling. II. Oxidation of

2,6-disubstituted phenols. *J. Polym. Sci.* **1962,** *58*, 581-91.

165. Finkbeiner, H.; Hay, A. S.; Blanchard, H. S.; Endres, G. F., Polymerization by oxidative coupling. The function of copper in the oxidation of 2,6-dimethylphenol. *J. Org. Chem.* **1966,** *31* (2), 549-55.

166. Van Aert, H. A. M.; Venderbosch, R. W.; Van Genderen, M. H. P.; Lemstra, P. J.; Meijer, E. W., Controlled molecular weight by the precipitation polymerization of 2,6-dimethylphenol. *J. Macromol. Sci., Pure Appl. Chem.* **1995,** *A32* (3), 515-23.

167. White, D. M., Reactions of poly(phenylene oxide)s with quinones. I. The quinone-coupling reaction between low-molecular-weight poly(2,6-dimethyl-1,4-phenylene oxide) and 3,3',5,5'-tetramethyl-4,4'-diphenoquinone. *J. Polym. Sci., Polym. Chem. Ed.* **1981,** *19* (6), 1367-83.

168. Staudt-Bickel, C.; Koros, W. J., Improvement of CO2/CH4 separation characteristics of polyimides by chemical crosslinking. *J. Membr. Sci.* **1999,** *155* (1), 145-154.

169. Wind, J. D.; Sirard, S. M.; Paul, D. R.; Green, P. F.; Johnston, K. P.; Koros, W. J., Carbon dioxide-induced plasticization of polyimide membranes: pseudo-equilibrium relationships of diffusion, sorption, and swelling. *Macromolecules* **2003,** *36* (17), 6433-6441.

170. Park, H. B.; Jung, C. H.; Lee, Y. M.; Hill, A. J.; Pas, S. J.; Mudie, S. T.; Van Wagner, E.; Freeman, B. D.; Cookson, D. J., Polymers with Cavities Tuned for Fast Selective Transport of Small Molecules and Ions. *Science (Washington, DC, U. S.)* **2007,** *318* (5848), 254-258.

171. Hayes, R. A. Polyimide gas-separation membranes. US4717393A, 1988.

172. Tran, A.; Kruczek, B., Development and characterization of homopolymers and copolymers from the family of polyphenylene oxides. *J. Appl. Polym. Sci.* **2007,** *106* (3), 2140-2148.

173. Gajbhiye, S. B., Membranes of poly(phenylene oxide) and its copolymers: Synthesis, characterization, and application in recovery of propylene from a refinery off-gas mixture. *J. Appl. Polym. Sci.* **2013,** *127* (4), 2497-2507.

174. Wang, F.; Sylvia, J. M.; Jacob, M. M.; Peramunage, D., Amphiphilic block copolymer membrane for vanadium redox flow battery. *J. Power Sources* **2013,** *242*, 575-580.

175. Wu, S. K.; Rabek, J. F., Benzophenone-initiated photocrosslinking of polynorbornene in the solid state. *Polym. Degrad. Stab.* **1988,** *21* (4), 365-76.

176. Christensen, S. K.; Chiappelli, M. C.; Hayward, R. C., Gelation of Copolymers with Pendent Benzophenone Photo-Cross-Linkers. *Macromolecules (Washington, DC, U. S.)* **2012,** *45* (12), 5237-5246.

177. Hendrix, K.; Van Eynde, M.; Koeckelberghs, G.; Vankelecom, I. F. J., Crosslinking of modified poly(ether ether ketone) membranes for use in solvent resistant nanofiltration. *J. Membr. Sci.* **2013,** *447*, 212-221.

178. Meier, I. K.; Langsam, M.; Klotz, H. C., Selectivity enhancement via photooxidative surface modification of polyimide air separation membranes. *J. Membr. Sci.* **1994,** *94* (1-3), 195-212.

179. Robeson, L. M.; Burgoyne, W. F.; Langsam, M.; Savoca, A. C.; Tien, C. F.,

High performance polymers for membrane separation. *Polymer* **1994,** *35* (23), 4970-8.

180. Handa, Y. P.; Roovers, J.; Moulinie, P., Gas transport properties of substituted PEEKs. *J. Polym. Sci., Part B: Polym. Phys.* **1997,** *35* (14), 2355-2362.

181. Vu, D. Q.; Koros, W. J.; Miller, S. J., Mixed matrix membranes using carbon molecular sieves. I. Preparation and experimental results. *J. Membr. Sci.* **2003,** *211* (2), 311-334.

182. Baker, R. W.; Low, B. T., Gas Separation Membrane Materials: A Perspective. *Macromolecules (Washington, DC, U. S.)* **2014,** *47* (20), 6999-7013.

183. Bernardo, P.; Drioli, E.; Golemme, G., Membrane Gas Separation: A Review/State of the Art. *Ind. Eng. Chem. Res.* **2009,** *48* (10), 4638-4663.

184. Liu, Q.; Shaver, A. T.; Chen, Y.; Miller, G.; Paul, D. R.; Riffle, J. S.; McGrath, J. E.; Freeman, B. D., Effect of UV irradiation and physical aging on O2 and N2 transport properties of thin glassy poly(arylene ether ketone) copolymer films based on tetramethyl bisphenol A and 4,4'-difluorobenzophenone. *Polymer* **2016,** *87*, 202-214.

185. Rowlett, J. R.; Liu, Q.; Zhang, W.; Moon, J. D.; Dose, M. E.; Riffle, J. S.; Freeman, B. D.; McGrath, J. E., Gas transport properties and characterization of UV crosslinked poly(phenylene oxide-co-arylene ether ketone) copolymers. *J. Mater. Chem. A* **2016,** *4* (41), 16047-16056.

186. Bender, T. P.; Burt, R. A.; Hamer, G. K.; DeVisser, C.; Smith, P. F.; Saban, M., The Synthesis of Poly(arylene ether)s in Solution at Pilot-Plant Scale with Control

over Molecular Weight and End-Group Composition. *Org. Process Res. Dev.* **2002,** *6* (5), 714-720.

187. Chen, Y.; Guo, R.; Lee, C. H.; Lee, M.; McGrath, J. E., Partly fluorinated poly(arylene ether ketone sulfone) hydrophilic-hydrophobic multiblock copolymers for fuel cell membranes. *Int. J. Hydrogen Energy* **2012,** *37* (7), 6132-6139.

188. Lyle, G. D.; Grubbs, H.; Tchatchoua, C.; McGarth, J. E., Synthesis and characterization of poly(arylene ether)s derived from 1,1-bis-(4-hydroxyphenyl)-1-phenyl-2,2,2-trifluoroethane. *Polym. Mater. Sci. Eng.* **1993,** *69*, 238-9.

189. Wu, Y.; Gui, L.; Wang, H.; Shentu, B.; Weng, Z., Synthesis and Characterization of α,ω-bis(2,6-dimethylphenol)-poly(2,6-dimethyl-1,4-phenylene oxide) Oligomers in Water and the End-Group Modification. *Ind. Eng. Chem. Res.* **2013,** *52* (49), 17351-17359.

190. Fox, T. G.; Flory, P. J., The glass temperature and related properties of polystyrene. Influence of molecular weight. *J. Polym. Sci.* **1954,** *14*, 315-19.

191. Morawetz, H., Polymer photophysics and photochemistry—an introduction to the study of photoprocesses in macromolecules. *Journal of Polymer Science Part C: Polymer Letters* **1988,** *26*, 243-244.

192. Barnabeo, A. E.; Creasy, W. S.; Robeson, L. M., Gas permeability characteristics of nitrile-containing block and random copolymers. *J. Polym. Sci., Polym. Chem. Ed.* **1975,** *13* (9), 1979-86.

193. Hopfenberg, H. B.; Paul, D. R., Chapter 10: Transport Phenomena in

Polymer Blends. In *Polymer Blends*, Academic Press: New York: 1978; pp 445-489.

194. Robert, G. D. S., A Multiple Comparison Rank Sum Test: Treatments versus Control. *Biometrics* **1959,** *15* (4), 560-572.